Ultrasonic NDE testing of a Gradient Enhanced Piezoelectric Actuator (GEPAC) undergoing low frequency bending excitation

A Thesis

Presented to

The Academic Faculty

By

Dominique Gex

In Partial Fulfillment

Of the Requirements for the Degree

Master of Science in Mechanical Engineering

Georgia Institute of Technology

April 2004

Ultrasonic NDE testing of a Gradient Enhanced
Piezoelectric Actuator (GEPAC) undergoing low frequency bending excitation

Approved by:

Dr. Yves H. Berthelot, Advisor

Dr. Christopher S. Lynch

Dr. Laurence J. Jacobs

April 2, 2004

To Mom and Dad for their love and support

ACKNOWLEDGEMENTS

First and foremost, I would like to express my gratitude toward my advisors, Dr. Yves Berthelot and Dr. Cristopher Lynch for offering me the chance to work on this project.

I thank my committee member, Dr. Jacobs, for taking the time and interest to review my work..

I thank Billy Oates and Scott Herdic for answering my questions about piezoelectricity.

I thank Kyle Webber for his assistance in the manufacturing of actuators.

Last but not least, I thank my fellow graduate students and my friends, for all the great and unforgettable moments we spent in Atlanta during this year.

This work is sponsored by the Air Force Office of Scientific Research.

TABLE OF CONTENTS

LIST OF TABLES

LIST OF FIGURES

SUMMARY

Gradient Enhanced Piezoelectric Actuators (GEPAC) are thin piezoelectric plates embedded between two composites layers having different thermal properties. Compared to standard unimorph bending actuators, GEPACs offer superior performances for operations at low frequencies. Potential applications are in the area of multifunctional aircraft skins. In practice, delaminations or debonding within the actuator itself can occur, and it is highly desirable to develop an ultrasonic nondestructive method to monitor the integrity of the actuator in real time.

For this study, the composite material is unidirectional Kevlar-epoxy, with fibers oriented at 90° and 0° for the upper and lower layers to achieve different coefficient of thermal expansion. A thin PZT plate is inserted between the two layers, and extended copper foil is used for electrodes on the PZT. The first objective of the research is to demonstrate that, by using segmented electrodes, one can simultaneously launch an ultrasonic pulse (1 MHz) for NDE testing while the actuator is undergoing low frequency actuation (<100 Hz). The second objective is to show that the ultrasonic signal can be used to detect damage induced during fatigue testing of the actuator. The third objective is to use the technique to monitor the integrity of a composite plate containing several embedded GEPACs.

CHAPTER I

INTRODUCTION

Gradient Enhanced Piezoelectric Actuators, or GEPACs, consist of very thin piezoelectric plates embedded between several composite layers with different thermal expansion coefficients. The actuators are designed to place the active ceramic layer in residual compression. Compared to traditional actuators, GEPACs provide superior performance in the bending mode for operations at low frequencies. They can be of high interest in aeronautics for the construction of "multifunctional skins". As with other unimorph designs, GEPACs change their curvature in response to an applied voltage. One could therefore actively control the shape of an airfoil to improve aerodynamic performance or actively damp vibration.

Bending mode actuators that produce large deflections are commercially available, most notably as the Rainbow™ (Heartling 1994) and the Thunder™ (Mossi 1999) actuators. These devices are based on using residual stresses to improve the piezoelectric response of the actuator. These devices use stainless steel or other metal as a substrate to the PZT plate. Goo (2001) recognized the benefit of using fiber composites instead of metal. Lynch et al. (Bechet 2003, Hopkinson 2003, Lynch 2003) built such actuators and finite element models and called them GEPAC.

While GEPACs have great potential for a variety of applications, they may be susceptible to fatigue-induced damage. Delamination or debonding may occur between the PZT layer and the fiber composites, cracks in the thin PZT layer may also be present

either after manufacturing of the actuator, or possibly, after millions of cycles of use (fatigue).

The objective of the present research is to show that ultrasonic Non Destructive Evaluation (NDE) can be used to monitor the structural integrity of the actuator itself while it is performing its low frequency bending actuation. Preliminary work by Bechet (Bechet 2003) included a finite element model of ultrasound in a GEPAC actuator, using Abaqus/explicit, and proof-of-concept experiments. For simplicity of modeling and experimentation, Bechet (Bechet 2003, Berthelot 2003) had modeled the PZT plate sandwiched between two steel plates.

In a GEPAC actuator, the PZT plate is sandwiched between several layers of fiber composite materials. The goal of this thesis is to demonstrate experimentally that ultrasonic NDE can be used in a GEPAC actuator to monitor its structural intergrity while not interfering with the primary function of the actuator in the low frequency bending mode.

The thesis is organized as follows. The chapter 2 provides some background informations on currently available bending actuators, as well as the design and manufacturing of GEPAC actuators in our laboratory at Georgia Tech. Chapter 3 is devoted to operations of ultrasonic non destructive evaluation and low frequency actuation in a GEPAC. The aim is to study the propagation of acoustic wave in the actuator and to observe the effect of actuation on ultrasonic testing. Chapter 4 is about fatigue testing of a GEPAC. In this part, a fatigue experiment is conducted (up to 53 millions cycles of actuation) and the actuator is regularly inspected by ultrasonic NDE in

order to evaluate possibly degradation. Fatigue testing is performed on healthy actuators. Debonding defects are studied in this part. Chapter 5 shows experimental results obtained with a fibercomposite plate containing two thin embedded piezo ceramics separated by a distance of 180 mm. The purpose of this experiment was to show that ultrasonic NDE can be used not only to monitor the structural health of an actuator, but also to monitor structural health of a composite plate beteen two actuators over large distances. Experiments are reported for both healthy composite plates and for plates containing an artificial debonding defect. Finally, conclusions and summary are presented in the last chapter.

CHAPTER II

BACKGROUND

In 1880, Pierre and Jacques Curie observed that electric surface charges appear when mechanical stresses are applied to specially prepared crystals such as tourmaline, topaz or quartz (Jaffe 1971). The converse effect was demonstrated by the Curie brothers also in 1880. This conversion of mechanical to electrical energy is called piezoelectricity (Auld 1990). It is during world war I that piezoelectricity found its first application, with the sonar invention by Langevin. In the mid twentieth century, researchers showed that it was possible to develop prepared ceramic materials having much higher dielectric constants than natural crystal. The most common of these are Lead Zirconate Titanate $Pb(Ti,Zr)O_3$ (PZT) and Lithium Niobate ($LiNbO_3$).

Piezoelectric ceramics are usually plates (see for instance http://www.channelindustries.com) of various size and shapes. When a voltage is applied across the electrodes (see Figure 2.1), the material changes thickness. The amplitude δt of the change is related to the applied voltage through a piezoelectric coefficient, d_{33} which, for PZT materials, is less than 600×10^{-12} $m.V^{-1}$. One way to increase the displacement is to use a bending actuator. Basically, a bending actuator is composed of a piezoelectric plate that is bonded to an inactive substrate layer (Smits 1990). When a voltage is applied, the piezoelectric plate expands or contracts whereas the non piezoelectric plate keeps the same geometry, causing the actuator to bend. Large amplitude bending

actuators may be used either with DC voltage to change the shape of a surface, or with AC voltage to generate and/or actively control surface vibrations and sound radiation.

There are several types of bending actuators. Thunder (Thin Layer Unimorph Ferroelectric Driver and Sensor) unimorph actuator is made of a piezoelectric (PZT) plate bonded to a stainless steel plate (Hellbaum 1997).

Figure 2.1. Thunder unimorph actuator.

On the above photograph, one can observe that the thunder unimorph actuator is curved at rest. This phenomenon is due to the different thermal expansion coefficients (CTE) of both materials. Indeed, the piezoelectric plate is bonded to the steel plate at a high temperature (320 °C or 608 °F). Hence, upon cooling, the steel plate (which has a higher CTE than PZT) will retract more than the piezoelectric plate, causing the actuator to curve. A thin aluminum foil covers the PZT to keep the entire top surface connected in case of cracking.

Another type of bending actuator is the Rainbow (Reduced And Internally Biased Oxide Wafers) actuator (Haertling 1994). The principle consists in placing a PZT disk on a graphite piece and to heat the system up to 975 °C (1787 °F) so that the carbon can diffuse in the bottom of the PZT. This way, one side of the piezoelectric disk becomes inactive whereas the other side remains active. By applying an electric field to the disk, one can observe the same bending phenomenon as with the Thunder actuator.

Yoon et al. (Yoon 2001, Yoon 2002, Yoon 2003) used composite materials to manufacture Lightweight Piezo-Composite Curved Actuators (LIPCA). Lynch et al. (Hopkinson 2003) proposed a duel function bending actuator called Gradient Enhanced piezoelectric Actuators (GEPAC). The actuators are ultra thin piezoelectric plates embedded between two or more composite layers of fiber reinforced polymer composite materials. GEPACs exhibit a natural curvature (similar to the Thunder uniform actuator) because the composite's coefficient of expansion depends on the direction of the fibers (anisotropic properties of a composite). This asymmetric geometry creates residual stresses in the PZT which entail enhanced flexural strains in the actuator. Compared to steel uniform actuators, GEPACs are lighter and offer a possibly better integration in "smart skins" for the aeronautical industry. In addition, there is a built in NDE system.

CHAPTER III

SEGMENTED GEPAC ACTUATORS

3.1 Principle

To generate low frequency actuation and high frequency ultrasonic waves, the PZT ceramic of a GEPAC actuator needs separate electrodes. Figure 3.1 indicates how ultrasound can be launched from one side of the ceramic (A) to the other side (B), while undergoing low frequency actuation.

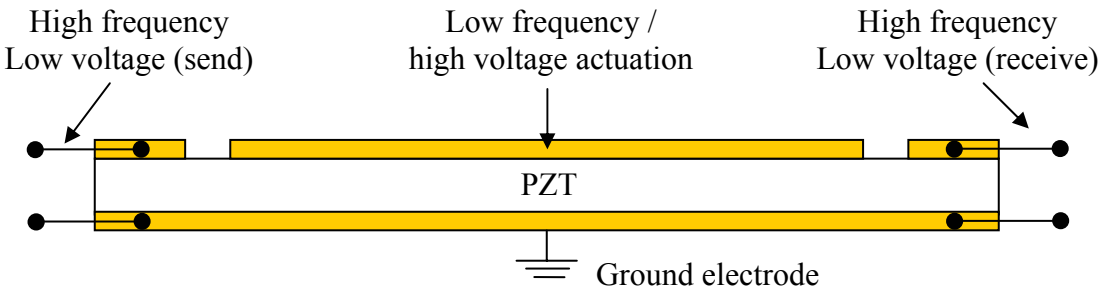

Figure 3.1. Sketch of a segmented PZT ceramic

In the work reported in this thesis, the low frequency range is from DC – 150 Hz while the high frequency is around 1 MHz. There is therefore no overlap of frequency range so that, at least in principle, it should be feasible to excite simultaneaoulsy both low frequencies and ultrasonic frequencies.

3.2 Piezoelectric Material

The piezoelectric crystal used is a PZT TRS-610 ($Pb(Ti,Zr)O_3$), manufactured by TRS Technologies, Inc (TRS Technologies website). It belongs to the soft PZT category, characterized by high dielectric strain and high hysteresis. The main properties for the TRS-610 are the Young's modulus, E_{11} = 64.5 GPa and the piezoelectric strain coefficient, d_{33} = 790 pC/N (TRS 2003), which relates the change in thickness to the applied voltage. The dimensions of the PZT are 71 × 21 × 0.25 mm (2.8 × 0.83 × 0.001 inch). In all the results presented in this thesis, the ultrasonic wavelength is much larger than the thickness of the PZT. The piezoelectric has small weight and thickness, which allows low frequency actuation up to 300 Hz.

3.3 Composite Material

In GEPACs actuators, The PZT ceramic is "sandwiched" between prepreg composite materials. Prepregs are thin sheets of composite fibers that have been impregnated with predetermined amounts of an even distribution of epoxy matrix (Mallick 1993). Prepregs can be found in three different categories: woven fiber, continuous unidirectional fibers and chopped fiber mats. The quantity of epoxy in Prepregs is calculated so that when composite is laid up, no additional resin needs to be added. There are different types of fibers, of which the most common are glass, carbon and epoxy. Given that carbon fibers are good electric conductors, they would create a short circuit between the top and bottom electrodes of the PZT. Instead, Kevlar fibers DA-4518K, manufactured by Adhesive Prepregs for Composite Manufacturers (APCM), have been used for the GEPACs' construction. Kevlar fibers are good insulators. They

also have a coefficient of thermal expansion (CTE) that depends on fiber orientation. Indeed, the CTE in the longitudinal direction (parallel to the fibers) is 3.6×10^{-6} K^{-1}, and CTE in the transversal direction (perpendicular to the fibers) is 54×10^{-6} K^{-1}. Hence, by using different orientations for the upper and lower composite layers, one can obtain a high natural curvature of the actuator and compressive residual stress in the PZT (which enhances the actuator performance and reliability). According to prepregs' manufacturer, composites have to be cured between 121 and 177 °C (250 and 350 °F). For this project, actuators are cured in the upper range (177 °C) which allows a higher curvature after cooling.

3.4 Actuator Design

As explained in the previous section, DA4518K prepregs and PZT TRS-610 are used for the construction of GEPACs. According to David P. Hopkinson's thesis (Hopkinson 2003), a good configuration is to use two composite layers below the PZT and three composite layers above the PZT.

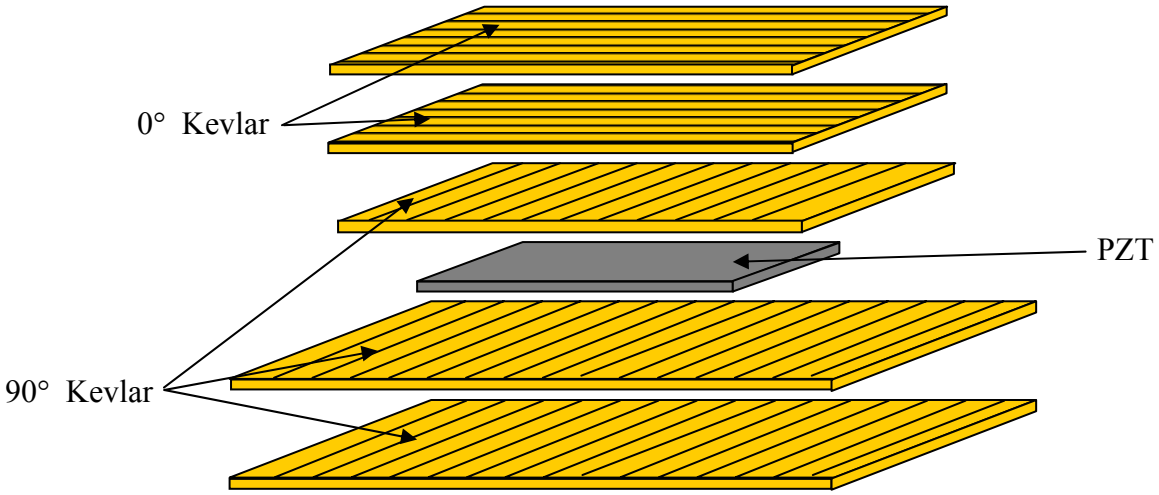

Figure 3.2. Composition of GEPAC

Both unidirectional Kevlar layers below the PZT have a transversal orientation (90°). The layer just above the PZT has also the same fiber orientation (90°) whereas both top layers have a longitudinal orientation (0°).

3.5 Fabrication of a segmented actuator

The first step is to cut out the composite layers. When the composite is at 4 – 10 °C, it is delicate to handle because it can separate easily along fiber direction. The best way is to let it rest at room temperature for a while so that the epoxy resinsoftens and keeps the Prepregs integrity. Once cut, the samples are stored at 4 °C – 10 °C.

The second step consists in segmenting the electrodes on the piezoelectric. PZT has a copper layer electrode on both sides. The upper electrode must be divided in three electrodes. The PZT is placed on a flat aluminum plate. The areas to be removed are fully exposed whereas the future electrodes are protected by an adhesive tape. This operation is

delicate because one has to remove a copper layer of severals microns on a PZT support which is highly brittle and has a thickness of 0.25 mm (0.001 inch). The first approach (Bechet 2003) is to use a sand blaster device. This technique works for a 0.5 mm-thick PZT, but it does not work well on thinner samples, even when the sand blaster is set at minimum power. When operation is over, the copper layer is perfectly removed, but one can observe cracks on the PZT.

The second approach is to use sandpaper of small granulation. The PZT needs to be placed on a perfectly flat surface. If not, the least stress will cause a crack in the piezoelectric ceramic. When fixing the PZT, it is important not to stick the adhesive tape directly on the PZT, because due to its small thickness, it would be impossible to remove the tape without breaking the ceramic. Instead, a thin transparent plastic sheet is used as indicated in Figure 3.3. The resulting segmented electrodes are shown in Figure 3.4.

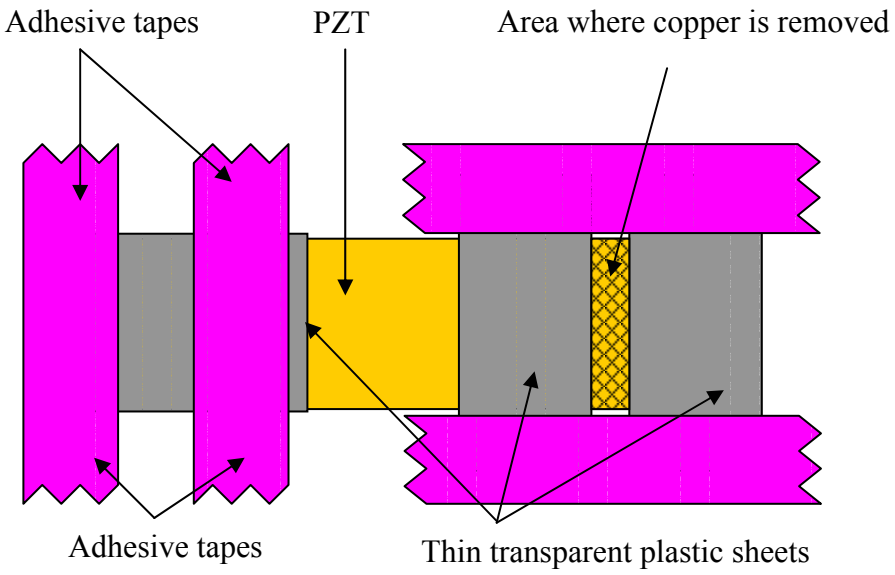

Figure 3.3. Assembly to segment the electrode

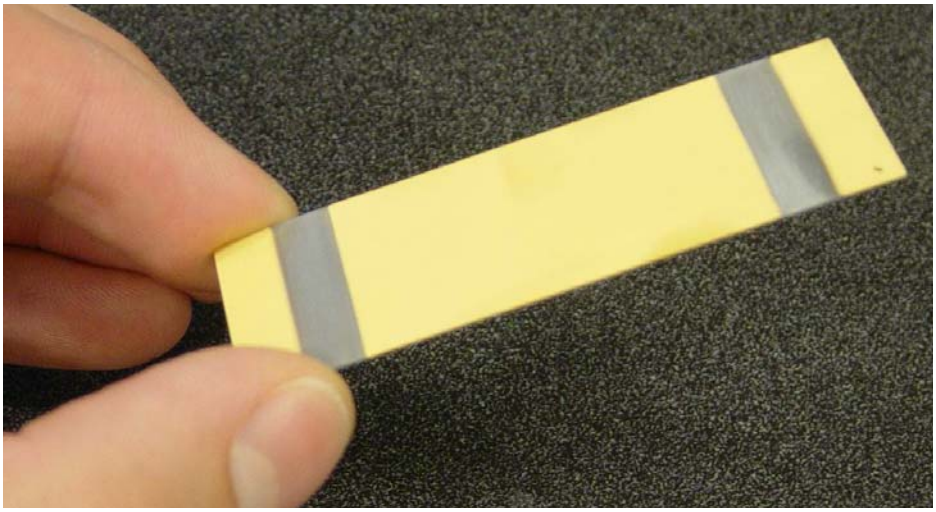

Figure 3.4. Segmented Actuators

Curing is done in an autoclave. A vacuum is applied to release air bubbles that might otherwise remain trapped within or between the layers thus causing debonding. Finally a pressure (30 psi) is applied to remove the excess resin from the GEPAC actuator.

Figure 3.5. Mold for the curing of GEPAC

An aluminum plate (12 × 12 inches) is used as a “mold” (see Figure 3.5). Before putting actuators on it, the mold is painted with a release agent in order to prevent the samples from bonding to it. The actuators are then placed on the aluminum plate and covered with a release film that prevents the top of specimens from bonding to the flexible bag covering the plate. A bleeder cloth is installed on the release film to absord the excess resin flowing out from samples. A sealant tape is placed around the perimeter of the aluminum plate and a cellophane vacuum bag covers the whole assembly. The round part on Figure 3.5 is a connector to pull a vacuum in the mold. It is placed between the bleeder cloth and the cellophane vaccum bag.

Figure 3.6. Autoclave

The mold is placed in an autoclave as shown in Figure 3.6. The cure cycle is as follows: the temperature increases at the beginning as rapidly as possible in order to prevent the resin from partially curing. When it reaches 177 °C (350 °F), a period of 5 minutes is observed in order for the mold and actuators to reach entirely the required temperature (177 °C). The assembly stays one hour at this temperature. Then, actuators cool down during two hours in the autoclave. The temperature and the pressure decrease slowly until they reach ambiant values.

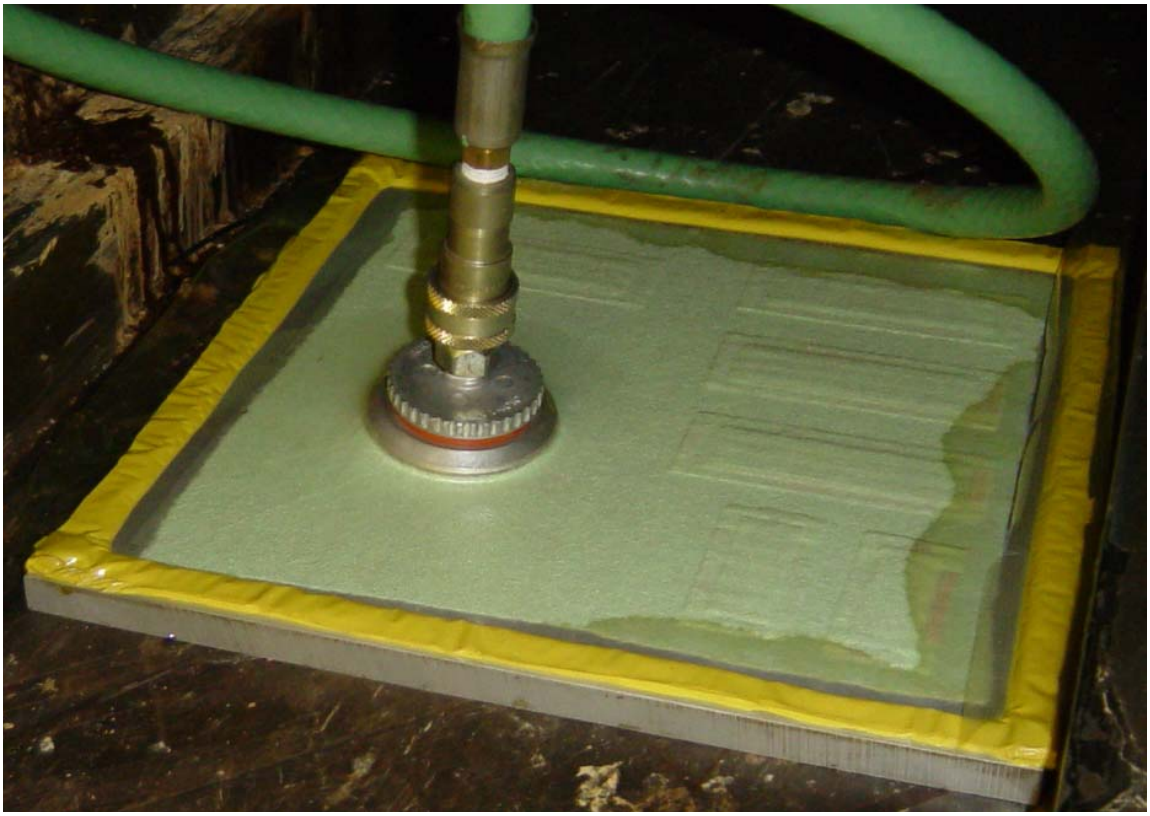

Figure 3.7. Mold in the autoclave right after the cure cycle

Figure 3.7 shows the mold after curing cycle in the autoclave. One can see the shape of the actuators under the cellophane bag, because of vacuum. On three sides of the mold, there is an excess of resin that has flowed out of the actuators and has been absorbed by the bleeder cloth. The cellophane bag, the bleeder cloth and the release film are easily removed. The actuators stick to the aluminum plate but they can be removed with a razor blade. Once removed, they reveal the characteristic curved shape of GEPAC actuators.

Figure 3.8. GEPAC (after curing)

Electrical wires are soldered to the copper foil for ultrasonic non destructive evaluation (NDE) and actuation (see Figure 3.9).

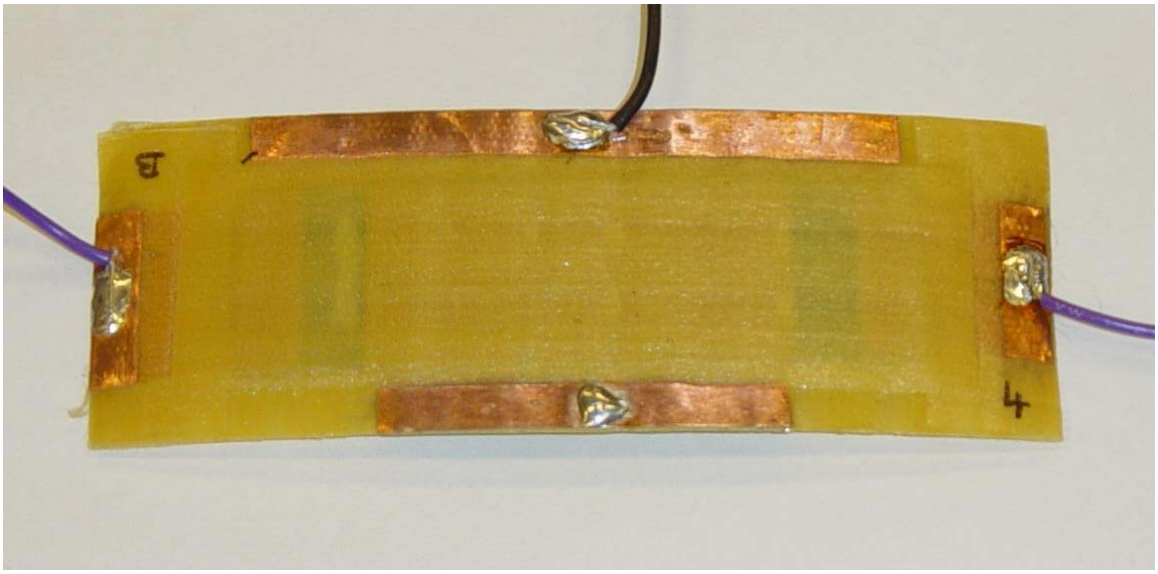

Figure 3.9. Soldered wires on GEPAC actuator

CHAPTER IV

ACTUATION AND ULTRASONIC NDE ON GEPAC ACTUATORS

4.1 Non Destructive Evaluation (NDE) of a GEPAC actuator

4.1.1 NDE of a traction free GEPAC

The first experiment consists in sending an ultrasonic pulse in a GEPAC actuator at rest. In this case, no high voltage low frequency is applied and only two electrodes are used, as shown in Figure 4.1. The wave generator (HP 33120A) sends one cycle of a sinusoidal pulse of 1 MHz with amplitude 5 V between the bottom and one of the top electrodes. The other top electrode is connected to an oscilloscope (TDS 420) where the received signal is displayed.

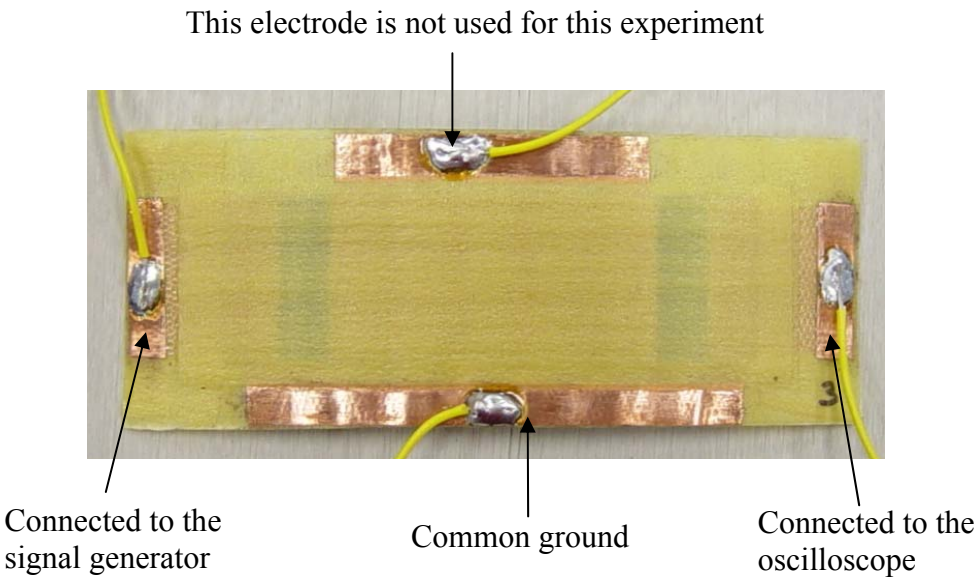

Figure 4.1. Segmented GEPAC

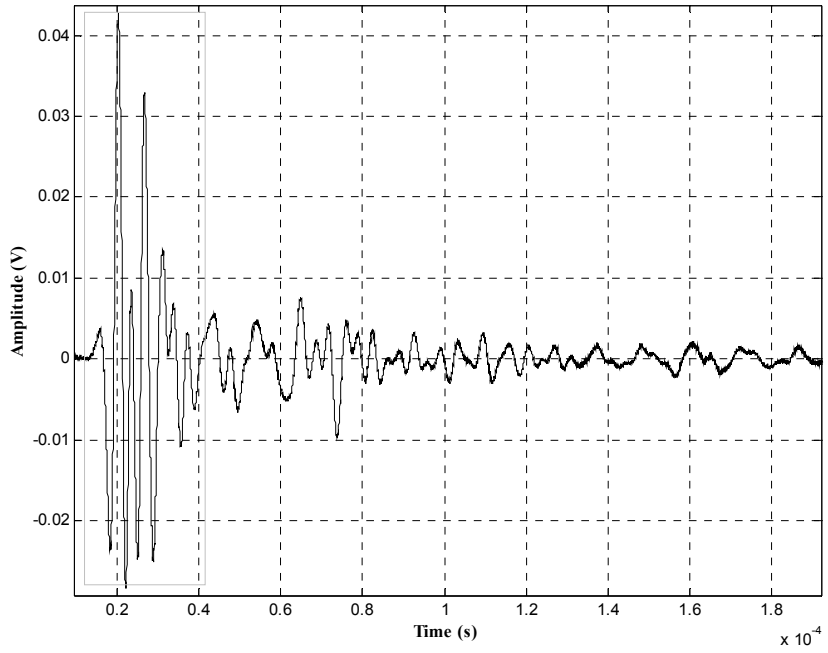

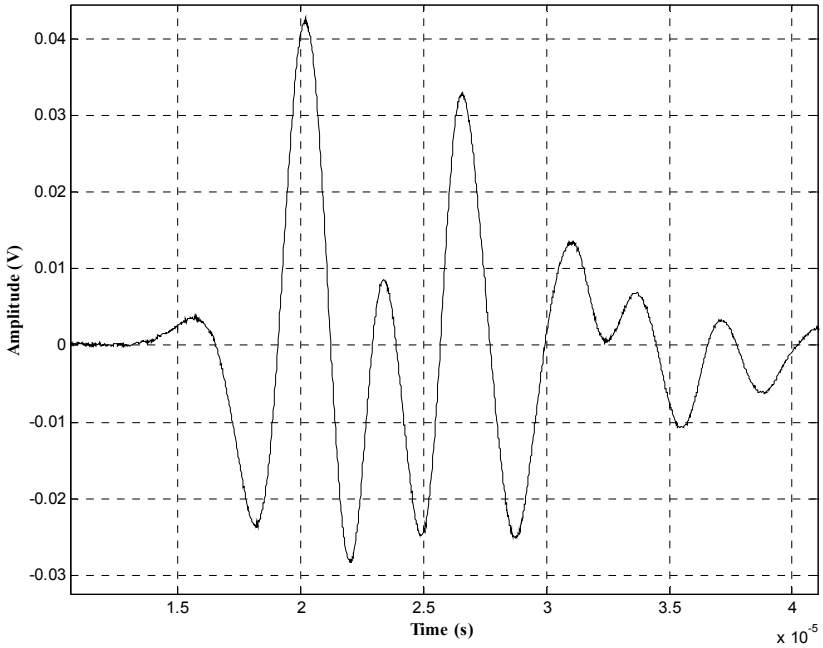

Figure 4.2. Ultrasonic Signal for a healthy GEPAC

The received ultrasonic waveform is shown in Figure 4.2. It takes about 13 µs for the wave to cover the distance between both electrodes. The length of the PZT is 71 mm. The width of electrodes is 6.5 mm. The separating distance between both electrodes is 58 mm. Hence, the quasilongitudinal wave travels at 4460 $m.s^{-1}$ in the GEPAC. This velocity is quite difficult to predict because of the propagation in layered anisotropic plates (Chimenti 1997). The complexity of the received signal is due to the complexity of the medium through which it travels. The medium is a series of layered viscoelastic fiber-epoxy composites glued to a thin piezoelectric ceramic. Propagation of ultrasound in layered composite plates is quite difficult to model (Nayfeh 1995).

Nevertheless, the received signal is extremely repeatable, and variations in the signal waveform would be indicative of a change in the medium.

4.1.2 NDE of a GEPAC broken before curing

In some cases, the thin PZT ceramics were accidentally cracked during the assembly of the GEPAC actuator. Ultrasonic monitoring of these actuators was performed before and after curing.

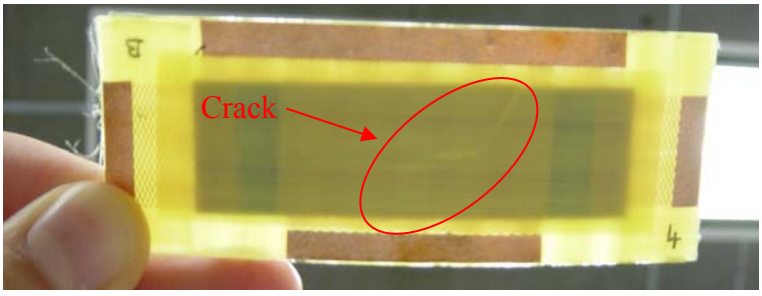

Figure 4.3. Broken PZT in a segmented GEPAC

(a crack is barely visible inside the oval)

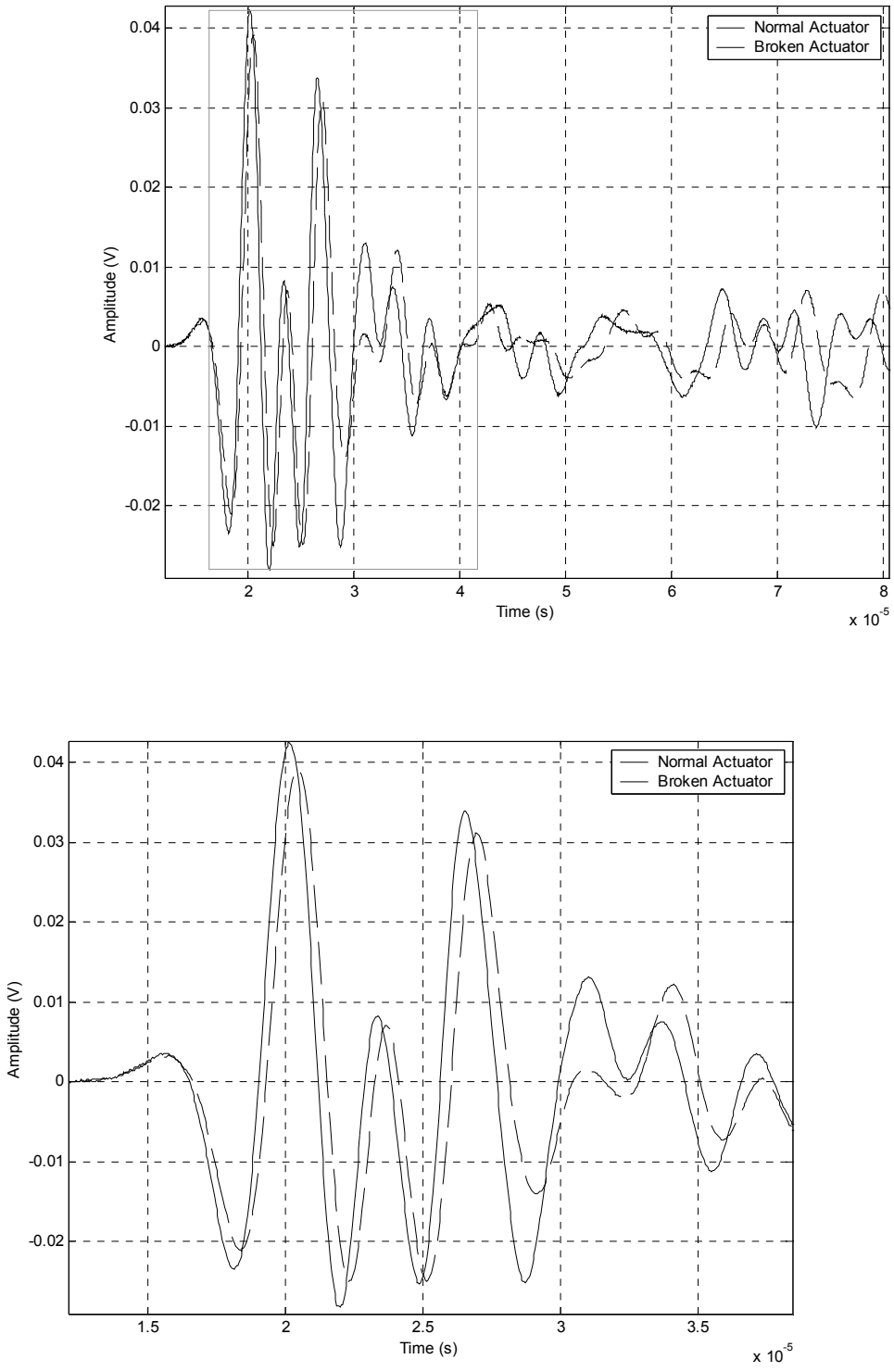

Figure 4.4. Ultrasonic signal for a GEPAC broken before curing

Figure 4.4. shows the ultrasonic response of a normal and a broken actuator, for the case of an actuator that was damaged before curing. A crack is barely visible in the oval in Figure 4.3. There is little difference between the healthy and the damaged actuator. This phenomenon is most likely due to the epoxy resin that has filled up the space between both parts of the piezoelectric ceramic during curing. Hence, the broken PZT performs as one-piece PZT. The amplitude of the response corresponding to the broken GEPAC is slightly smaller than the one of a healthy actuator. This phenomenon of amplitude reduction is consistent with intuitive expectations, given that now, the wave has to go across an interface between the PZT and the resin. A small part of energy is lost at this interface. Another interesting point is the gap between both curves, always for the first arrivals. The crack produces a delay of about 0.35 μs.

4.1.3 NDE of a GEPAC broken after curing

The behavior of a GEPAC that has been damaged *after* its manufacturing is studied in this part. The GEPAC actuator was bent beyond its mechanical limits on purpose until it cracked. Figure 4.5 shows that debonding defects / cracks have been created between the PZT and the upper composite layer.

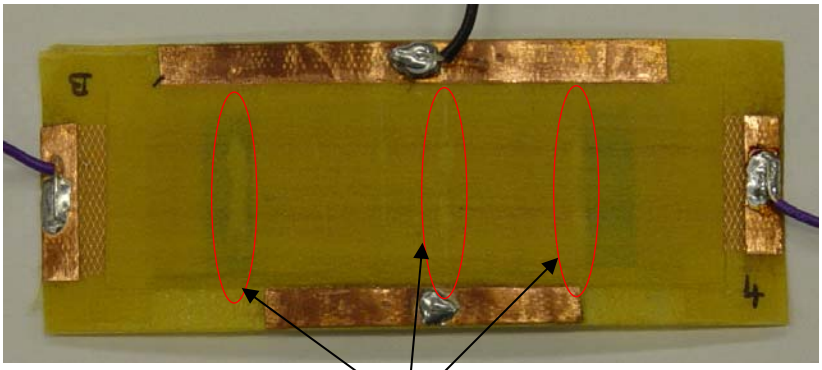

Figure 4.5. Broken segmented GEPAC after curing

The ultrasonic response is shown on Figure 4.6 and compared to the response before breaking the actuator. In this case, the ultrasonic signals are very different for a healthy or a damaged actuator.

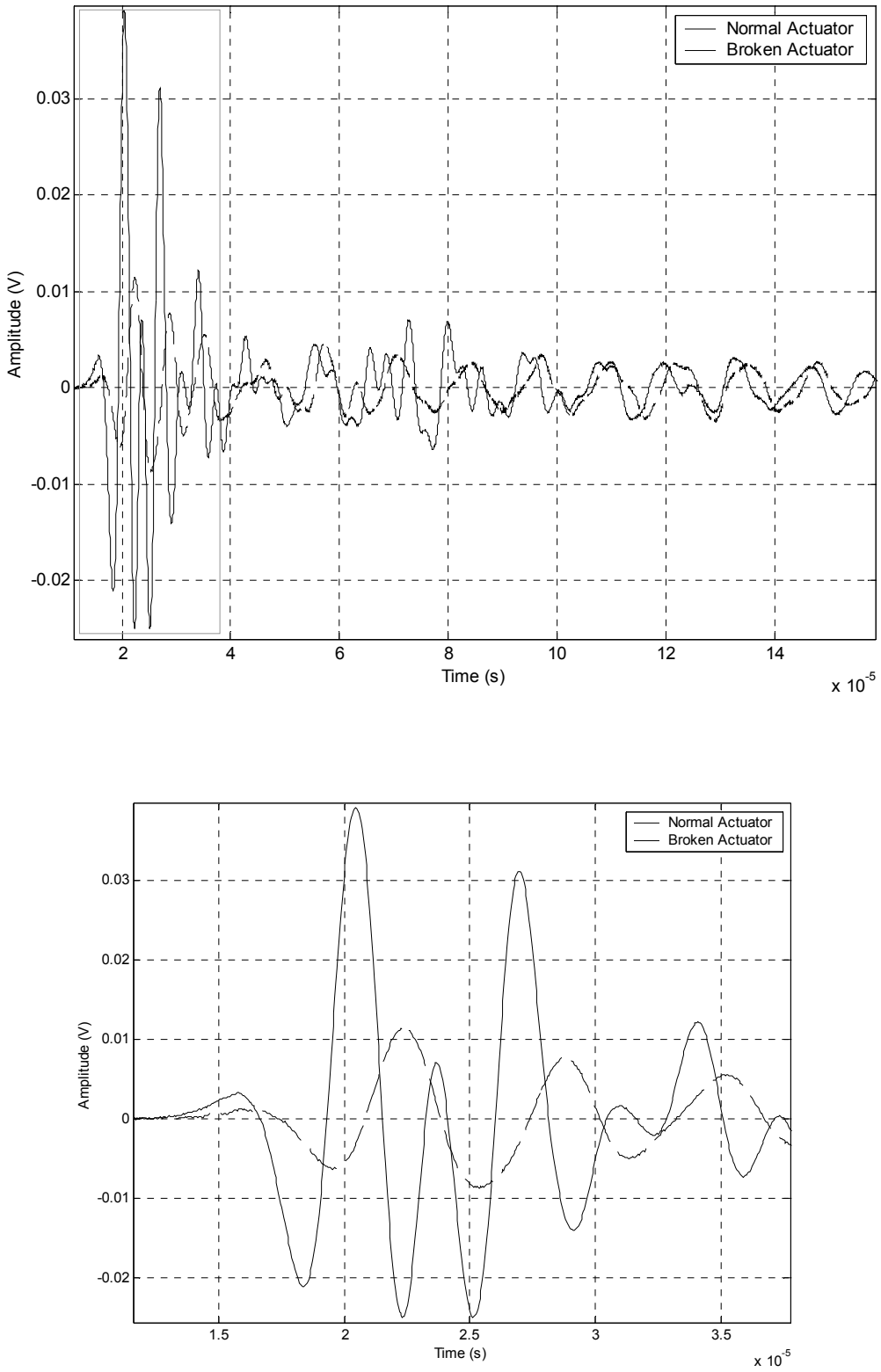

Figure 4.6. Ultrasonic signal for a GEPAC broken after curing

In summary, defects in GEPACs are not always easily detectable with ultrasonic NDE. If the defect is present in the PZT before the curing cycle, it will be certainly filled up by epoxy resin in the oven during the curing process. In this case, it may be difficult to detect the defect with ultrasound but the low frequency actuator response would clearly reveal the defective ntaure of the actuator. If a defect occurs during the use of GEPAC, it is possible to detect it with ultrasound because the signal is significantly modified.

4.1.4 Comparison between different healthy GEPACs

In this section, the response of different GEPACs having the same characteristics is studied to characterize sample-to-sample variability of the ultrasonic signature. Figure 4.7 exhibits these actuators. They have been manufactured at the same time and cured in the same mold.

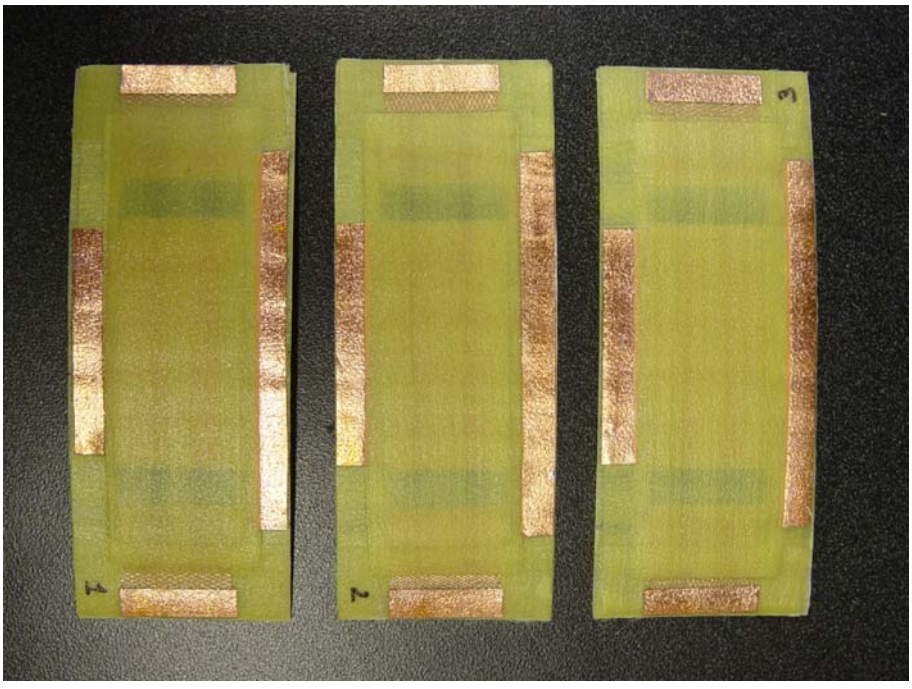

Figure 4.7. Three identical healthy GEPACs

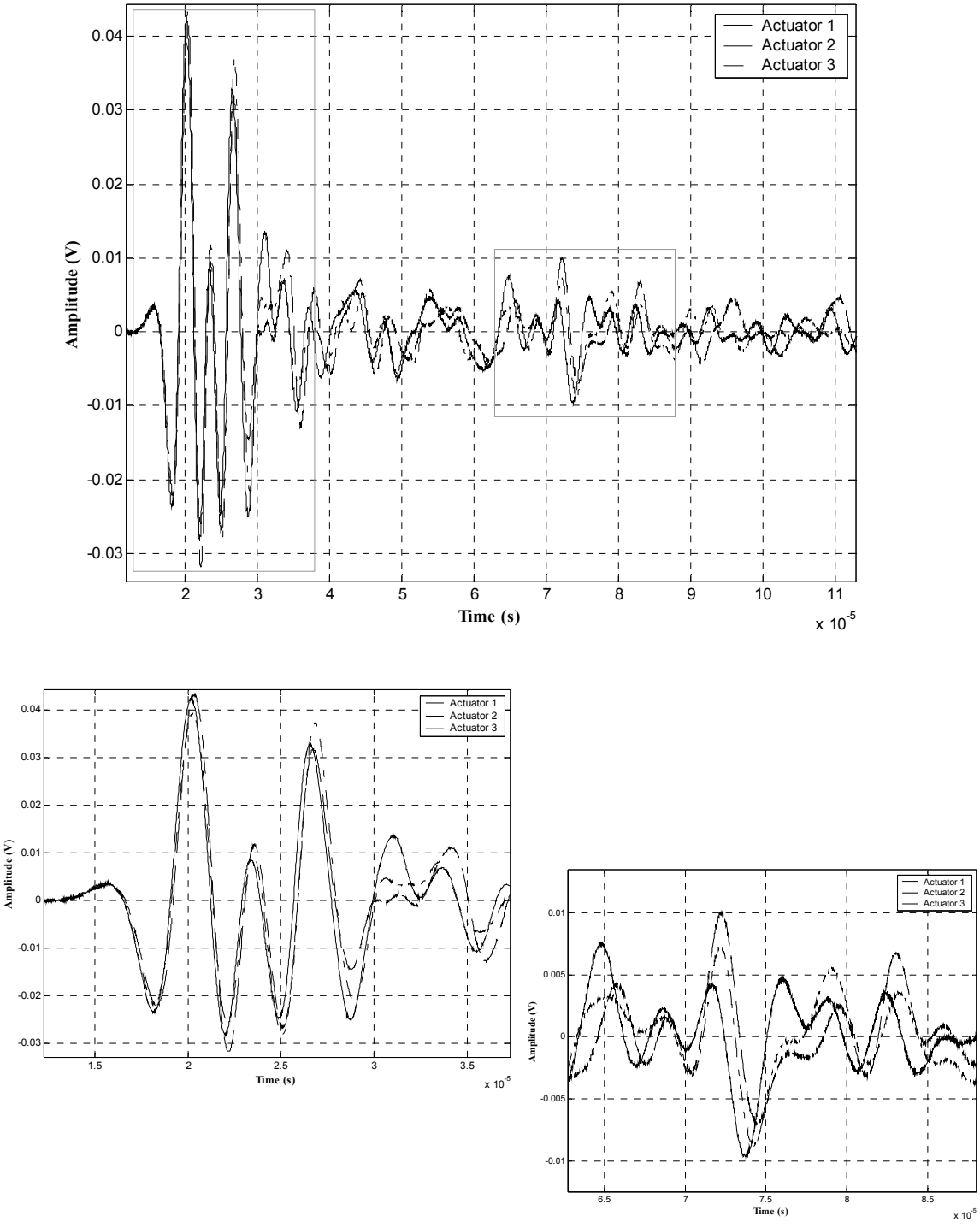

Figure 4.8. Comparison of ultrasonic response between three healthy actuators

(a) up to 110 μs; (b) up to 37 μs; (c) 63 – 88 μs

The experiment is performed under the same conditions as previously. Actuators are traction free. As shown in Figure 4.8, the first arrivals ($t < 30$ μs) are almost identical. The rms value of the signal ($0 < t < 30$ μs) was calculated for the 3 actuators. It represents the energy of the received signal integrated over all frequencies. The relative error in rms is 2.25 % and it represents the sample-to-sample variability of the signal.

Table 4.1. RMS values of the ultrasonic signal corresponding to different actuators

	RMS value for $0 < t < 30$ μs (mV_{RMS})	% variability with respect to actuator 1
Actuator 1	14.43	0
Actuator 2	14.11	2.25
Actuator 3	14.75	2.20

Later arrivals show much more relative variability. This is not surprising because, for late arrivals, each signal represents a very large number of reflections throughout the sample (this superposition of reflections is somewhat analogous to reveberation of sound in a room). Slight differences between the actuators (such as dimensions, assembly, etc...) are therefore accentuated for late arrivals since the signal has travelled through the length of the actuators several times.

4.2 Low frequency actuation and ultrasonic NDE

The main function of a GEPAC is to operate as a smart skin, in bending mode, at DC or low frequencies. The aim of this section is to demonstrate that actuation does not interfere with the operation of ultrasonic NDE so that continuous monitoring of structural integrity can be achieved during normal operation of the actuator.

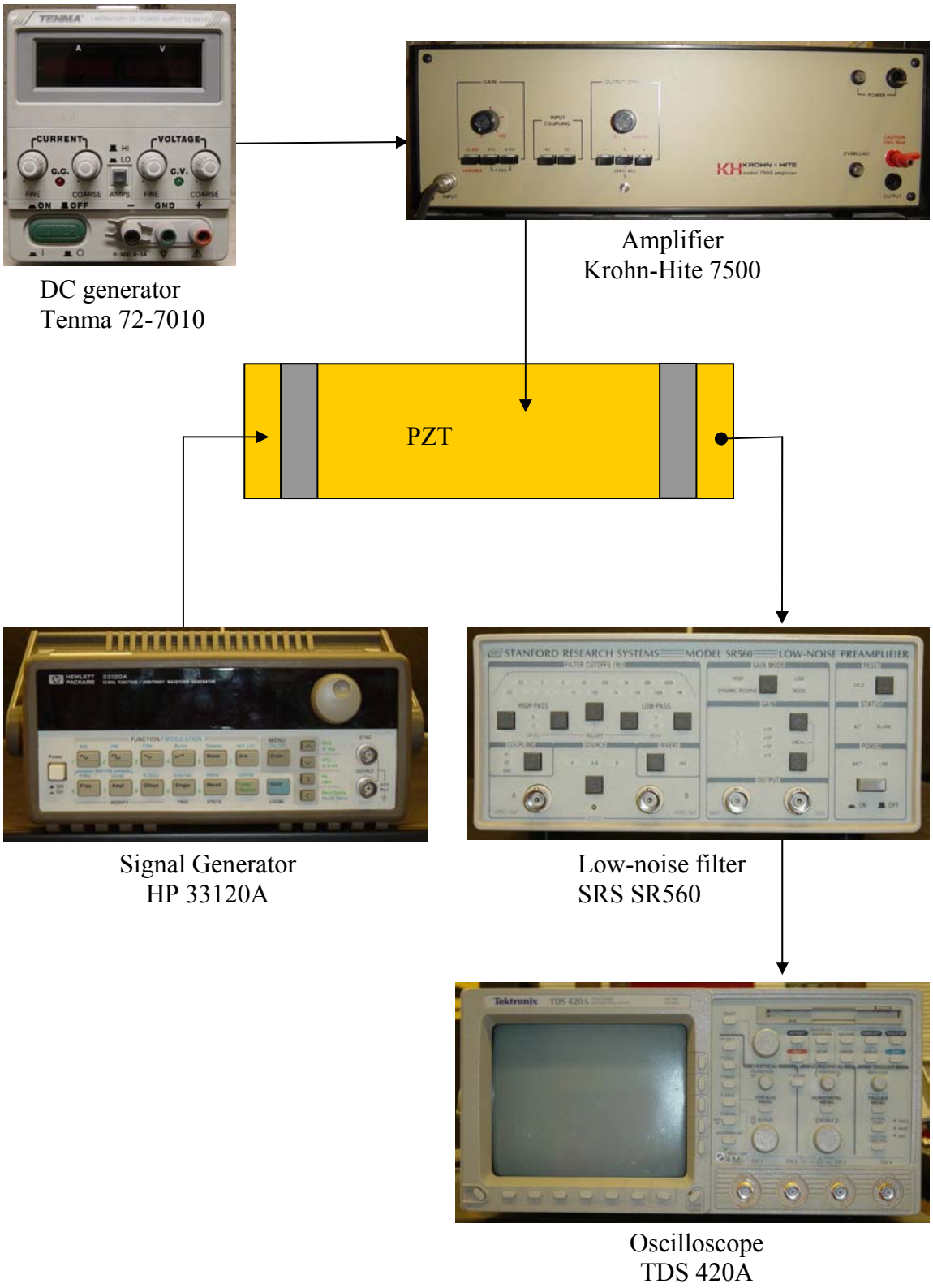

Figure 4.9. Assembly to test ultrasonic NDE during actuation

4.2.1 DC actuation

The first experiment is to apply a large DC bias voltage to the actuator, to see if it affects the ultrasonic waveform in the actuator. Figure 4.9 gives a sketch of the experiment. A DC generator (Tenma 72-7010) sends a continuous signal adjustable between 0 to 170 volts to a Krohn-Hite amplifier (KH 7500) with a ×10 gain. The DC voltage is applied between the top central electrode and the bottom electrode (ground). For the ultrasonic NDE, single period of a sinusoidal pulse of 1 MHz with 5 V of amplitude is generated by the HP 33120A and applied to one side of the actuator. The utrasonic pulse is received on the other side. A preamplifier and a low pass filter (SRS SR560) are used. The signal is displayed on a digital oscilloscope (TDS 420A).

Figure 4.10 shows the received ultrasonic signal when the DC voltage was 0, 100 and 170 V respectively. As expected, the ultrasonic signals are almost identical regardless of the applied DC voltage. It is interesting to note that even very late arrivals (see Figure 4.11) are unaffected by the DC voltage. The late arrivals are not noise, as one might think. They represent the characteristic signature (reverberation) of ultrasound in the actuator. This experiment shows that it seems possible to monitor the integrity of GEPACs during actuation.

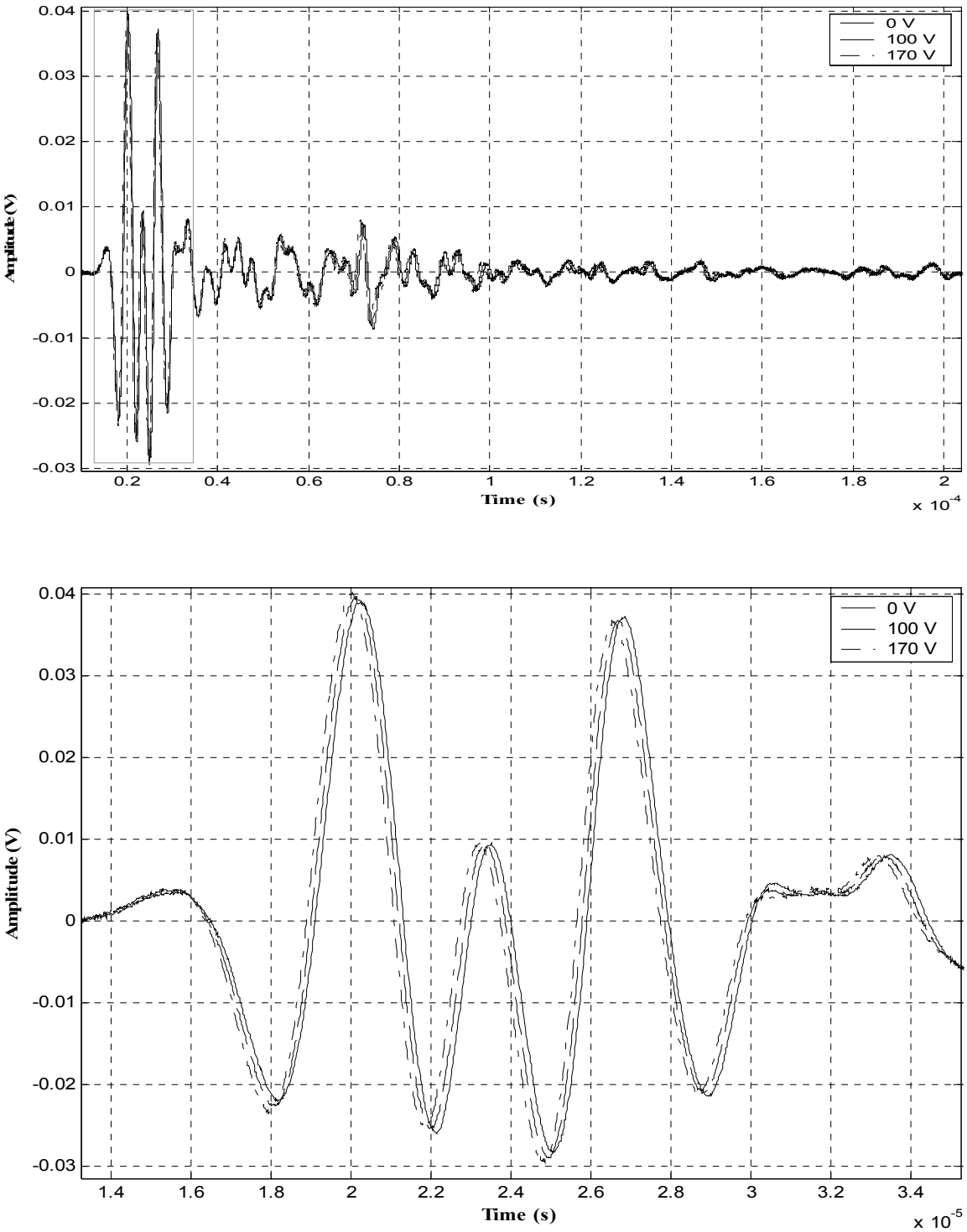

Figure 4.10. Ultrasonic signals in the actuator for different values of high voltage between the central top and bottom electrodes of the PZT

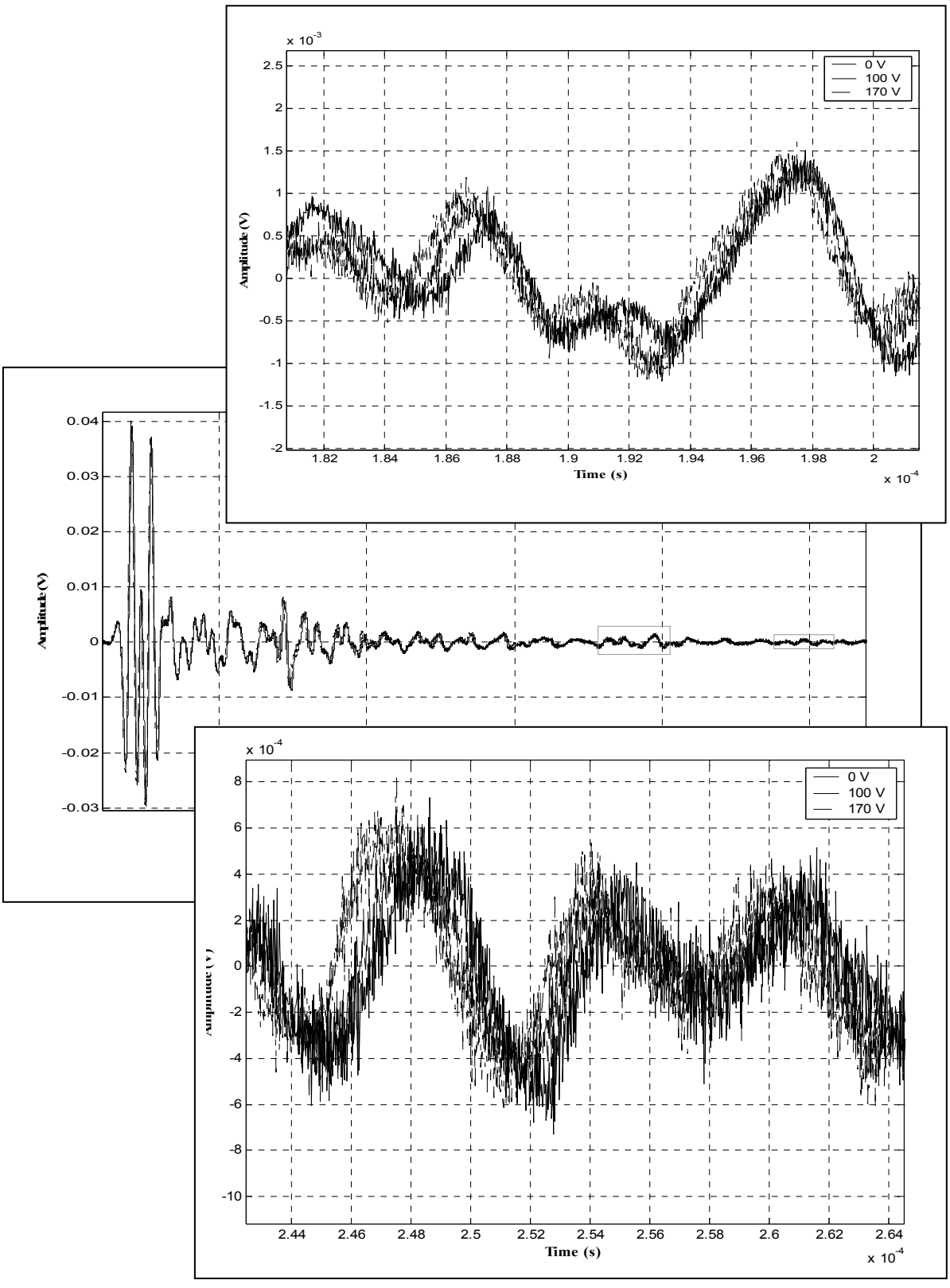

Figure 4.11. Insight on the late arrivals of the response signals

4.2.2 Low frequency mechanical flexion

A high voltage applied to the actuator has the effect of bending it. It would be interesting to know if the mechanical bending of the actuator affects the ultrasonic signal. If it does not, one can use mechanically induced bending, instead of electrically induced bending to test the samples, thus avoiding electical noise due to the high voltage amplifier. Fatigue testing of the actuators (see chapter V) could be done with mechanical actuation.

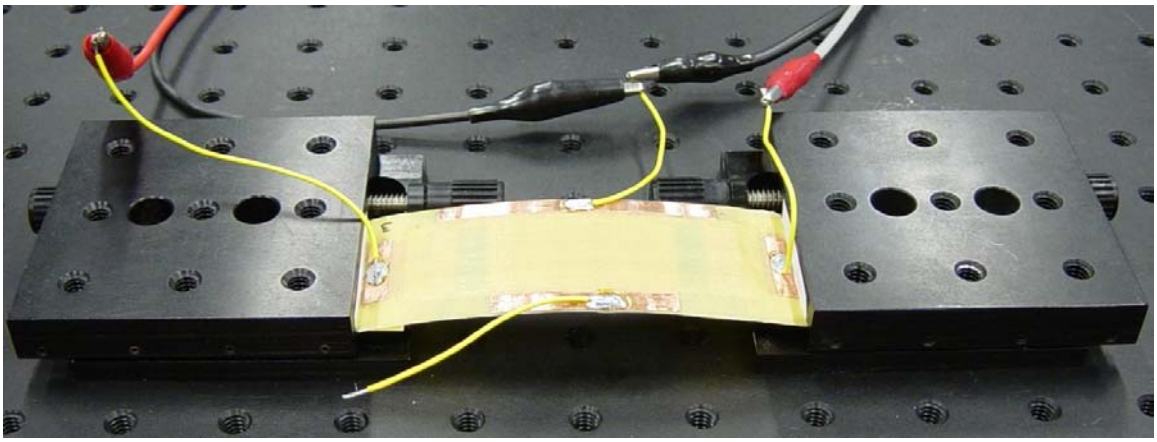

Figure 4.12. Picture of the assembly for mechanical bending of the actuator

Two jaws are used to bend the actuator. One is fixed and the other is placed on a translation stage. The GEPAC is placed between both jaws. Table 4.2 gives the projected length, d, of the actuator on the horizontal axis, the dome height, f, and the resulting radius of curvature, ρ, for four positions of the translating jaw.

Table 4.2. Values of height and lenght of the actuator for each measure

Length d	Height f	Radius of curvature ρ
100.01 mm	17.46 mm	187.77 mm
99.61 mm	18.25 mm	167.84 mm
99.22 mm	19.05 mm	151.48 mm
98.82 mm	19.84 mm	138.11 mm

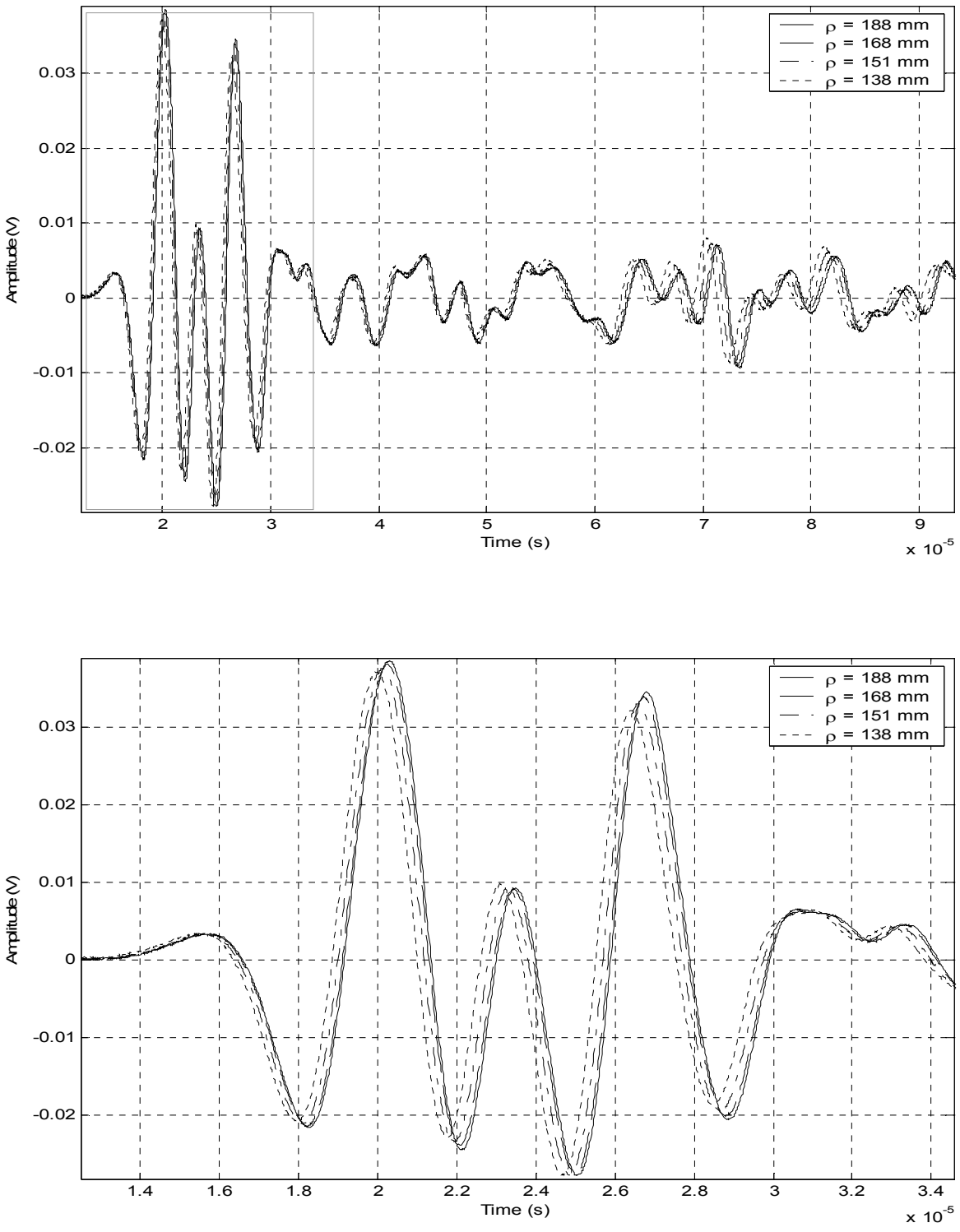

Figure 4.13. Ultrasonic signals for different radius of curvature ρ of the actuator

The ultrasonic signals recorded for these four radii of curvature are chown in Figure 4.13. Mechanical flexion has the same effect as actuation with high voltage. When the actuator is bent, there is a small lag between ultrasonic signals but the ultrasonic waveform is almost identical regardless of the applied mechanical force, as shown in Figure 4.14.

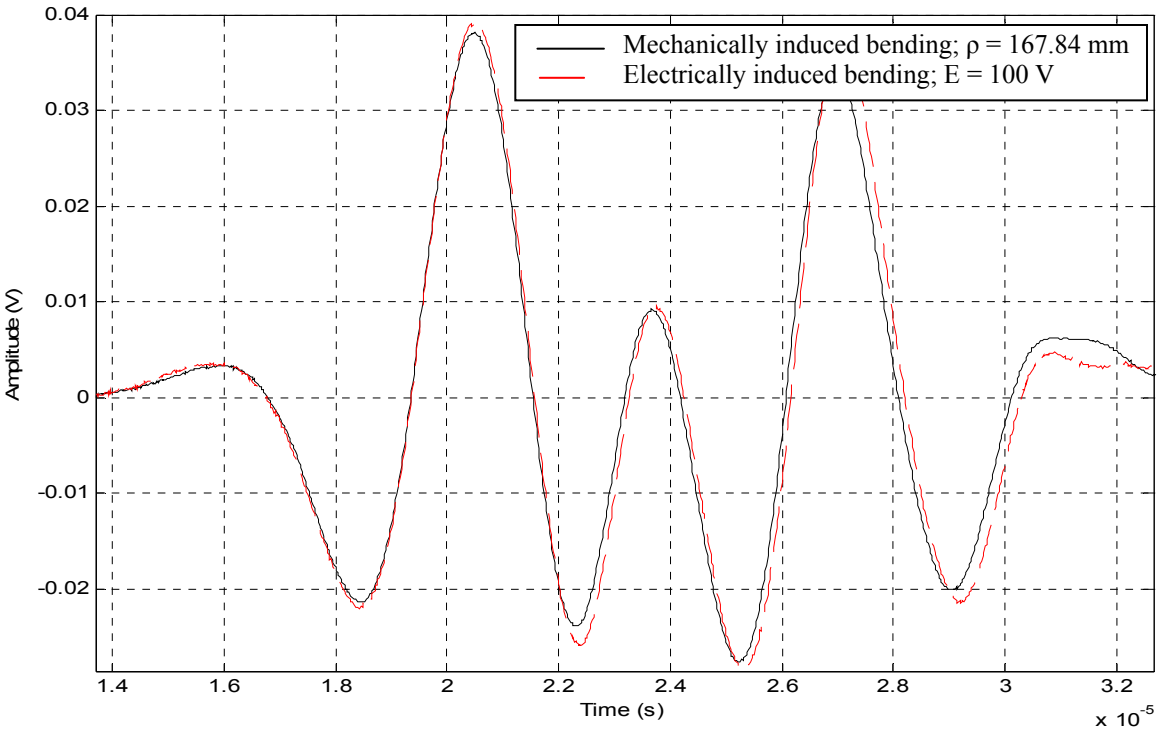

Figure 4.14. Early arrivals of the ultrasonic signal

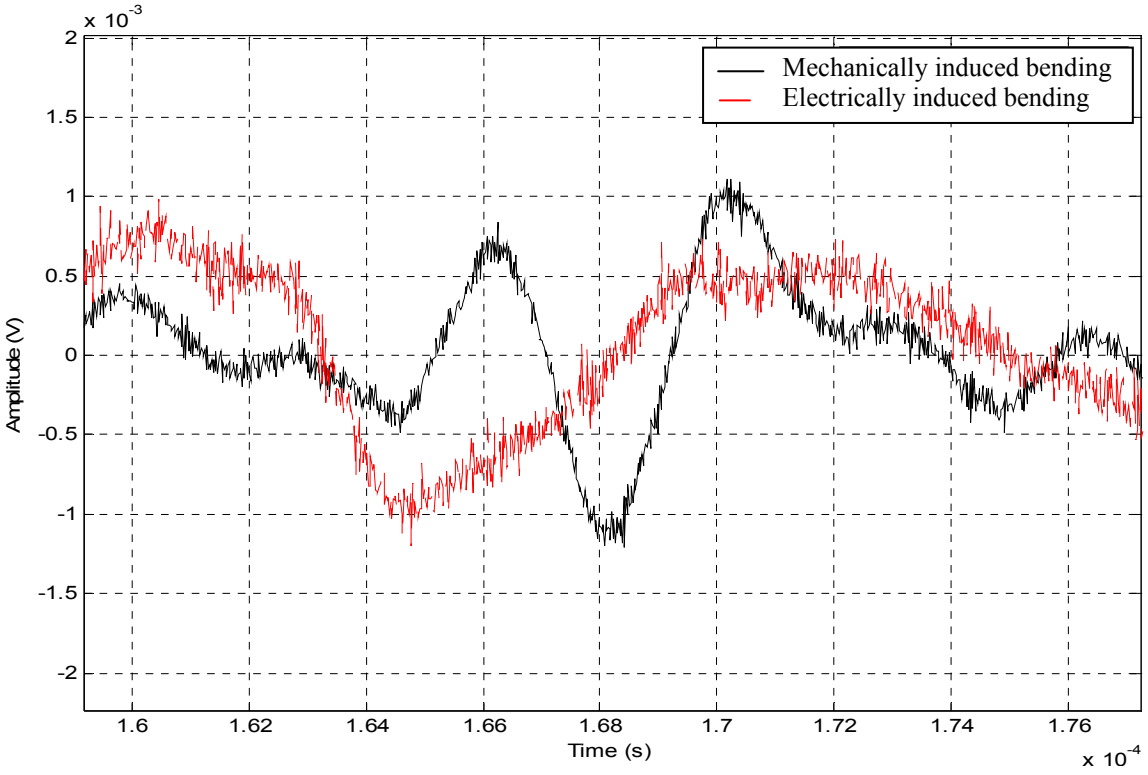

Figure 4.15. Phenomenon of noise on late arrivals

Figure 3.15 shows the late arrivals of the ultrasonic waves. The differences between the ultrasonic signals shown in Figure 3.15 is attributed to the difference in boundary conditions between the mechanical and electrical actuation. Note also that the ultrasonic signal (late arrivals) is more noisy with the electrical actuation than with the mechanical acutation.

4.3 Simultaneous low frequency actuation and ultrasonic NDE

Now, the interest is to use low frequency actuation and ultrasonic NDE simultaneously. The same devices and set up are used to achieve this. The low frequency actuation uses a signal with 150 V of amplitude and ranges from 0 to 150 Hz. The ultrasonic signal is one cycle of a pulse at 1 MHz with an amplitude of 5 V. The resulting

signal correponding to different frequencies of actuation are plotted on Figure 4.16. Furthermore, the rms value for each signal are shown in table 4.3.

Table 4.3. RMS values of the ultrasonic signal corresponding to different frequencies of actuation

Frequency of actuation	RMS value for 0 < t < 30 μs (mV_{RMS})	% variability with respect to "No actuation"
No actuation	10.12	0
50 Hz	10.06	0.63
100 Hz	10.01	1.17
150 Hz	9.87	2.54

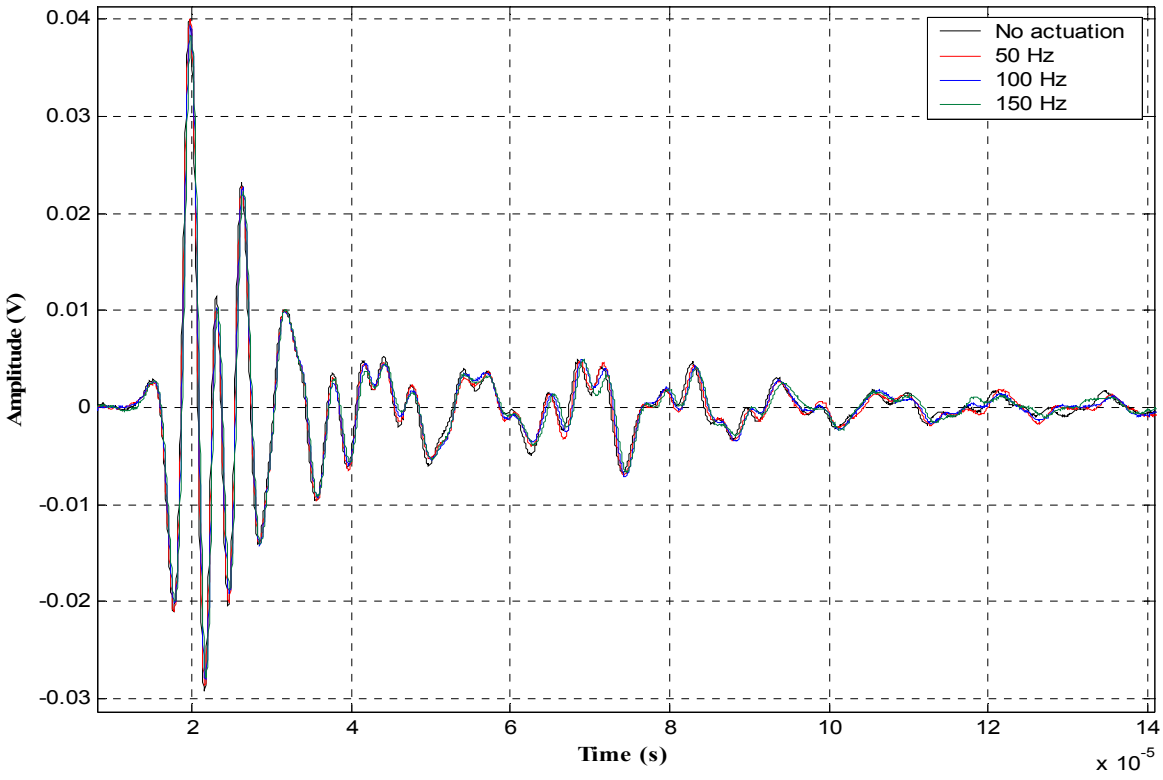

Figure 4.16. Ultrasonic response of the actuator during actuation at different frequencies

The ultrasonic response is not really affected by the low frequency actuation. By computing the rms value ($0 < t < 30$ μs) for the different signals, one can see that the difference increases with the frequency of actuation, but the variability of the value reaches only 2.54 % at 150 Hz. The repeatability is good and suggest the possibility of monitoring the integrity of the actuator during low frequency actuation.

4.4 Concluding remarks

In this chapter, it was established that

- Ultrasonic signals in a GEPAC actuator are extremely repeatable, even for very late arrivals.
- Ultrasonic signals between similar GEPAC actuators are almost identical for early arrivals. Late arrivals differ because of intrinsic differences in the manufacture of individual acutators.
- Ultrasonic signals can be used to detect cracks in the actuator (PZT ceramic) if the crack occurs after curing. If it occurs during manufacturing, resin fills up the crack and ultrasonic signals are not significantly affected by the presence of resin-filled cracks.
- Ultrasonic signals are not significantly affected by the electrical actuation of the GEPAC (DC or low frequency), so that NDE monitoring can be performed during normal actuator operations.
- Mechanically induced bending of the actuator has the same effect as electically induced bending. The fatigue tests can be performed with either electrical or mechanical actuation.

- It is possible to monitor the integrity of an actuator during low frequency actuation up to 150 Hz.

CHAPTER V

DELAMINATION AND FATIGUE TESTING ON GEPACS ACTUATORS

It has been seen that the actuator bends when a high voltage is applied to its central electrode. But what are the consequences of these flexions on the integrity of the actuator over millions of cycles? There are two main issues. The first one is the eventual rupture of the PZT which is very thin (0.25 mm) and very brittle. The second issue is that a debonding defect may occur at the interface between two layers, and particularly at the interface between the piezo ceramic and the composite because of shearing that occurs when two layers are under bending.

In this chapter, fatigue tests of GEPAC actuators are conducted using ultrasonic NDE characterization. The first set of experiments deals with actuation off the bending resonance frequency. The second set of data is for actuation at the resonance frequency of the actuator.

5.1 First fatigue experiment: off resonance, up to 1.7×10^6 cycles

5.1.1 Overview

It has been seen previously that the maximum electrical field for the PZT is 2 $MV.m^{-1}$. Hence, the maximum input voltage with the PZT plate of 0.25 mm is 500 V. The amplifier Krohn-Hite 7500 cannot be used for this experiment since its highest output voltage is 200 V. Instead, Kepco high voltage power supply BHK 1000 (voltage up to 1000 V) is used.

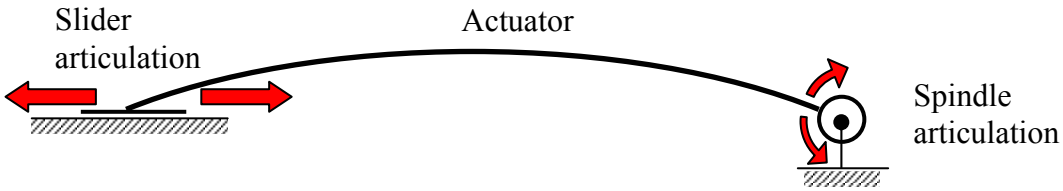

Figure 5.1. Boundary conditions during the fatigue experiment

During the experiment, the GEPAC is resting on a table, as indicating in Figure 5.1. One end of the actuator is attached with an adhesive tape. It is equivalent to a spindle articulation. The actuator can "turn" around its end. The other end just rests on the table. As indicated in Figure 5.2, the actuator is placed under a Linear Variable Differential Transducer (LVDT). It is composed of a rod that moves through a coil. A magnetic core is attached to the rod, and produces a voltage that is proportional to the displacement of the core when passes through the coil. The distance between the table and the center of the actuator is referred as the dome height. The LVDT is used to measure the dome distance with micron accuracy.

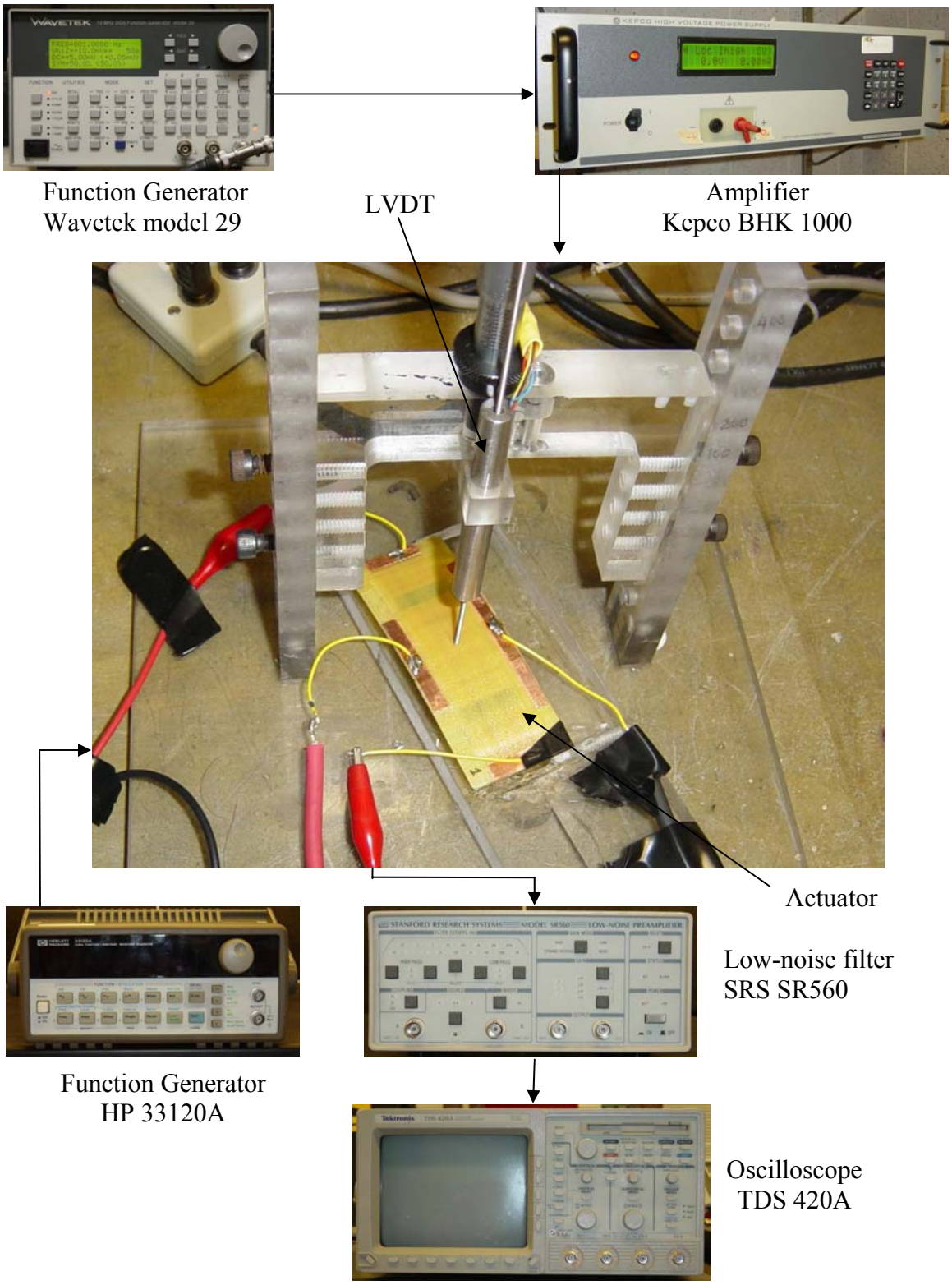

Figure 5.2. Assembly for a fatigue experiment

The output of the LVDT is calibrated using a Schaevitz ATA 2001 LVDT signal conditioner. This device is connected to the oscilloscope TDS 420A, where the signal is displayed and stored. A peculiarity of this amplifier is that the ground is positive. For a common PZT, it would not be a problem, but for a segmented PZT, it is. Indeed, segmented piezo ceramic are designed to be used with two different devices at the same time, grounds of which are plugged to the same electrode. In this case, it is not possible to send an ultrasonic signal during actuation. Nevertheless, the amplifier BHK 1000 is used for fatigue test. It will be unplugged before each ultrasonic measure. The configuration for low frequency actuation is illustrated in Figure 5.3. For ultrasonic NDE, the amplifier is switched off. The function generator HP 33120A and the oscilloscope TDS 420A are used to generate and receive ultrasound. At this stage, the ground is connected to the bottom electrode of the PZT (see Figure 5.4).

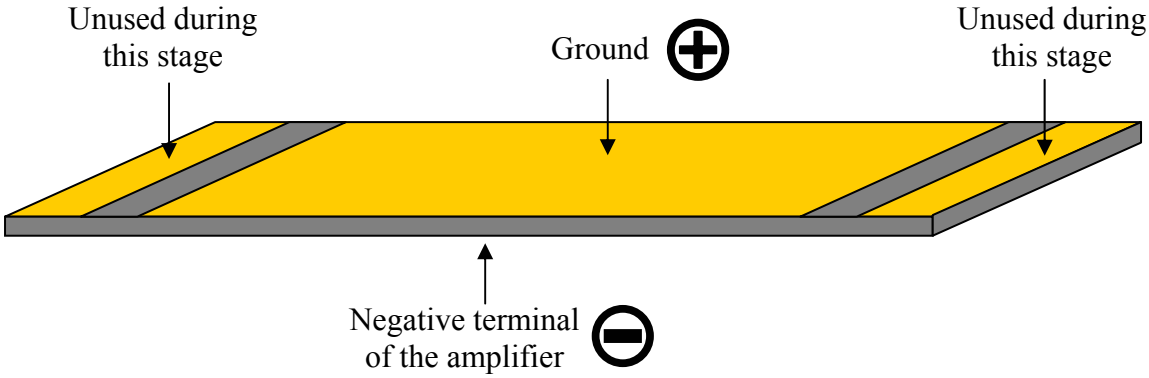

Figure 5.3. State of connection during actuation

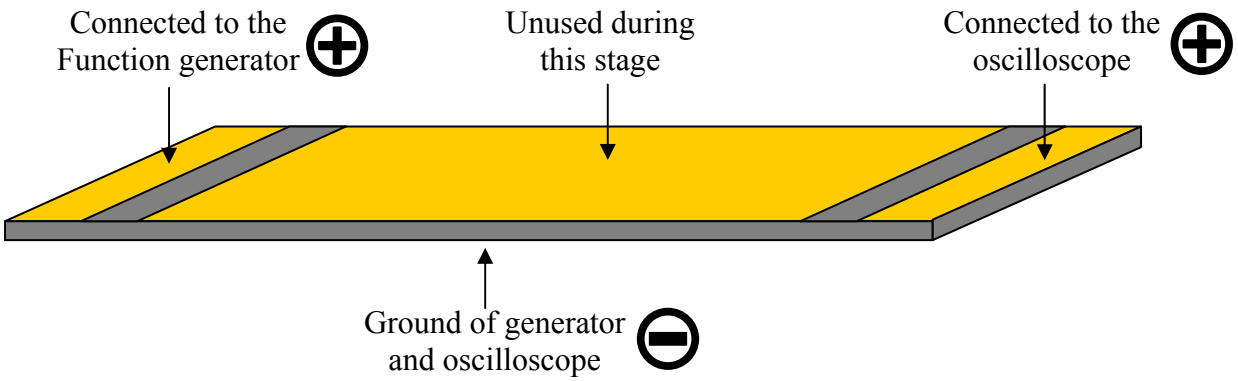

Figure 5.4. State of connection during ultrasonic NDE

The actuator is subjected to a continuous, low frequency sinusoidal displacement to test its endurance. The function generator Wavetek model 29 generates a positive sinusoidal signal with a frequency of 10 Hz and an amplitude of 5 V. The signal is sent to the Kepco BHK 1000 amplifier where it is amplified a hundred times. For ultrasonic NDE, we use the same signal as in previous experiments. The function generator HP 33120A generates one cycle of a sinusoidal signal at 1 MHz with amplitude 5V. The received signal is filtered by the SRS SR560 and displayed on the oscilloscope.

5.1.2 Displacement of the actuator

Table 5.1 gives the data used to calibrate the LVDT.

Table 5.1. LVDT calibration

Displacement [inch]	Displacement [mm]	Voltage [mV]
0.004	0.1016	371
0.008	0.2032	777
0.012	0.3048	1174
0.016	0.4064	1578

According to these measurements, 1 V corresponds to 0.253 mm. This calibration is used to determine the dome height of the actuator. The actuator is at rest when there is no voltage in the PZT. The dome height displacement is taken to be zero in this position. Figure 5.5 shows the output signal and the displacement of the actuator after 100,000 cycles at 10 Hz. The maximum displacement of the actuator dome height is almost 0.4 mm. With a DC signal of 500 V, this displacement reaches 0.6 mm. But at a frequency of 10 Hz, the actuator does not have enough time to reach this upper limit. Furthermore, it is interesting to compare the output (displacement) with the input (generator signal). The generator function is a perfect positive sinusoidal signal of 10 Hz having an amplitude of 5 V. Figure 5.5 indicates that, although both signals start at the

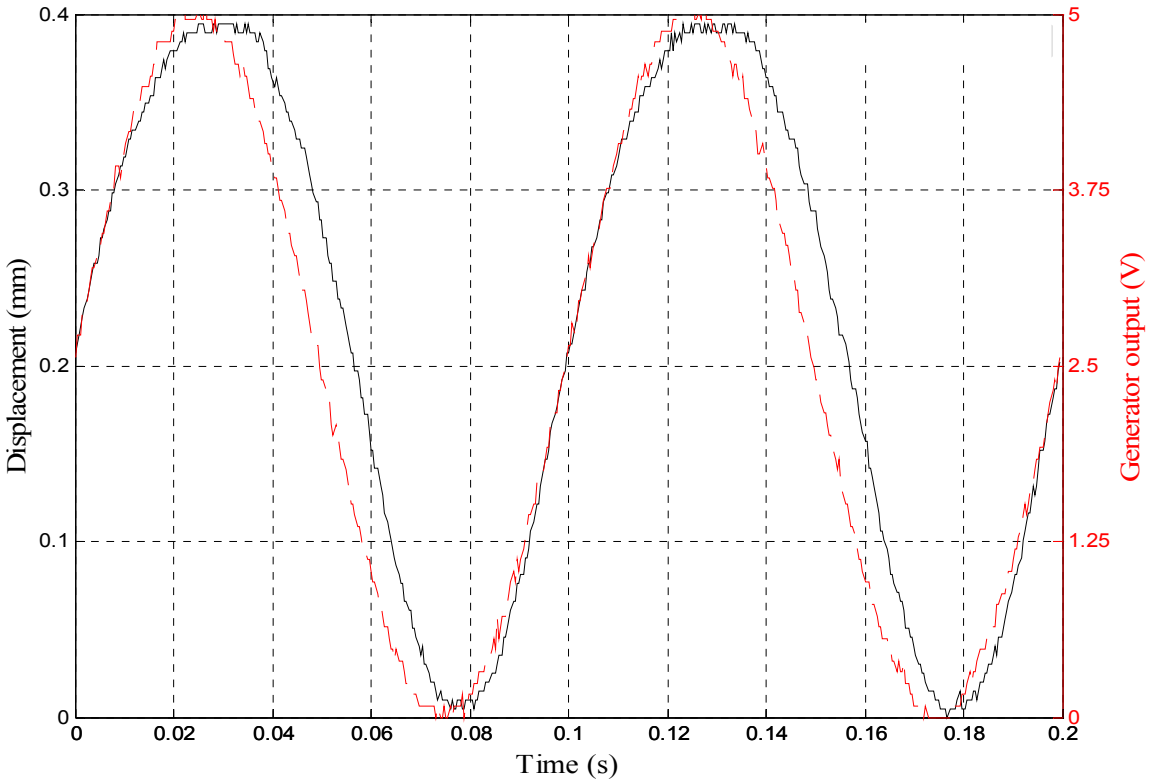

Figure 5.5. Dome height displacement and generator output for N = 100,000 cycles

same point, a lag occurs when the voltage decreases, but it disappears at the end of one period. This is characteristic of an hysterisis. The graph representing the displacement versus the voltage illustrates this phenomenon (see Figure 5.6). When the voltage is increasing, the displacement goes along the lower arm of the cycle. When decreasing, the displacement moves along the upper arm. Graphs 5.5 and 5.6 have been plotted for a number of 100,000 cycles.

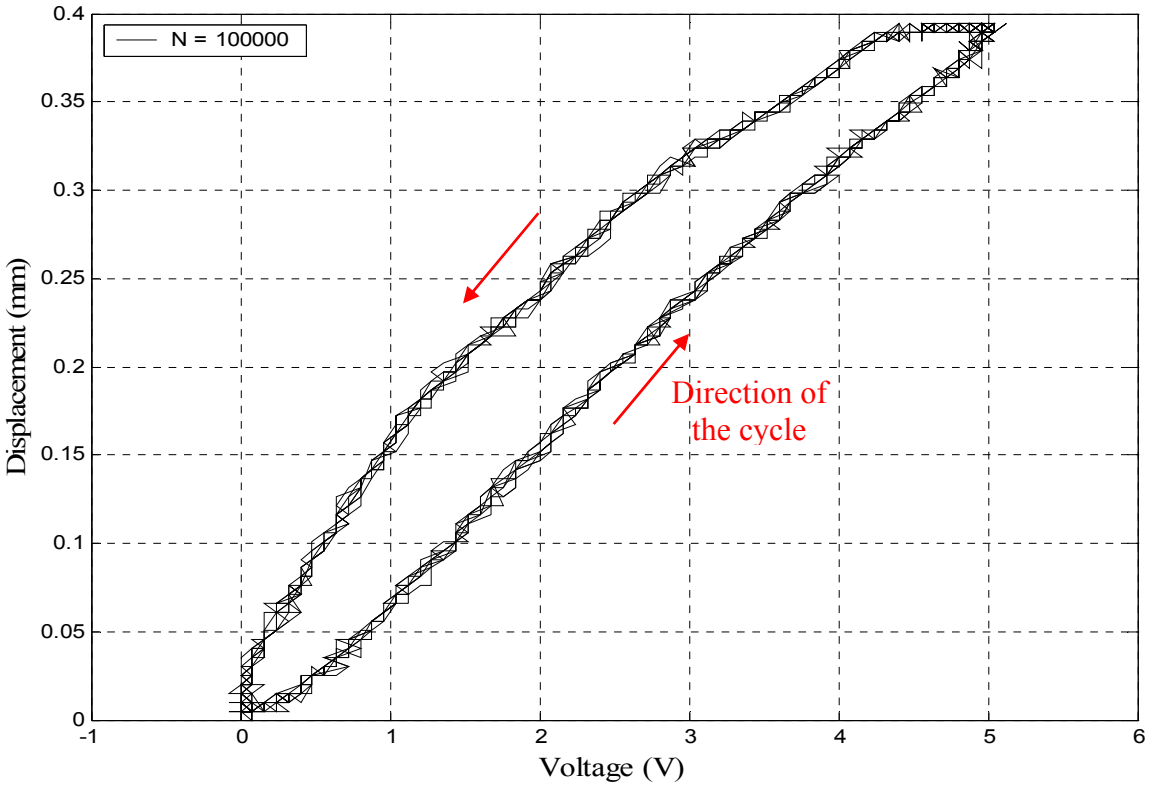

Figure 5.6. Hysteresis cycle of displacement vs voltage for N = 100,000

The fatigue test had been done up to 1.7 million cycles. The different curves representing the displacement and the hysteresis until 850,000 cycles are available in appendix A. There is virtually no difference between signals after 850,000 cycles and

after the first bending. The actuator seems to have a good resistance to fatigue, at least, until 0.85 million cycles.

5.1.3 Ultrasonic NDE during fatigue experiment

An ultrasonic signal is used to control the integrity of the actuator between each series of test. The amplifier is turned off and unplugged. Then, the generator and the oscillator are connected to the ground electrode. A pulse of 5 V and 1 MHz is sent in the actuator. The received signals are plotted on Figure 5.7 before any low frequency actuation (N=0 cycles) and after N=50,000 cycles (10 Hz).

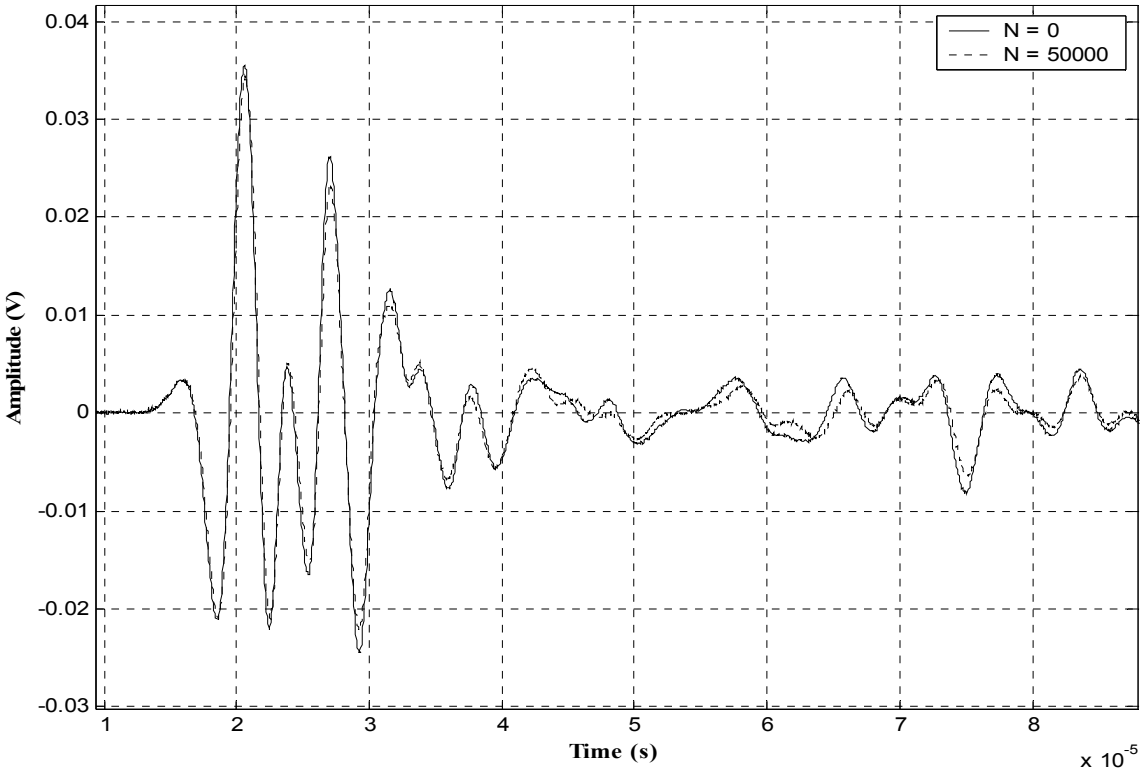

Figure 5.7. Received ultrasonic signals after N=0 and N=50,000 cycles at 10 Hz

Figure 5.7 indicates that both signals have almost the same shape. There is a very small drop in the amplitudes of the peaks for the signal after 50,000 cycles. Ultrasonic signals are plotted for N=50,000, 400,000 and 1.7 million cycles in Figure 5.8. Again, there is virtually no difference between these three signals. Even last arrivals are similar, which confirms that they really correspond to the signature of the actuator. After 1.7 million cycles at 10 Hz and 500 V, the actuator shows no damage.

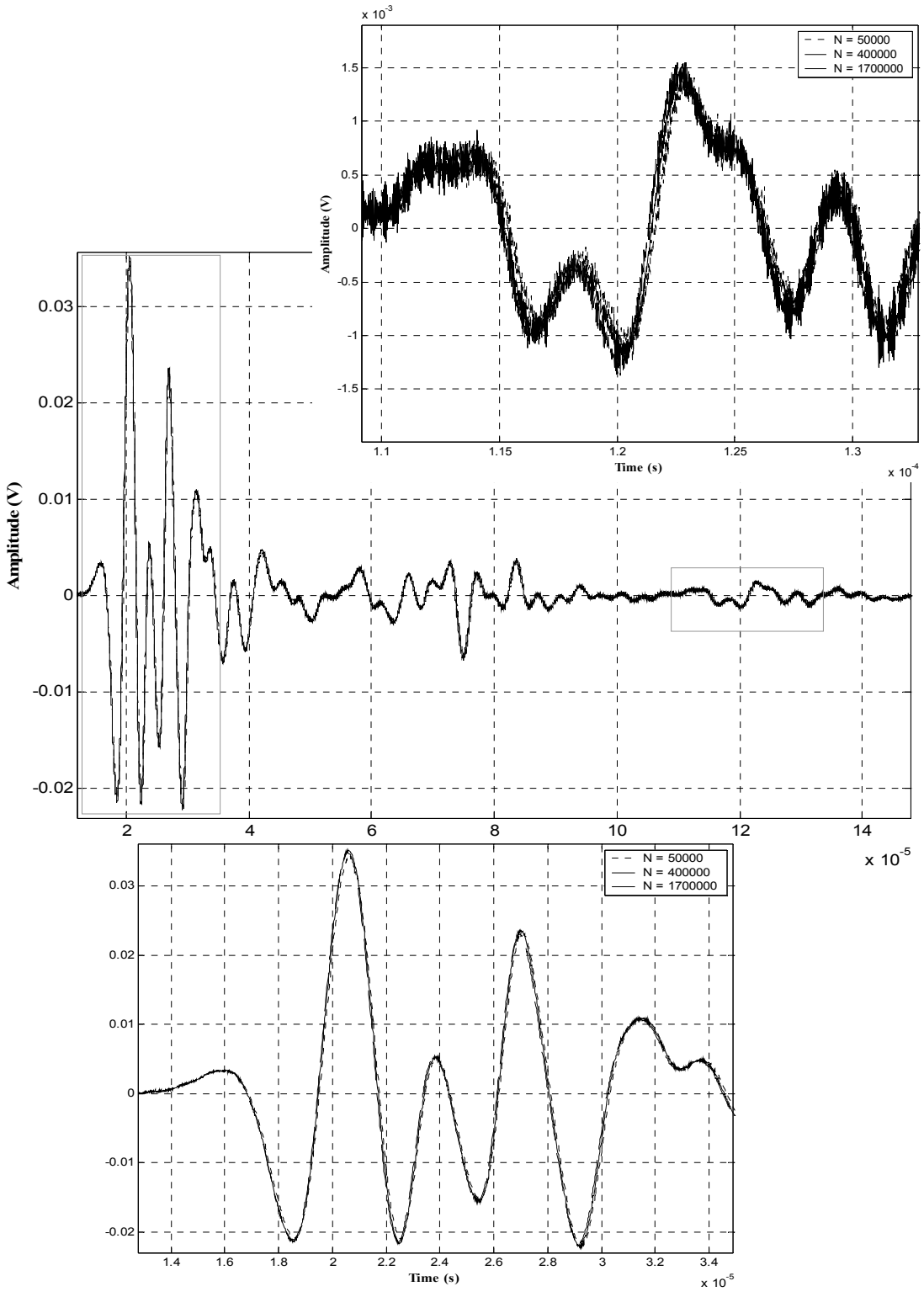

Figure 5.8. Received ultrasonic signals after N=50,000, 400,000 and 1.7 million cycles

5.2 Second fatigue experiment: at resonance, up to 5.3×10^7 cycles

5.2.1 Overview

It is possible that, if the actuator was driven at its resonance frequency, it would show some damage earlier in the fatigue cycle. This hypothesis is the subject of the following section.

5.2.2 Resonance frequency of a GEPAC

The first step consists in finding the resonance frequency of the actuator. The actuator is placed under the LVDT and fixed with an adhesive tape at one end. A signal having an amplitude of 200 V and a variable frequency is sent to the actuator. By observing the amplitude of the LVDT output, it should be possible to determine the resonance frequency. This method works at low frequencies (up to 25 – 30 Hz) but at higher frequencies the LVDT rod cannot follow the actuator because of its light mass.

Another solution is to use strain gages bonded above and below the dome actuator. The strain gages are connected to a Micro Measurements 2100 signal conditioner in a quarter bridge arrangement. The output of the signal conditioner is displayed on an oscilloscope. The resonance frequency occurs when the amplitude of the strain signal is maximum. The actuator is placed on a table and fixed as previously. The output of the amplifier is connected to the electrodes and delivers a signal of 200 V. The signal becomes noisy as the frequency is increased. This noise is due to the boundary conditions. At low frequencies, the free end of the actuator can slide on the table during bending, but above 20 or 30 Hz, the free end has no time to go back and forth, it rebounds on the table. And each time that it hits the table, it creates noise in the strain gage signal.

To avoid this source of noise, one end of the actuator is clamped while the other is free, as shown in Figure 5.9. In this experiment, the actuator is clamped in a vertical position to avoid bending caused by gravity. A positive sinusoidal signal of 200 V and variable frequency activates the GEPAC. For each frequency, the amplitude of the strain gage output signal is recorded. It is this amplitude that characterize the flexion (and so the dome height) of the actuator.

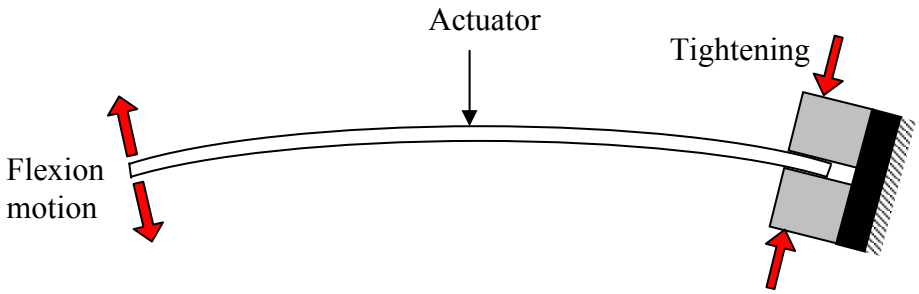

Figure 5.9. Top view of the actuator during the second fatigue experiment

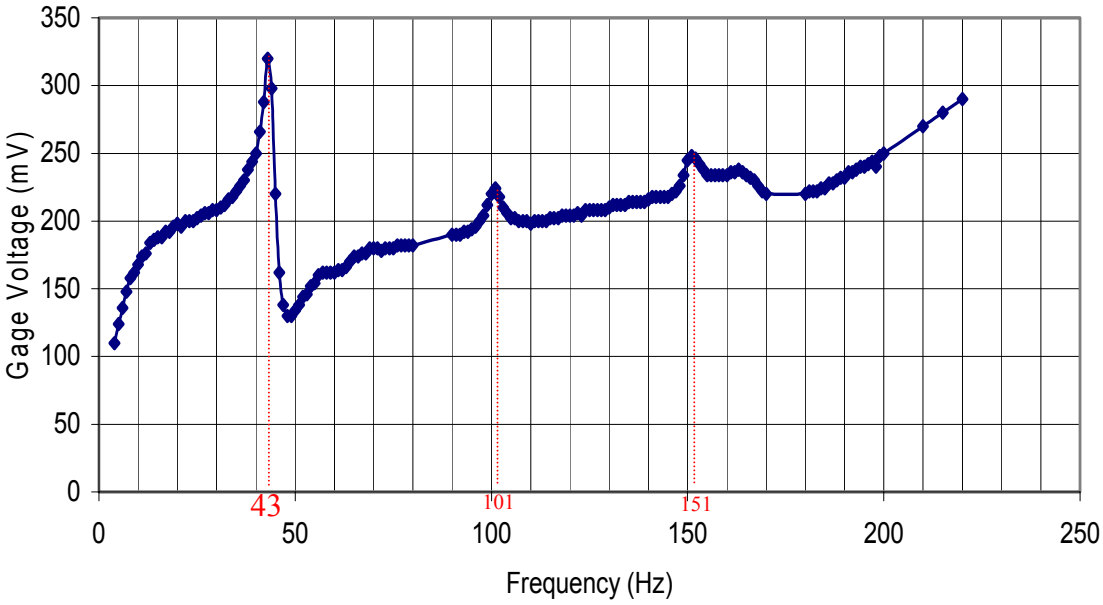

Figure 5.10. Amplitude of the actuator displacement as a function of frequency

The result is plotted on Figure 5.10. The first resonance occurs at a frequency of 43 Hz. One can observe a second resonance at 101 Hz and a third one at 151 Hz

5.2.3 Fatigue experiment at the resonance frequency

The second fatigue experiment is conducted at 43 Hz. A photograph of the experimental set up is shown in Figure 5.11. The actuator has the same boundary conditions as in the previous experiment. One end is fixed whereas the other is free. In this position, it is not possible to use the LVDT to measure the dome displacement.

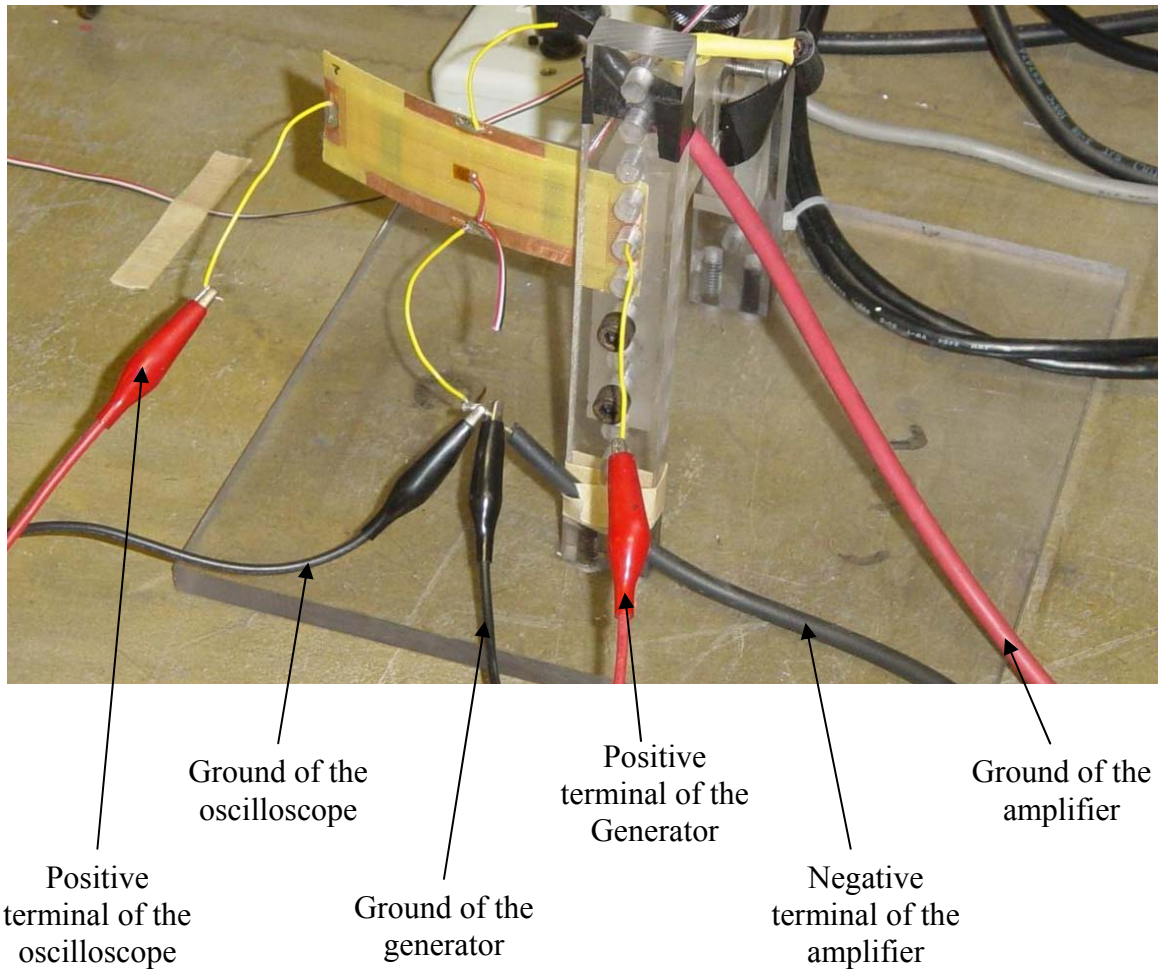

Figure 5.11. Assembly for the second fatigue experiment

As for the previous fatigue experiment, the amplifier has to be turned off in order to make an ultrasonic test so the electrical grounds of the oscilloscope and the generator are connected to the negative terminal of the amplifier for an ultrasonic NDE. During the fatigue, the peak-to-peak amplitude of the vibration of the free end reaches 8 mm.

5.2.4 Experimental results

Figure 5.12 shows the ultrasonic signals of the actuator before the beginning of the fatigue experiment and after 24.43 millions cycles. The signals are almost identical,

both for the first arrivals and for the late arrivals. The fatigue test is continued. Figure 5.13. exhibits the ultrasonic response for 27 millions cycles.

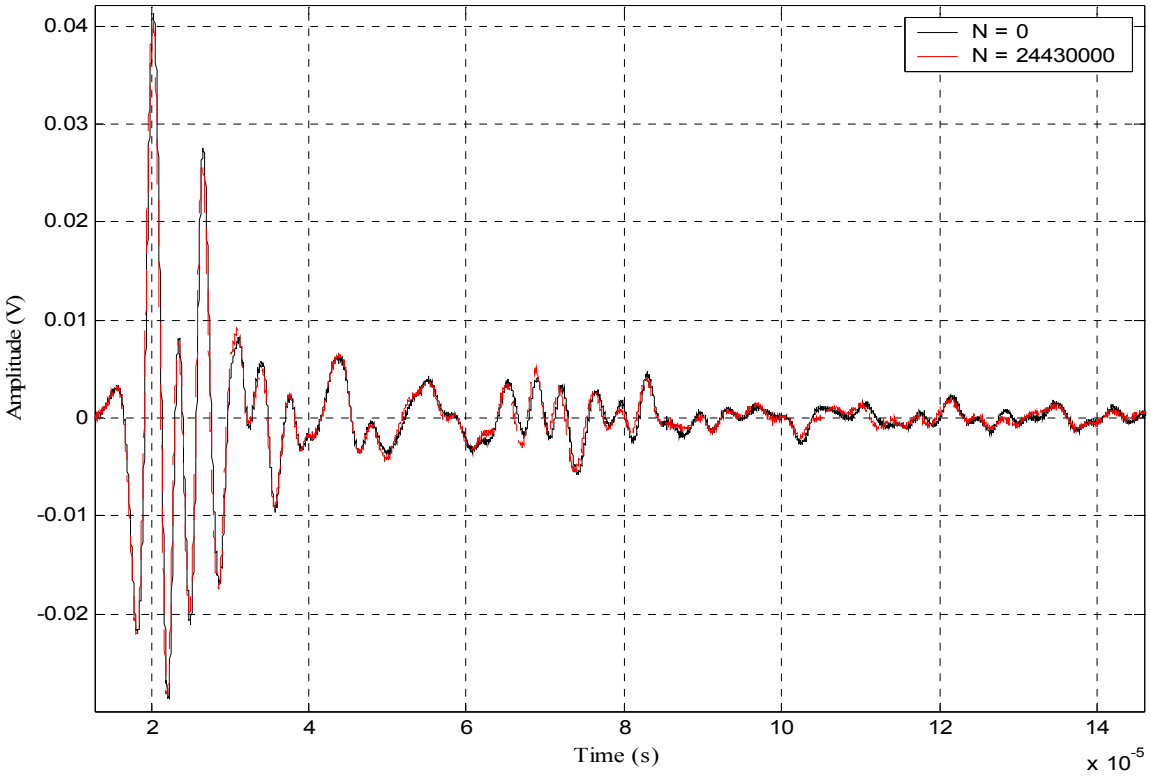

Figure 5.12. Ultrasonic response before the beginning of the fatigue test and after 24 millions cycles

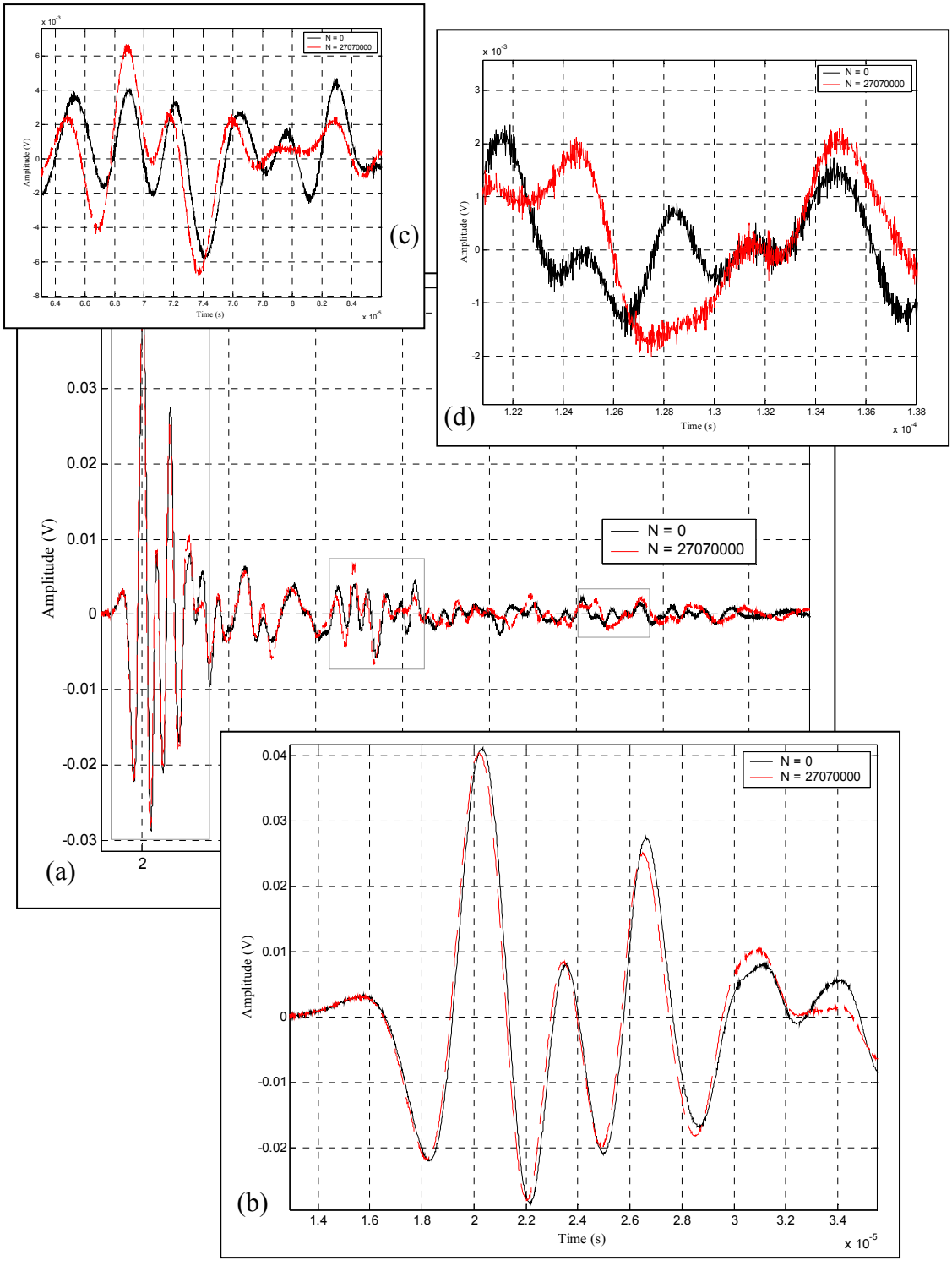

Figure 5.13. Ultrasonic response for N = 0 and N = 27 millions cycles

(a) 0 – 140 µs; (b) 13 – 35 µs; (c) 63 – 86 µs; (d) 121 – 138 µs

Again, for the first arrivals, the signals are almost identical. The only difference comes after 32 μs. For the late arrivals, the ultrasonic signals are quite different. Therefore, it appears that fatigue is more apparent in the late arrivals of the ultrasonic signal than in the early arrivals. This result may be expected if one considers that late arrivals represent ultrasound that has traveled many times through the sample, thus magnifying any defects in the sample. This result may be very useful for practical implementation of ultrasonic NDE health monitoring of a GEPAC actuator.

Next measurements are taken up to 53 millions cycles. Again, there is almost no difference between the signal at $N = 27 \times 10^6$ cycles and $N = 53 \times 10^6$ cycles as shown in Figure 5.14. However, it is interesting to note that there is very little difference beween the late arivals at $N = 27 \times 10^6$ and $N = 53 \times 10^6$ cycles.

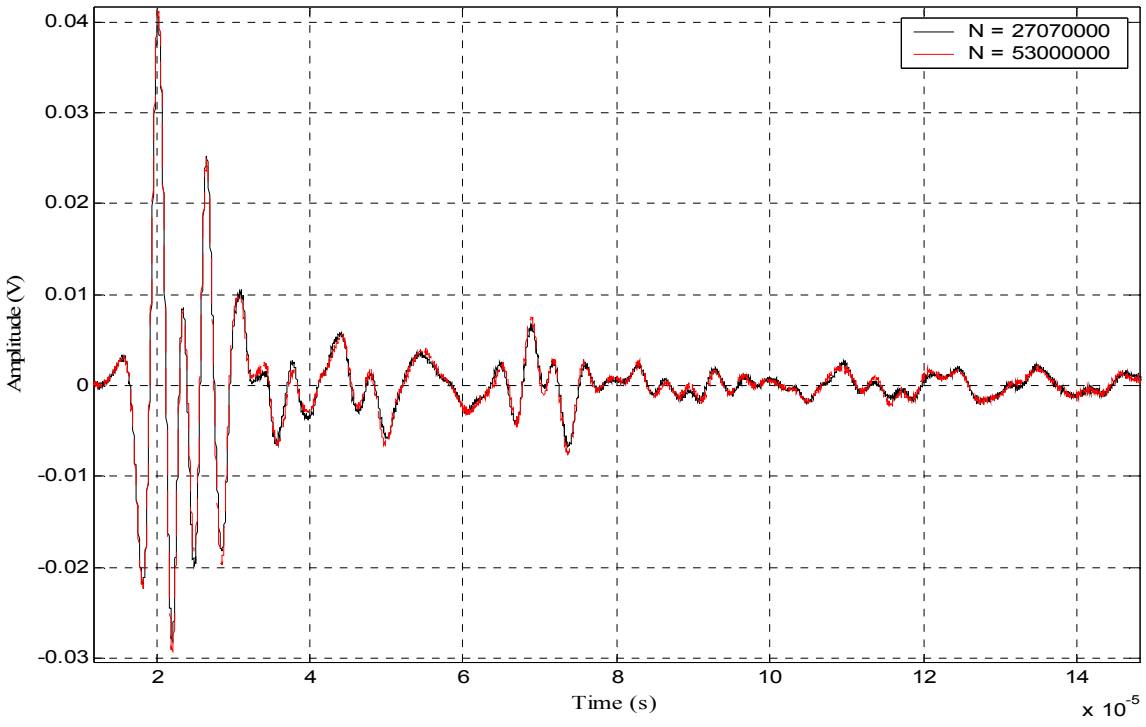

Figure 5.14. Ultrasonic response for 27 and 53 millions cycles

5.2.5 Mechanical flexion of actuator after fatigue experiment

The ultrasonic measurements have been made when the high voltage amplifier was disconnected. Hence, the actuator has its natural curvature. Perhaps a defect is visible when the actuator is in flexion. Another experiment is conducted to check this hypothesis. The actuator used during the fatigue test is mechanically bent between two jaws. The dome is displaced by 1.59 mm. Given that the length of the actuator is 102 mm, the corresponding radius of curvature is 154.5 mm.

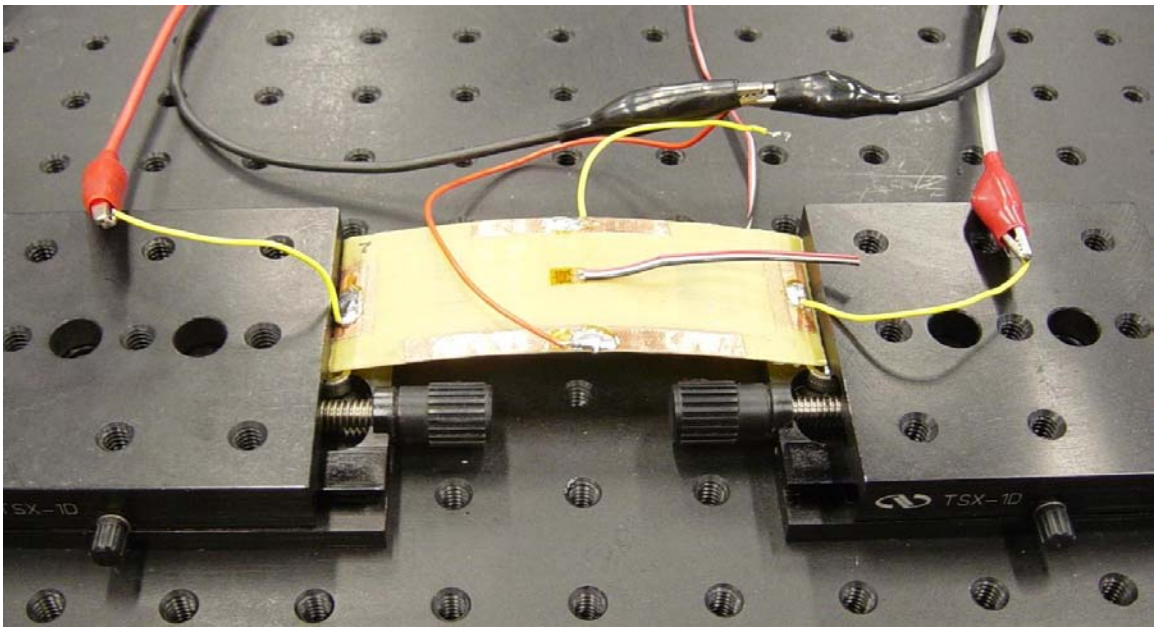

Figure 5.15. Assembly for ultrasonic NDE with mechanical bending after the fatigue test

A sinusoidal pulse of 5 V and 1 MHz (one cycle) is sent to the actuator. The received signal is plotted on Figure 5.15 when the actuator is at rest and when it is mechanically bent. It is noted that the actuator has been subjected to 53 millions bending cycles before this experiment. Again, both signals are very similar. Therefore, bending the actuator does not reveal a defect. It confirms the previous results: after ten of millions

of bending cycles, the actuator keeps its structural integrity. Furthermore, the dome displacement was the same at the end of the fatigue test.

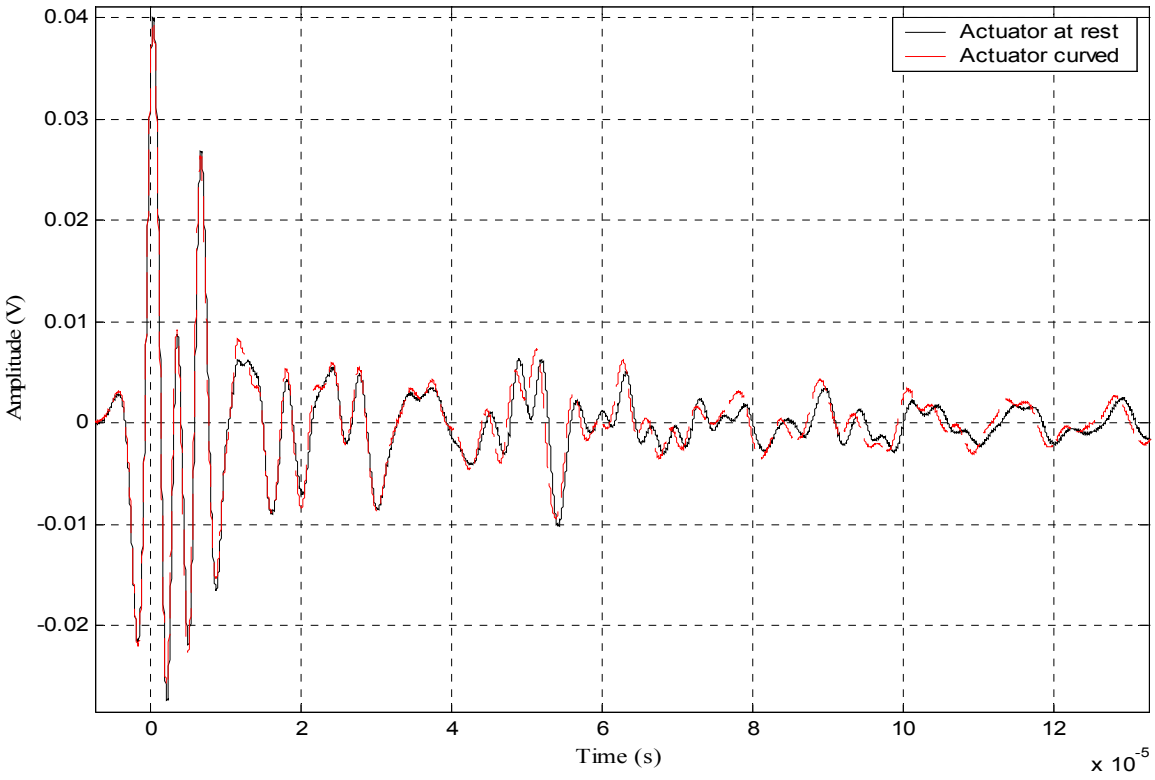

Figure 5.16. Ultrasonic response for the actuator after 53 millions cycles

5.3 Debonding defect in GEPAC

5.3.1 Simulated debonding defects

The aim of this section is to study the actuators with simulated debonding and to see how these defects affect the ultrasonic signal. Three new actuators are made. The dimensions of the PZT ceramic are 50.8 × 12.7 × 0.25 mm (2 × 0.5 × 0.01 inch). The first actuator is built without any defect. The second one has a defect that represents 30 % of the PZT length. The third one has a defect of 60 %. The debonding is simulated by

introducing a release film, the same one as used to prevent actuators from sticking to the mold during curing. The debonding defect is on the entire width of the actuator. The release film is located between the PZT and the three upper composite layers. The defect is placed in the middle of the actuator, right above the upper extended copper foil.

5.3.2 Experimental results

The experimental arrangement is identical to the one in Figure 4.9. A sinusoidal pulse of 5 V and 1 MHz (one cycle) is sent to the actuator containing no defect. The received signal is plotted on Figure 5.17.

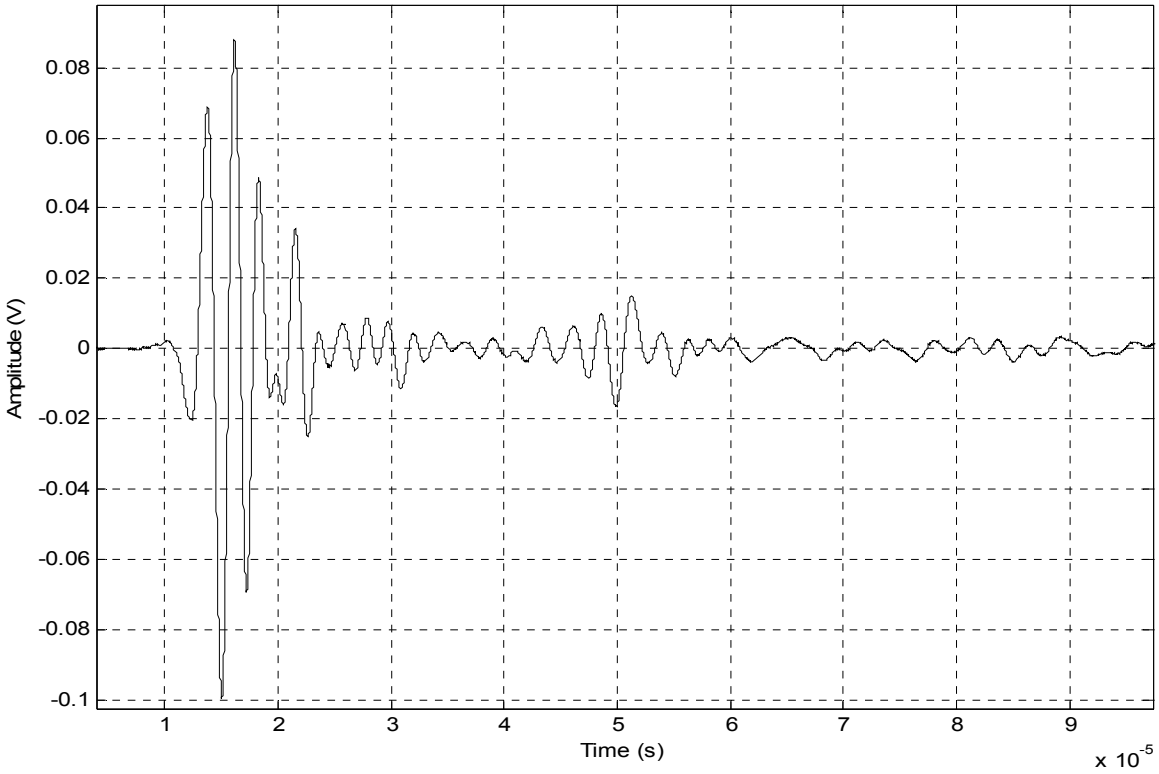

Figure 5.17. Ultrasonic signal for a healthy GEPAC

Compared to the signal of Figure 4.2 which corresponds to a healthy actuator with a PZT twice as thick (500 μm), the amplitude of the signal is about twice as large.

5.3.3 Ultrasonic signal for the actuator with a defect representing 30% of the PZT length

An ultrasonic measurement was made right after curing, when the release film was still inside the actuator. The release film was then pulled, but, as shown in Figure 5.18, only the edges of the film were successfully removed. Figure 5.19 shows a comparison of the ultrasonic signals received with the film inside and with the film partially removed.

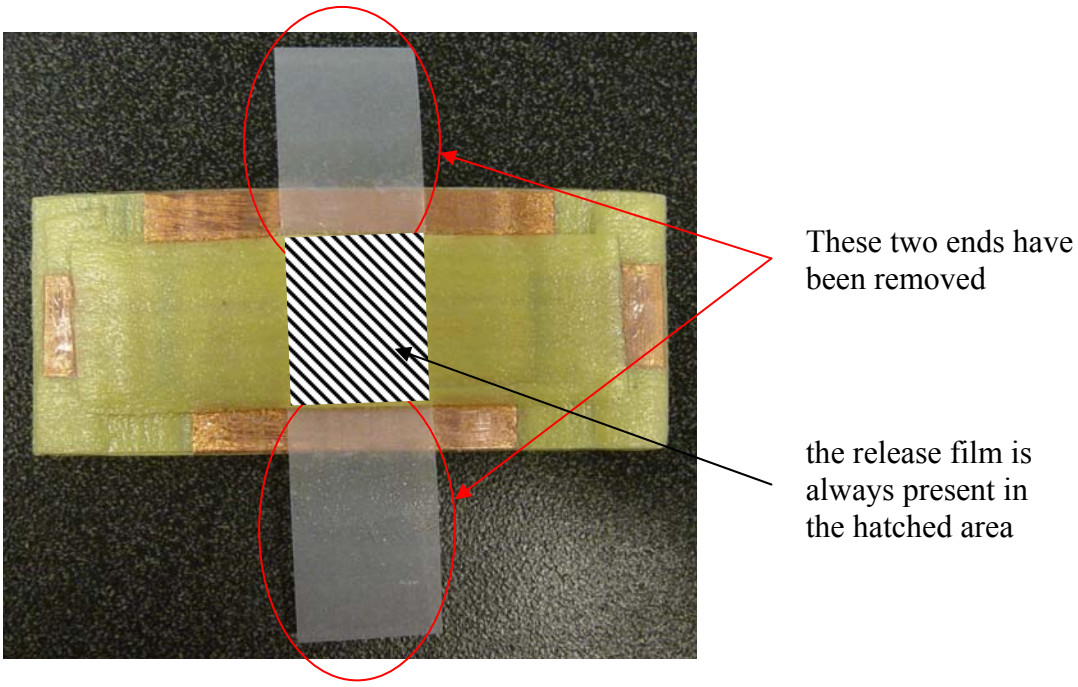

Figure 5.18. Actuator with a defect representing 30% of the PZT length

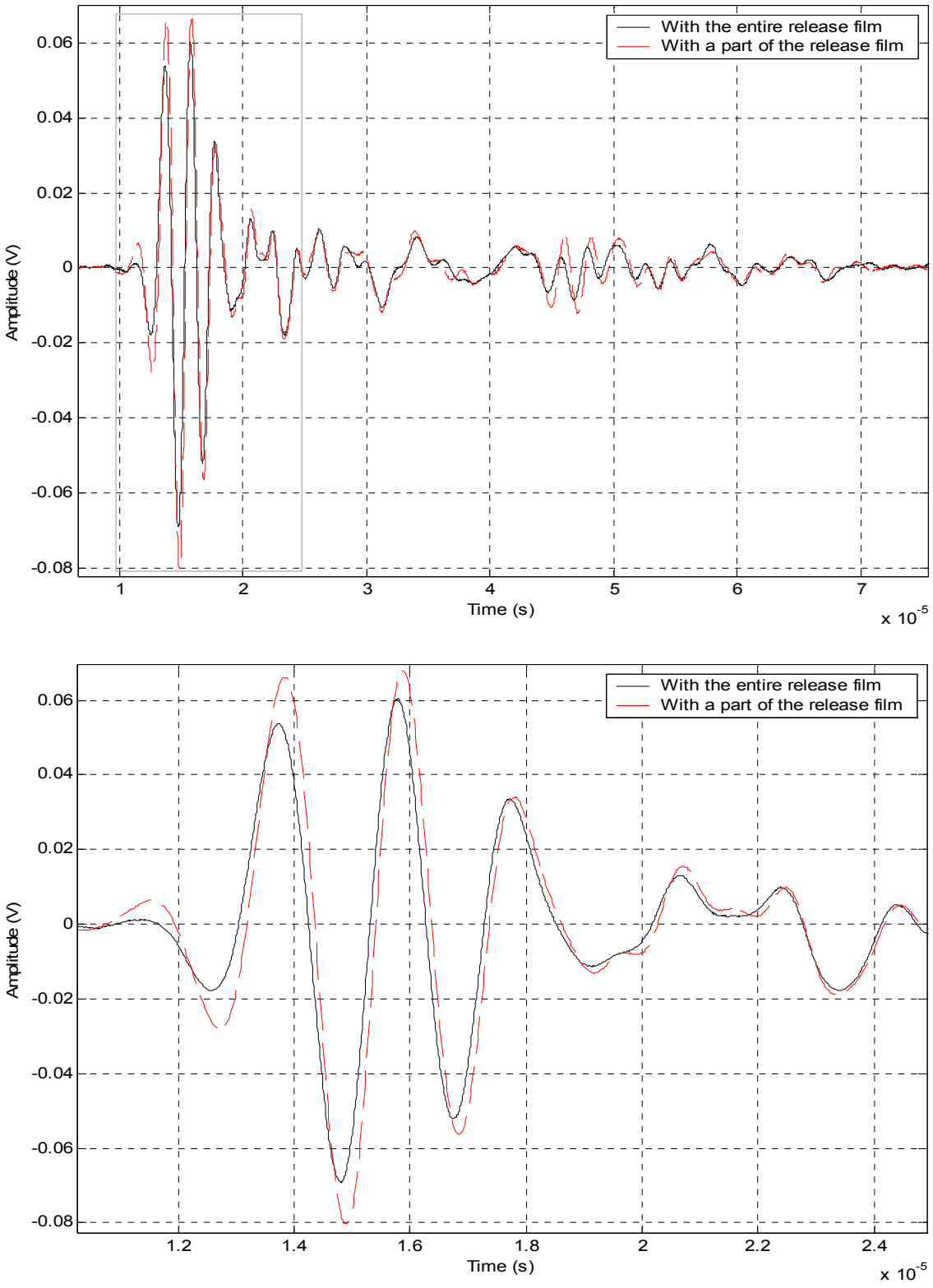

Figure 5.19. Received signal with the entire and a part of the release film for the actuator with a defect representing 30 % of the PZT length

Both signals exhibit nearly the same shape. The amplitude of the signal, when a part of the release film is removed, is slightly higher than that with the entire release film. The film acts as a damper. It absorbs a part of the transmitted energy. As regards timing, there is no noticeable difference between both signals. The release film does not delay the response signal.

5.3.4 Ultrasonic signal for the actuator with a defect representing 60% of the PZT length

The same measurements are taken for the actuator having a debonding defect representing 60 % of the PZT length. This time, the release film has been removed entirely because of its higher size. Hence, the actuator has a “perfect” debonding defect located between the PZT and the upper composite layers. The corresponding curves are plotted on Figure 5.20. Both signals exhibit some similarities for the first arrivals, but not for late arrivals. Given the many reflections occuring in the actuator, it is almost impossible to determine the effect of debonding defect regarding late arrivals. It is then necessary to focus on first arrivals to compare the curves. As far as amplitude, the observation is the same as before. When the release film is removed, the amplitude of the signal is higher. For timing, the absence of release film introduces a slight delay for the wave propagation. Though both curves begin at the same time, a lag appears between signals. One can conclude that presence of release film in actuators modifies the way of wave propagation. Removing partially or totally the release film produces different results. Hence, if one wants to study the effect of debonding defect on actuators, it is necessary to remove entirely the release film (if possible).

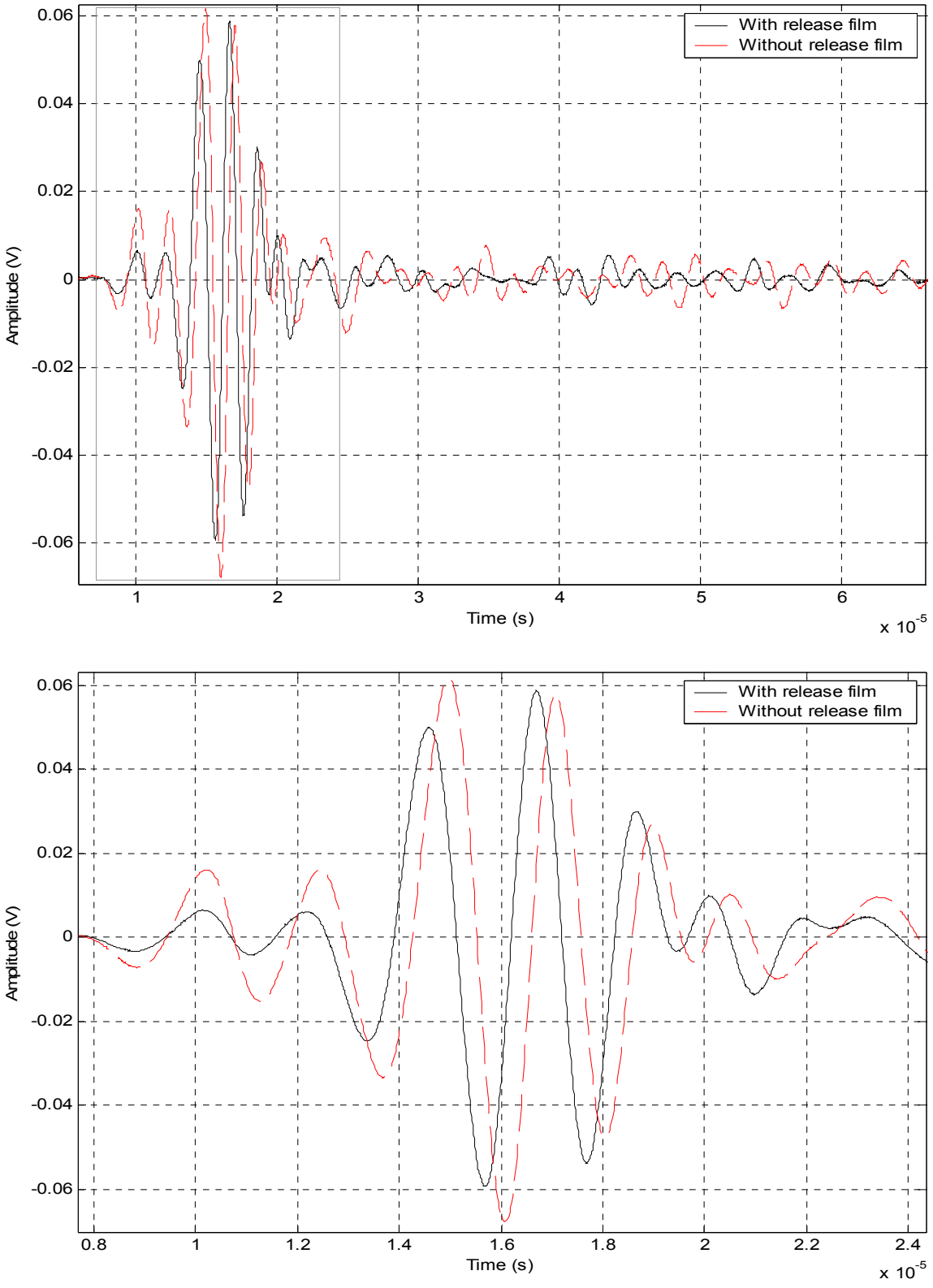

Figure 5.20. Received signal with and without release film for the actuator with a defect representing 60 % of the PZT length

5.3.5 Impact of debonding defect on the ultrasonic signal

For this experiment, the same sinusoidal pulse is sent through a healthy actuator without defect and a similar actuator having a debonding defect corresponding to 60 % of the PZT length. Received signals are plotted on Figure 5.21. The peak amplitude is higher when there is no defect in the actuator. A part of the initial energy is lost at the interface between the PZT and upper composite layers, where there is the debonding defect. The number of peaks and their location are different. For the healthy actuator, a second wave packet appears between 40 and 60 μs. But it does not exist for the debonding actuator. This last one has only the wave packet corresponding to the first arrivals, and then, the signal is composed of small oscillations corresponding to the late arrivals. Note also the difference of arrival time and shape for the first arrivals ($t < 12$ μs).

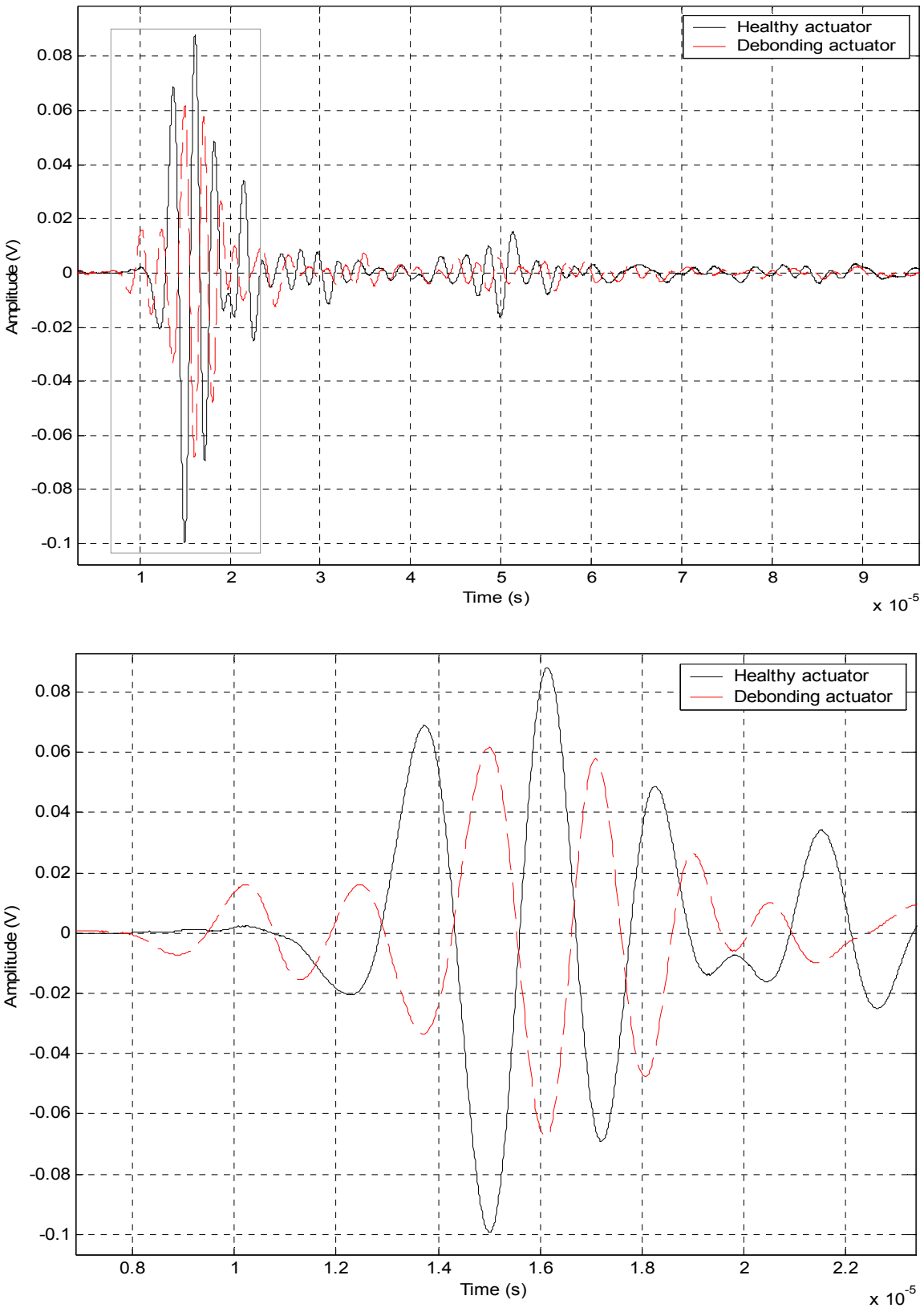

Figure 5.21. Ultrasonic response for a healthy and "debonded" actuator

It has been seen in section 4.2.3 that mechanical bending of the actuator is equivalent to electrical actuation. It is interesting to study the impact of the debonding defect on the ultrasonic signal when the actuator is curved. The same assembly as in section 4.2.3 is used to bend the GEPAC. The actuator with a debonding defect representing 30 % of the PZT length is used for this experience. Three ultrasonic measurements are taken. The first one corresponds to the actuator at rest. The second and third ones correspond to a radius of curvature of 121 and 105 mm, respectively. Results are plotted on Figure 5.22.

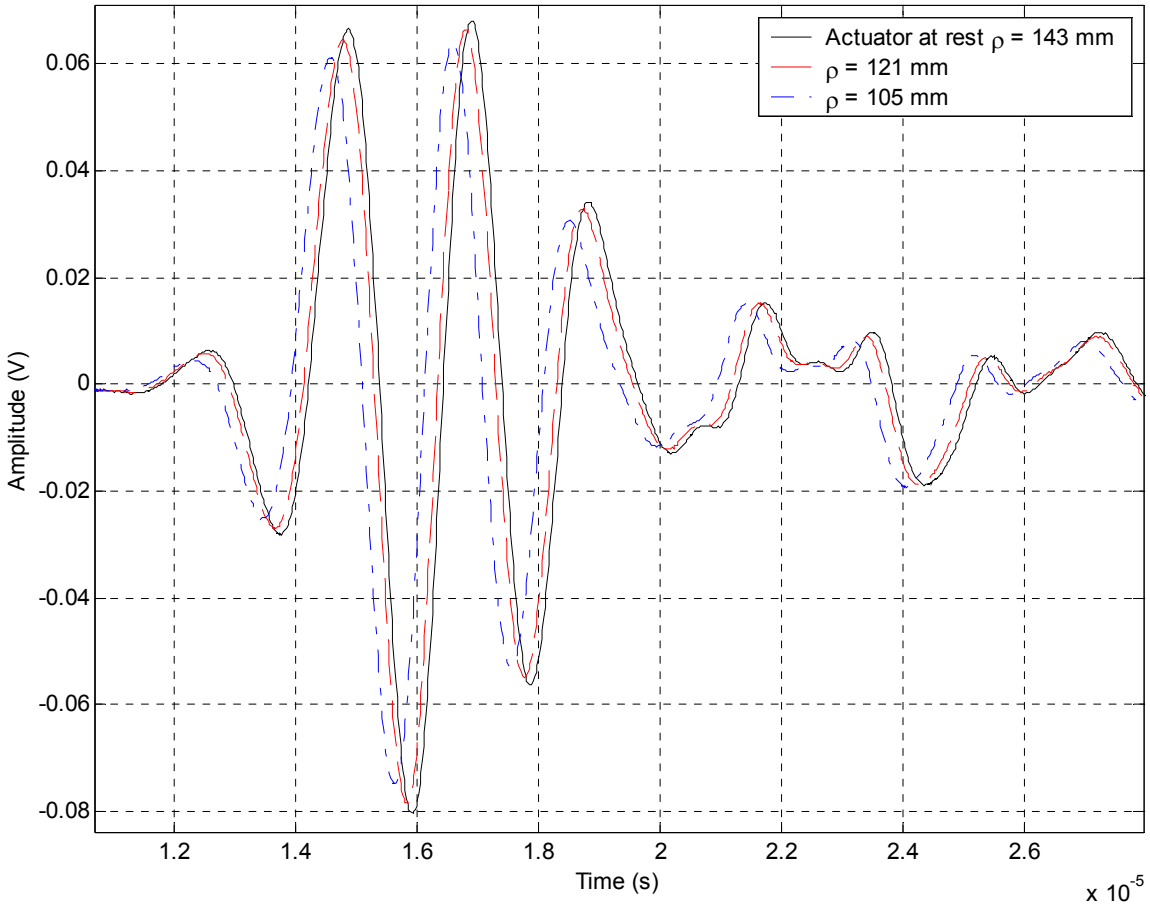

Figure 5.22. Ultrasonic signal of a debonding actuator for different level of actuation

The observation is exactly the same as for healthy actuators. The shape of curves remains identical. The debonding defect does not introduce changes in the signal during actuation. The actuator with a 60 % PZT length defect gives the same results. Hence, the ultrasonic NDE method can be used to detect debondings during actuation of this device.

CHAPTER VI

ULTRASONIC NDE IN PLATES CONTAINING SEGMENTED GEPACS

6.1 Introduction

Actuators are expected to be used in large structures, like airplane skins for instance. Previous chapters have shown that it was possible to monitor the integrity of the actuator itself during low frequency actuation. The interest now is to study the ultrasonic NDE in the composite plate and to see if it is possible to monitor the plate integrity between two actuators separated by a large distance. For this study, two plates are manufactured and tested. The first one has no known defect, whereas a debonding defect is artificially introduced in the second plate.

6.2 Manufacturing of the plates

6.2.1 Design of the plates

Plates are manufactured with the same materials (Kevlar epoxy) as with previous actuators (see Chapt. 4, 5). Both lower unidirectional Kevlar layers have a transversal orientation (90°) compared to the length of the PZT plates. The layer just above PZT has also the same fiber orientation (90°) whereas both top layers have a longitudinal orientation (0°). The dimensions of each sample are 70 × 229 × 0.75 mm (2.76 × 9 × 0.03 inch). As shown in Figure 6.1, piezo ceramics (50.8 × 12.7 × 0.25 mm or 2 × 0.5 × 0.01 inch) are placed at each end of the plate. On Figure 6.2, one can observe the extended copper foil that constitute the connections to the electrodes. Each PZT ceramic has

segmented electrodes so that they can be used for low frequency actuation or for ultrasonic NDE (source or receiver). The piezo ceramics are separated by a distance of 183 mm. The composition of composite layers is identical to a simple actuator. Both lower layers and the one right above the PZT have a 90° fiber orientation (with respect to the PZT length). The last two upper layers have a 0° fiber orientation.

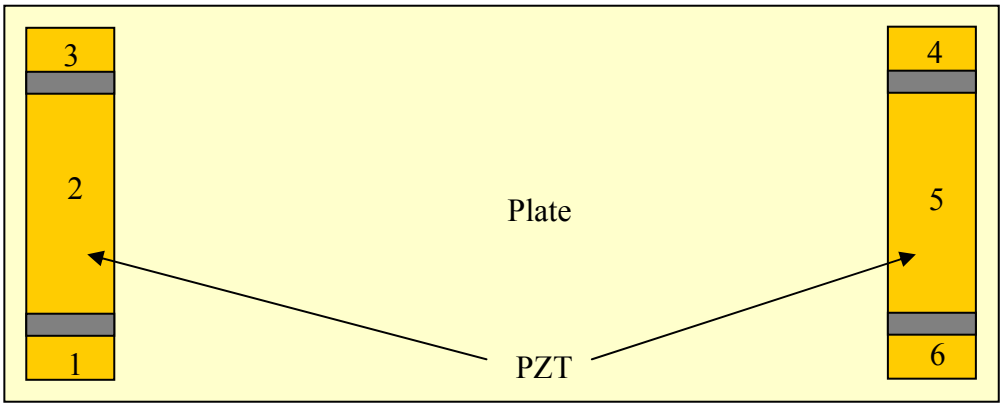

Figure 6.1. Sketch of a composite plate with two embedded segmented PZT

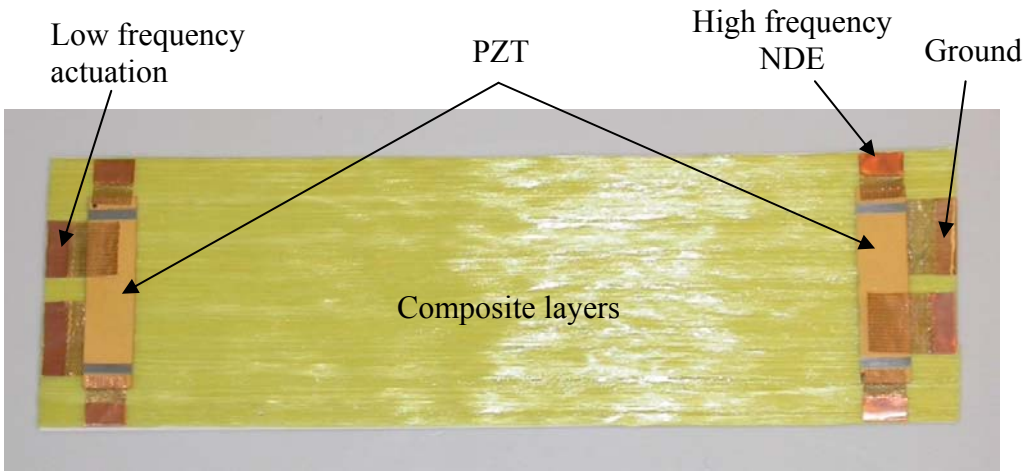

Figure 6.2. Composite plate with two PZT before upper layers are applied and before curing

6.2.2 Curing of the plates

The curing cycle is the same as for previous actuators, one hour at 177 °C and a pressure of 2 bars (30 psi). The aluminum plate is wide enough to cure both plates at the same time. As shown on Figure 6.3, a thin release film is used to simulate debonding defect. This film has a thickness of 20 µm and a length of 38.1 mm (1.5 inch). It is placed in the middle of the plate, between the two lower and three upper composite layers (at the same level than the PZT elements).

After curing, the curvature of the plates is higher in the center than at their extremities. This is due to the presence of piezo ceramics which stiffens the assembly at the two ends.

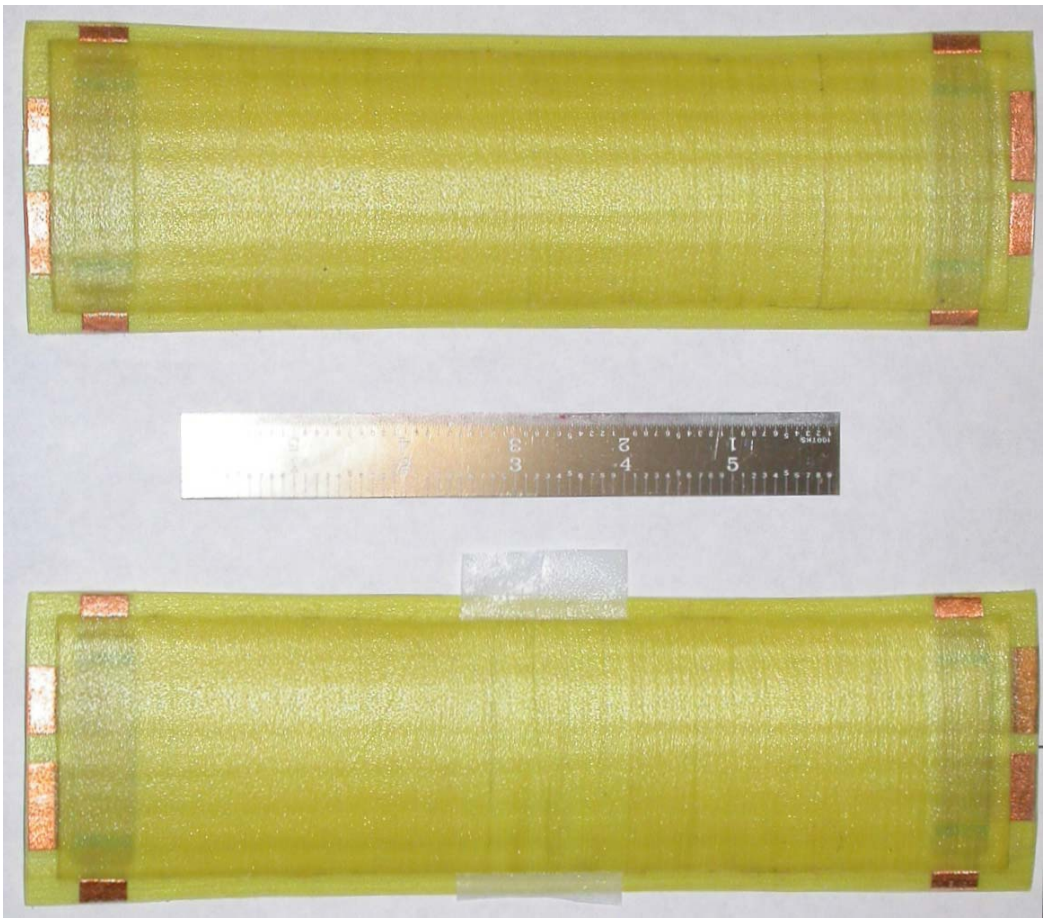

Figure 6.3. Plates with two piezo ceramics

6.3 Ultrasonic NDE in plates

6.3.1 Assembly for the ultrasonic testing

Figure 6.1 exhibits a plate with its piezo ceramics. Electrodes have been numbered in order to use any combination of them for ultrasonic NDE. Note that, if no low frequency actuation is present, electrodes 2 and 5 can be used for ultrasonic NDE. For instance, the ultrasonic signal can be sent to electrodes 1, 2, 3 and received on electrodes 4, 5 and 6, or sent to electrode 6 and received on electrode 3. It allows a good flexibility in the different measures.

A function generator (HP 33120A) sends a single cycle sinusoidal pulse of 5 V and 1 MHz to the electrode(s) of interest. The signal is received on the other end of the plate with chosen electrode(s). It is filtered by the low-noise filter SRS SR560 and sent to the oscilloscope TDS 420A. In the case of the plate, the signal has to cover a longer distance than just an actuator. As can be expected, the amplitude of the received signal is smaller and it is necessary to increase the gain of low noise filter. A gain of 5 is used for the experiments reported belows. All the possible combinations of send/receive electrodes were tested but for brevity, not all are reported below.

6.3.2 Ultrasonic NDE of the healthy plate

Figure 6.4 shows the recorded ultrasonic signal. On the caption, “Electrodes 123-456” means the signal is sent simultaneously to electrode 1, 2, 3 and received simultaneously with electrodes 4, 5 and 6 (see Figure 6.1). The caption “electrode 2-5” means that the signal is sent from electrode 2 and received with electrode 5.

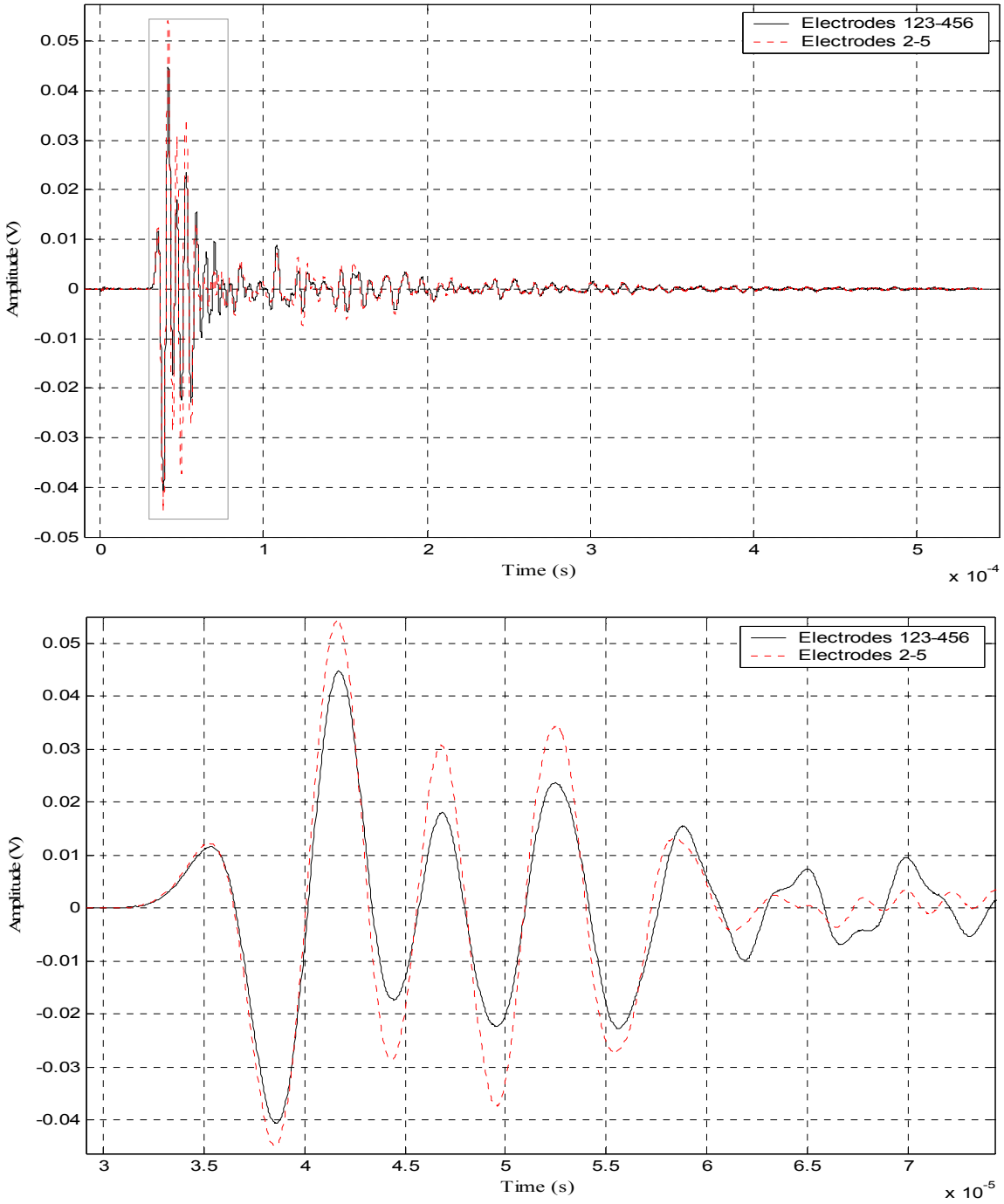

Figure 6.4. Ultrasonic signal in the healthy plate

As expected, the received signals are almost identical for both cases. There is just a slightly higher amplitude for the electrodes 2-5. The signal-to-noise ratio is acceptable

considering that the ultrasonic waves propagates perpendicular to the fiber direction over 180 mm. It should be possible to perform ultrasonic NDE over even longer distances. The length of these plates was limited by the aluminum mold used for curing.

Although not documented here for brevity, excellent signal repeatability was ovserved during the experiment even over several days of experimentation. Also, reciprocity was observed by reversing the send and receive electrodes.

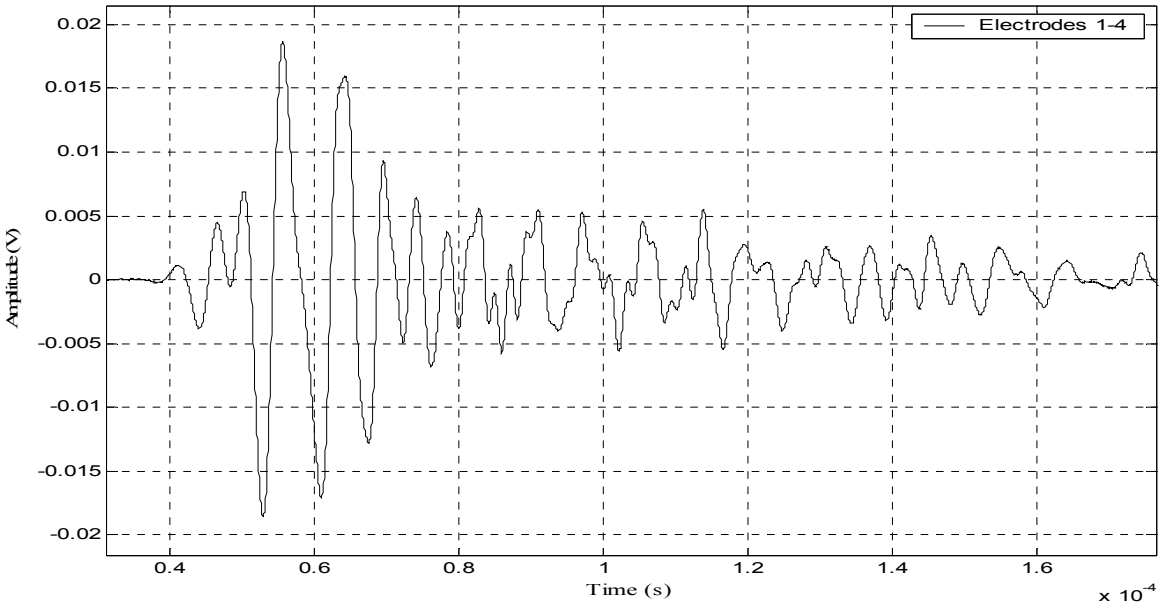

Figure 6.5. Ultrasonic response in a healthy plate using electrodes 1 and 4

All combinations of electrodes give a repeatable signal with adequates signal-to-noise ratio. For instance, a pulse can be sent to electrode 1 and received with electrode 6. The above figure exhibits the response corresponding to a signal launched from electrode 1 and received with electrode 4.

6.3.3 Comparison between healthy and debonding plates

The second plate is manufactured with a debonding defect. This defect is 1.5 inch long and is located at the center of the plate. As for the healthy plate, the debonding plate is tested with different combinations of electrode connections. The experiment is performed first with the release film inserted in the plate, then, with the film removed.

On Figure 6.6, one can see the difference of response signals between the healthy and defective actuators. Both signals begin at the same time, but the amplitude is smaller for the defective plate and the peaks do not occur at the same time. A simple way to detect the presence of the defect would be to measure the root mean-square amplitude of the signal. A drop in root mean-square value would be indicative of the presence of a defect.

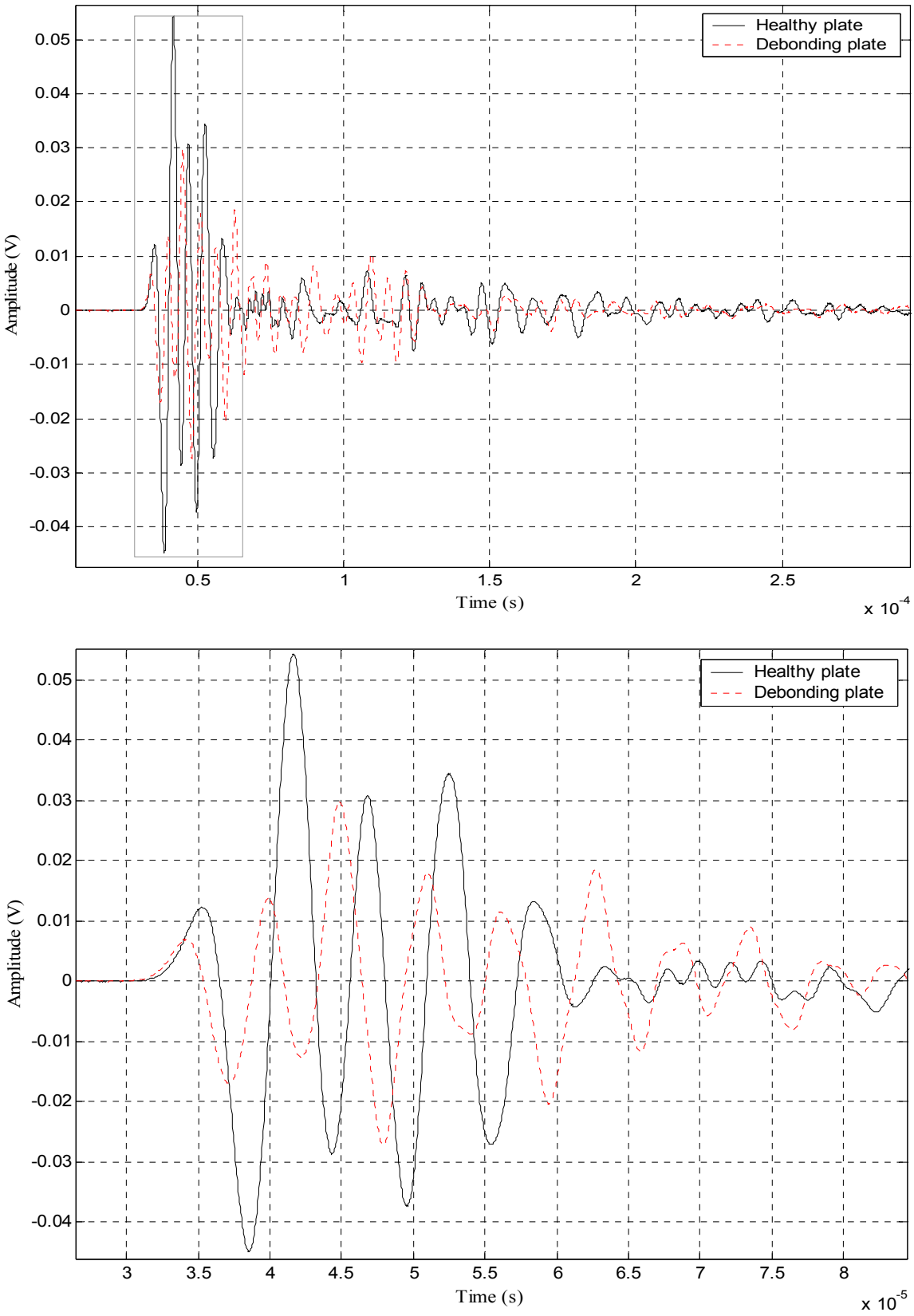

Figure 6.6. Comparison between healthy and debonding cases using electrodes 2 and 5

Table 6.1 shows the RMS values calculated for the ultrasonic signals (over a duration of 300 μs). It is calculated for different combination of electrode connections, for the healthy plate on one hand and the debonding case on the other hand.

Table 6.1. Root Mean Square values of the ultrasonic signal received for different combination of electrode connections

Electrodes		RMS value for the healthy plate (mV_{RMS})	RMS value for the defective plate (mV_{RMS})	Ratio healthy/defective
Send	Receive			
2	5	5.29	3.33	1.59
1	6	3.23	1.69	1.90
3	4	3.35	1.42	2.36
1	4	2.33	1.21	1.93
3	6	2.51	1.04	2.39
123	456	4.26	2.68	1.58
12	65	4.64	2.91	1.59
23	45	4.82	3.02	1.59

A duration of 300 μs is used for the calculation of the RMS value. Table 6.1 shows that the best combination is to use 3→4 or 3→6 for send/receive electrodes, or alternatively 1→4 or 1→6.

6.4 Ultrasonic NDE in a plate during low frequency actuation

6.4.1 Presentation of the experiment

The aim of this part is to see if the ultrasonic NDE is compatible with low frequency actuation in the plate. For this experiment, the function generator HP 33120A sends a pulse of 5 V and 1 MHz (one cycle) to a PZT. The other PZT is connected to the low-noise filter SRS SR560. The filtered signal is then displayed on the oscilloscope TDS

420A. For the low frequency actuation, the same signal generator is used. It sends its signal to the amplifier Krohn-hite 7500. This device is limited to 200 V peak. The generator produces a signal of 1.5 volts which is amplified a hundred times. The frequency ranges from 1 to 150 Hz.

At first, the high voltage is only applied to the central electrode of the piezo ceramic connected to the function generator. The "receiving" piezo is not submitted to low frequency actuation. The ultrasonic response is stored for different frequencies of actuation. For the second experiment, the high voltage is applied to the receiving piezo only. In the last experiment, both piezo ceramics are submitted to a high voltage.

6.4.2 NDE with low frequency actuation applied on the "sending" PZT of the plate

The healthy plate is used for this experiment. The ultrasonic pulse is sent to electrode 3 and received on electrode 4 (see Figure 6.1). For the low frequency actuation, a voltage of 150 V is applied to electrode 3 and the frequency can be set from 10 to 150 Hz.

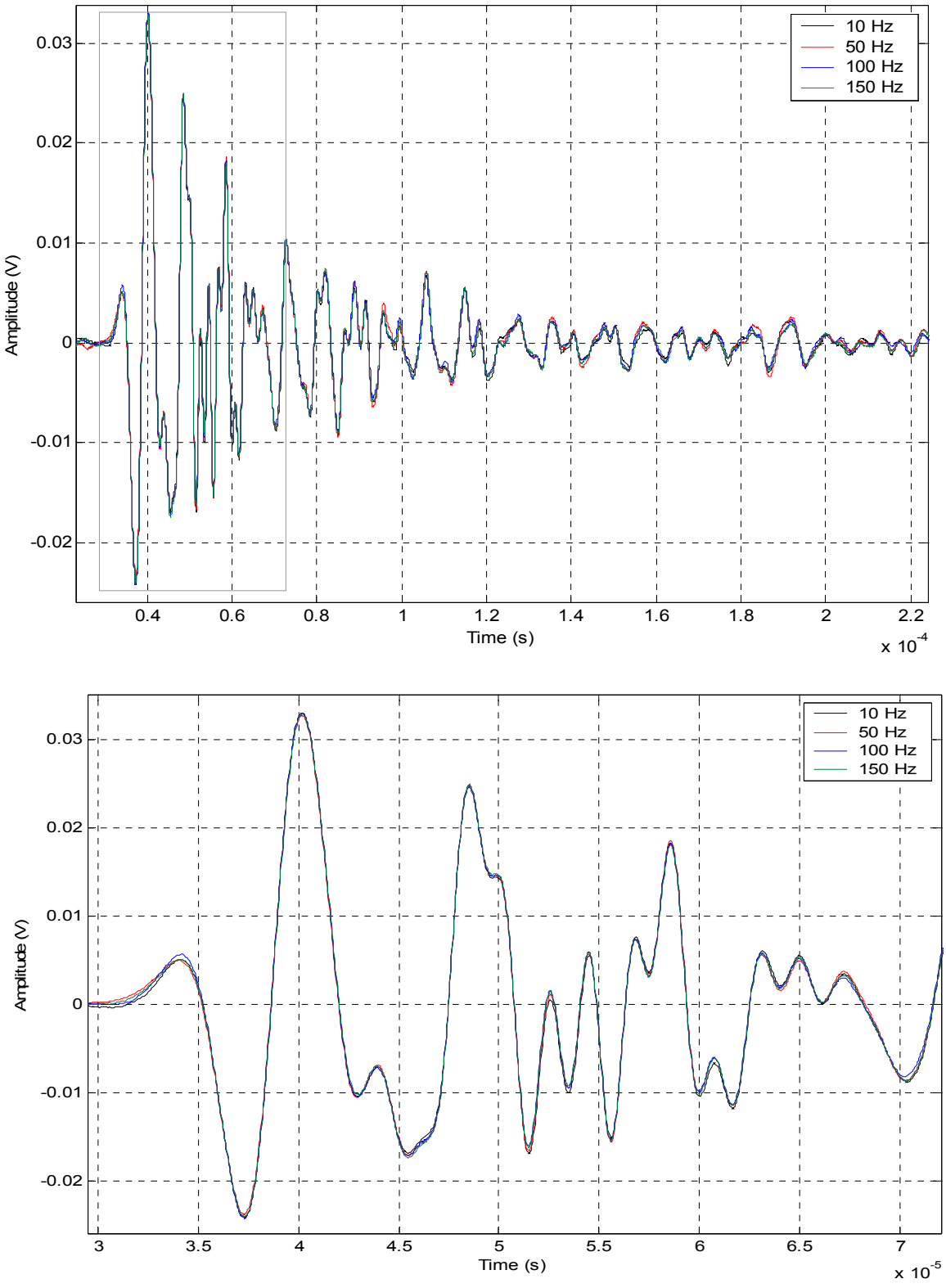

Figure 6.7. Ultrasonic response in the healthy plate during a low frequency actuation at 150 V and under different frequencies – high voltage applied on sending electrode

The results are shown in Figure 6.7. They correspond to a low frequency actuation signal of 10, 50, 100 and 150 Hz. The ultrasonic signal is sent continuously in the plate and is superimposed to the low frequency actuation. One can observe that signals are almost identical. The actuation applied to the "sending" PZT does not interfere with the ultrasonic signal.

6.4.3 NDE with actuation applied on the "receiving" PZT of the plate

The same experiment is performed, but this time, the low frequency high voltage signal is applied to the PZT connected to the oscilloscope (receiving PZT). The received signals are plotted on Figure 6.8. As expected, the low frequency of actuation does not interfere with the ultrasonic signals. The same experiment is performed for other different combinations of electrode connections with similar results. Hence, it is possible to monitor the integrity of the plate during low frequency actuation ranging from 1 to 150 Hz.

6.4.4 NDE with actuation applied on both "sending" and "receiving" PZT of the plate

To test the reliability of previous results, actuation is applied to both piezo ceramics. Furthermore, the defective plate is used for this experiment. The amplitude of the signal is smaller, and it may be more difficult to obtain a "good" signal. At first, electrodes 3 and 4 are used. Received signals are plotted on Fig 6.9 (a). The amplitude of responses are twice smaller than for the healthy plate, but signals are still visible. Though there is a debonding defect in the plate, the ultrasonic response is almost the same regardless the frequency of actuation (at 150 V). The RMS value corresponding to

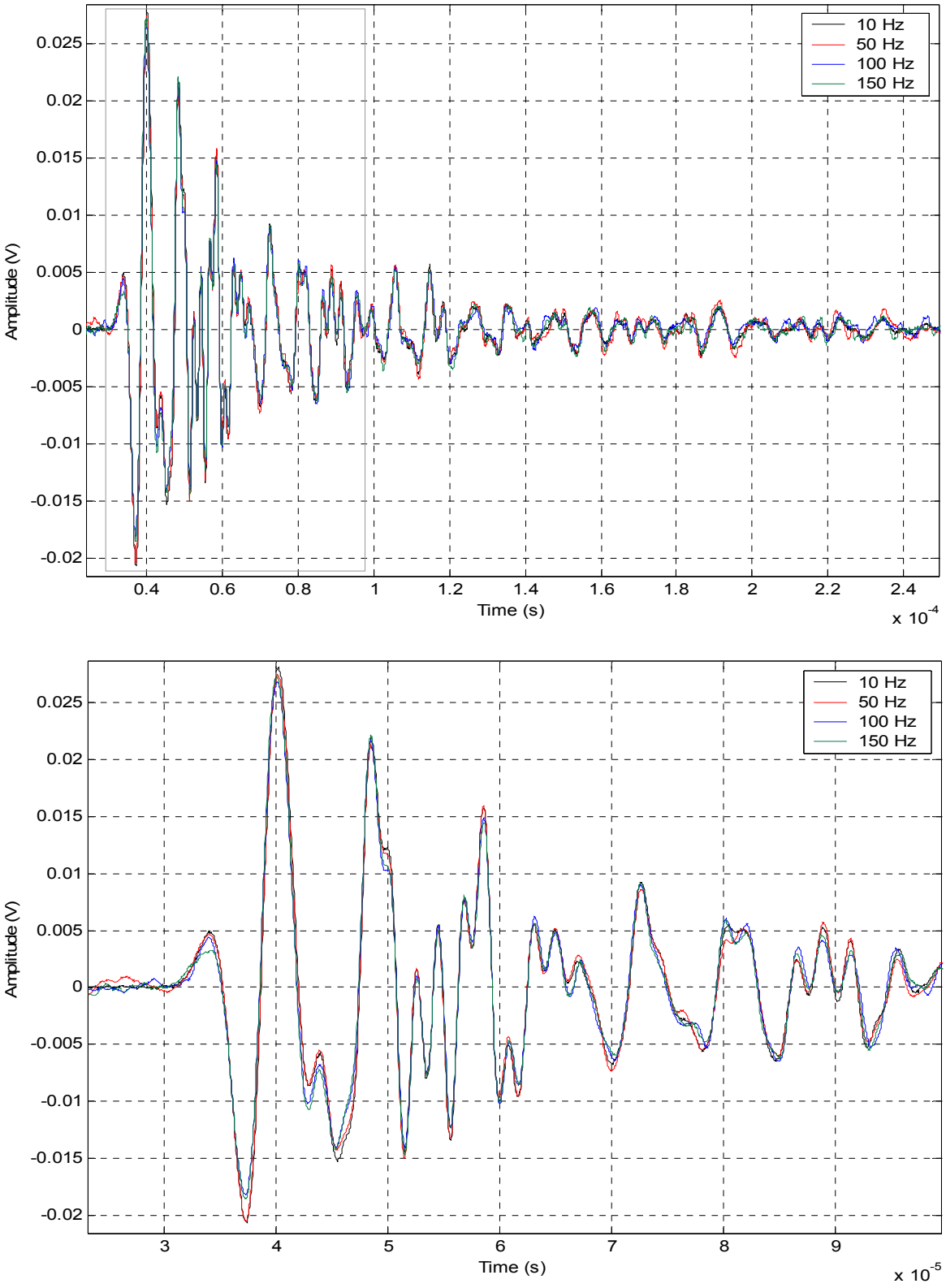

Figure 6.8. Ultrasonic response in the healthy plate during a low frequency actuation at 150 V and under different frequencies – high voltage applied on receiving electrode

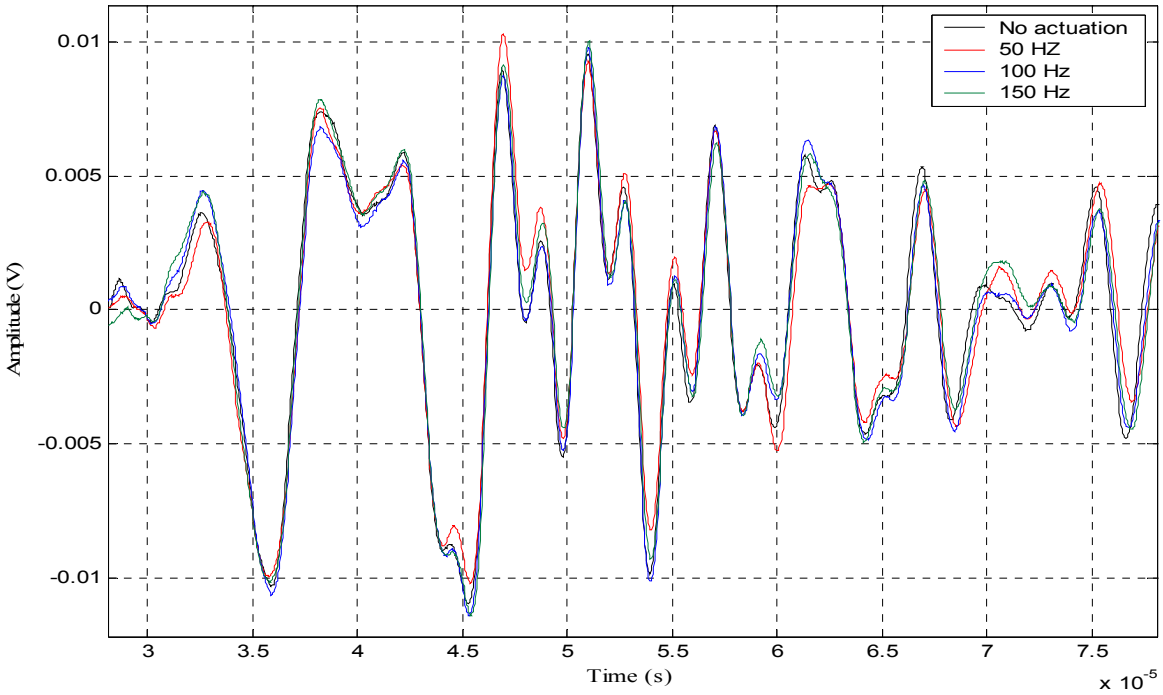

(a) Between electrodes 3 and 4

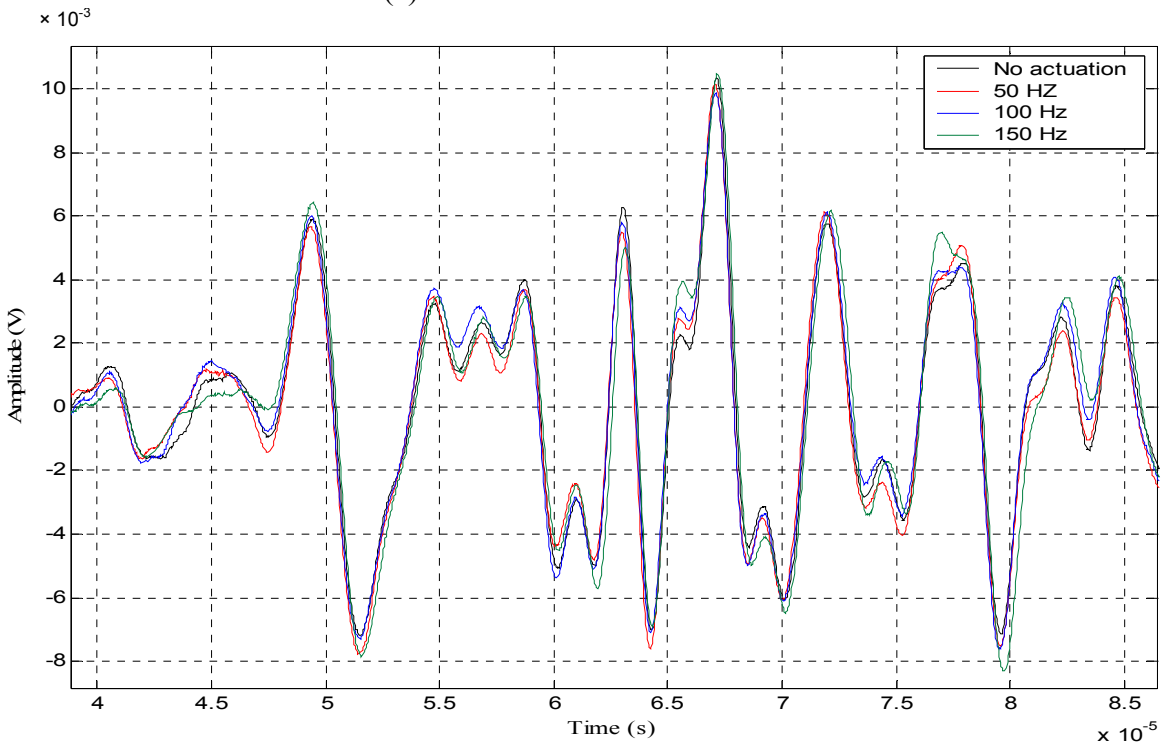

(b) Between electrodes 1 and 4

Figure 6.9. Ultrasonic responses in the debonding plate during a low frequency actuation at 150 V and under different frequencies – high voltage applied on receiving electrode

"no actuation", "50 Hz", "100 Hz" and "150 Hz" are respectively 0.00234, 0.00227, 0.00215 and 0.00215. These values are almost identical. Again, the ultrasonic NDE is not affected by the low frequency actuation.

Similar results are obtained using electrode 1 (send) and 4 (receive) as shown in Figure 6.9 (b). In summary, low frequency actuation does not interfere with ultrasonic NDE testing of the plate.

6.5Conclusion

Several conclusions can be drawn from this study:

- PZT elements embedded in fiber-epoxy layers can be used for ultrasonic monitoring of the plate assembly when the source and receiving elements are separated by 180 mm, even with fiber direction of some layers perpendicular to the propagation of the ultrasound.
- There is a noticeable difference between the ultrasound signal that propagates in a healthy composite and one that propagates in a damaged composite with a simulated debonding defect. A simple method to assess the presence of the defect is to measure the RMS signal of the first part of the signal. This simple method, however, does not allow one to localize the defect, or to characterize its length with precision.
- Low frequency actuation (150V, 1-150 Hz) of the plate (through either or both PZT actuators) does not interfere with NDE operations.

CHAPTER VII

CONCLUSIONS

Gradient Enhanced Piezoelectric Actuators, or GEPACs, are very thin piezoelectric plates embedded between several composite layers with different thermal properties. The anisotropic properties of the composite, and particularly the coefficient of thermal expansion leads to residual stresses that improves the actuator performance for low frequency actuation under high voltage (up to 500 V). These types of actuators are used primarily in the bending mode. Possible applications include "smart" active wings where the shape can be attered to improve performance. These actuators could also be embedded in an aircraft fuselage to provide means of actively controlling vibrations and interior noise. Because of the very thin (250 to 500 μm) piezoactive elements, it is important to be able to monitor the structural health integrity of these actuators while they are under low frequency actuation. The primary objective of this thesis was to establish that, by segmenting the electrodes of the actuator, one can perform ultrasonic nondestructive evaluation (NDE) of the actuator to detect the presence of cracks or debonding.

GEPAC actuators have been manufactured with multiple layers of unidirectional Kevlar fiber epoxy (0° / 0° / 90° / PZT / 90° / 90°) and cured in an autoclave at 177°C at 30 psi. The top electrode of the PZT was segmented by gently rubbing sandpaper. In all the results presented in this thesis, the input voltage for the ultrasonic signal was one cycle of a 1 MHz sine wave with amplitude of 5 V. At this frequency, the wavelenght is

much longer than the thickness of the PZT. Nevertheless, because of the multi-layered structure and the anisotropy of each layers, the received ultrasonic signal is rather complicated.

Experiments showed that the repeatibility of the signal was excellent, not only for the early arrivals but also for the very late arrivals, which correspond to the "reverberation" of ultrasound in the sample. Despite the complexity of the signal, the reverberation signature for a given GEPAC is very repeatable.

It was also established that utrasonic signals can be used to detect cracks in the actuator if the crack occurs after curing. If it occurs during manufacturing, resin fills up the crack and ultrasonic signals are not significantly affected by the presence of resin-filled cracks.

In this thesis, it was also established that the low –frequency, high voltage, high amplitude actuation of the device does not interfere with the high-frequency, low voltage, low amplitude of ultrasonic signals. It is therefore possible to monitor the structural integrity of the GEPAC actuator in real time while it undergoes low frequency actuation.

Fatigue testing of the GEPAC actuators was studied by measuring ultrasonic signals during life cycle up to 53 million cycles. No visible signs of fatigue could be observed up to 24 million cycles. Even late arrivals (ultrasonic reverberation) was remarkably similar for N=0 and N=24 $\times$ 10^6 cycles. After 27 million cycles, the main early part of the ultrasonic signal remained unchanged, but the late arrivals were noticeably different for N=0 and N=27 $\times$ 10^6 cycles. These experiments suggests that changes in the late arrivals (ultrasonic reverberation of the sample) are more sensitive to early signs of fatigue than the main ultrasonic signal. This result may be very useful for

practical implementation of structural health monitoring of GEPAC actuators with ultrasound NDE. Interestingly when the fatigue test was continued up to 53×10^6 cycles, no changes could be detected for either the early or the late arrivals.

Finally, experiments were conducted with two GEPAC actuators embedded in a Kevlar/epoxy plate, and separated by a distance of 180 mm. It was observed that (a) ultrasound (1 MHz pulse) propagates over this distance with enough amplitude that it can be used for NDE; (b) there is a noticeable difference between the ultrasonic signals in a healthy and a damaged composite plate. To artificially create debonding between the layers of the Kevlar epoxy plate, a release film was introduced during the manufacturing between two layers and removed after curing. A simple method to assess the presence of a defect is to measure the rms-signal amplitude of the received pulse. This method, however, does not allow one to localize the defect.

GEPAC with segmented electrodes are therefore promising for ultrasonic NDE monitoring of structural integrity of actuators and skins in aeronautical applications. Future work could include the problem of large arrays of embedded GEPAC actuators for large scale applications.

APPENDIX A – DISPERSION CURVES

In a linearly elastic medium, the relation between the stresses (τ) and the strains (ε) can be written as follows:

$$\tau_{ij} = C_{ijkl} \cdot \varepsilon_{kl} \quad \text{i,j,k,l} = 1,2,3 \qquad \text{(A.1)}$$

C_{ijkl} are the components of the elastic stiffness tensor (C). They are called the elastic constants. C is a fourth order tensor which is generally composed of $3^4 = 81$ independent elements. But the strain and stress tensors (respectively ε and τ) are symmetrical. So, the elastic constants are invariant by permutation of indexes i with j and k with l $C_{ijkl} = C_{jikl} = C_{ijlk}$

There are 36 independent components left in the stiffness tensor. The Voigt's notation allows classifying these components in a square matrix of dimension 6×6 by using the indexes contraction: ij→I and kl→J

$$11 \rightarrow 1 \; ; \; 22 \rightarrow 2 \; ; \; 33 \rightarrow 3 \; ; \; 23 = 32 \rightarrow 4 \; ; \; 13 = 31 \rightarrow 5 \; ; \; 12 = 21 \rightarrow 6$$

Equation A.1 can be rewritten as following: $\tau_I = C_{IJ} \cdot \varepsilon_J$

In general case, the behavior of a material is determined by 21 elastic constants which are non-zero numbers and independent. It is convenient to take into account the symmetries of material.

- One symmetrical plane

The mechanical properties of a material are assumed to be symmetrical with respect to a plane (for example, the plane of coordinate X3 = 0). In this case, eight elastic constants are equal to zero: $C_{14} = C_{24} = C_{34} = C_{64} = C_{15} = C_{25} = C_{35} = C_{65} = 0$

$$C = \begin{bmatrix} C_{11} & C_{12} & C_{13} & 0 & 0 & C_{16} \\ C_{12} & C_{22} & C_{23} & 0 & 0 & C_{26} \\ C_{13} & C_{23} & C_{33} & 0 & 0 & C_{36} \\ 0 & 0 & 0 & C_{44} & C_{45} & 0 \\ 0 & 0 & 0 & C_{45} & C_{55} & 0 \\ C_{16} & C_{26} & C_{36} & 0 & 0 & C_{66} \end{bmatrix}$$

There are 13 independent components.

- Orthotropic material

An orthotropic material has two perpendicular symmetrical planes. The stiffness matrix is defined by 9 independant elastic constants.

$$C = \begin{bmatrix} C_{11} & C_{12} & C_{13} & 0 & 0 & 0 \\ C_{12} & C_{22} & C_{23} & 0 & 0 & 0 \\ C_{13} & C_{23} & C_{33} & 0 & 0 & 0 \\ 0 & 0 & 0 & C_{44} & 0 & 0 \\ 0 & 0 & 0 & 0 & C_{55} & 0 \\ 0 & 0 & 0 & 0 & 0 & C_{66} \end{bmatrix}$$

There are 9 independent components.

- Transversely isotropic material

In a transversely isotropic material, there is invariance of elastic constants with respect to a rotational axis. It is noted that the medium is already orthotropic since all planes containing the rotational axis are symmetrical plane. If the axis X1 is a symmetrical axis, there are the following relations: $C_{22} = C_{33}$; $C_{12} = C_{13}$; $C_{55} = C_{66}$; $C_{44} = ½ (C_{22} – C_{23})$

$$C = \begin{bmatrix} C_{11} & C_{12} & C_{13} & 0 & 0 & 0 \\ C_{12} & C_{11} & C_{13} & 0 & 0 & 0 \\ C_{13} & C_{13} & C_{33} & 0 & 0 & 0 \\ 0 & 0 & 0 & C_{44} & 0 & 0 \\ 0 & 0 & 0 & 0 & C_{55} & 0 \\ 0 & 0 & 0 & 0 & 0 & C_{55} \end{bmatrix}$$

There are 5 independent components.

- Isotropic material

In this case, the stiffness matrix is defined by 2 independent coefficients (the Lamé's coefficients):

$$\lambda = \frac{E.\nu}{(1+\nu)(1-2\nu)} \quad \text{and} \quad \mu = \frac{E}{2(1+\nu)} \tag{A.2}$$

with E: Young modulus of the material

ν: Poisson ratio

The elastic constants are defined by

$$C_{11} = C_{22} = C_{33} = \lambda + 2\mu$$
$$C_{44} = C_{55} = C_{66} = \mu$$
$$C_{12} = C_{13} = C_{21} = C_{23} = C_{31} = C_{32} = \lambda$$
$$C_{44} = 1/2 \times (C_{11} - C_{12})$$

In general the elastic wave quation can be written in the form (Auld 1990)

$$\frac{\partial \tau_{ij}}{\partial x_j} - \rho \frac{\partial^2 u_i}{\partial t^2} = 0 \qquad \text{i,j = 1,2,3} \tag{A.3}$$

where τ is the stress tensor and u_i is the displacement vector of the particles in the direction Xi.

Substituing equation A.1, one obtains:

$$C_{ijkl} \frac{\partial \varepsilon_{ij}}{\partial x_j} - \rho \frac{\partial^2 u_i}{\partial t^2} = 0 \qquad \text{i,j,k,l = 1,2,3} \tag{A.4}$$

To obtain a wave equation in terms of u, it is necessary to find an expression for ε in terms of u. The strain tensor can be expressed by the following relation:

$$E = \frac{1}{2}\left[grad\vec{u} + grad\vec{u}^{T} + grad\vec{u}^{T} \times grad\vec{u}\right] \tag{A.5}$$

Under the assumption of small disturbances, the strain state is represented by the linearised strain tensor:

$$E = \frac{1}{2}\left[grad\vec{u} + grad\vec{u}^{T}\right] \tag{A.6}$$

In index notation:

$$\varepsilon_{ij} = \frac{1}{2}(u_{i,j} + u_{j,i}) \qquad \text{i,j = 1,2,3} \tag{A.7}$$

with $u_{i,j} = \frac{\partial u_i}{\partial x_j}$

By combining the relations (A.4) and (A.7), the following set of three equations is obtained:

$$C_{ijkl}\frac{\partial u_k}{\partial x_j \partial x_l} - \rho\frac{\partial^2 u_i}{\partial t^2} = 0 \qquad \text{i,j,k,l} = 1,2,3 \qquad \text{(A.9)}$$

This is the general equation of propagation for a wave in a material.We consider now propagation in an orthotropic plate (figure A.1) of thickness 2×h. The coordinate axes X1, X2 and X3 correspond to the three principal directions of the plate.

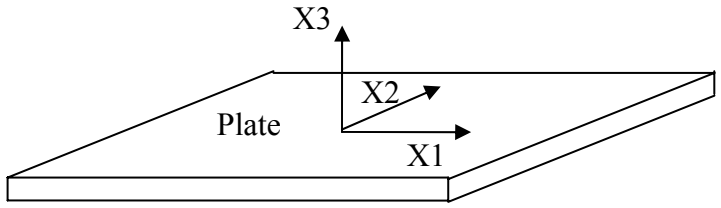

Figure A.1. Sheet of paper modelled as an orthotropic plate

We consider propagation of Lamb waves in the X1 direction. Given the nature of this type of waves, the displacements of the particles occurs in the X1 and X3 directions. In other terms, there is no displacement in the X2 direction $\Rightarrow u_2 = 0$.

By using Voigt's notation for the elastic constants, the equation (A.9) can be written as following:

$$\begin{aligned}\rho\frac{\partial^2 u_1}{\partial t^2} &= C_{11}u_{1,11} + C_{13}u_{3,13} + C_{55}(u_{1,33} + u_{3,13}) \\ \rho\frac{\partial^2 u_3}{\partial t^2} &= C_{33}u_{3,33} + C_{13}u_{1,13} + C_{55}(u_{1,13} + u_{3,11})\end{aligned} \tag{A.10}$$

For harmonic propagation at frequency f = ω/2π, the particle displacement are given by:

$$\begin{aligned}u_1 &= U_1\exp[i(k_1x_1 + k_3x_3 - \omega t)] \\ u_3 &= U_3\exp[i(k_1x_1 + k_3x_3 - \omega t)]\end{aligned} \tag{A.11}$$

In the previous equations, the parameters are:

- U_1: amplitude of displacement u_1
- U_3: amplitude of displacement u_3
- k_1: wave number (in the direction X1)
- k_3: wave number (in the direction X3)
- ω: angular frequency

By replacing the expression of u1 and u3 in the equations of propagation (A.10):

$$\begin{aligned}\rho u_1\omega^2 &= C_{11}U_1k_1^2 + (C_{55} + C_{13})U_3k_1k_3 + C_{55}U_1k_3^2 \\ \rho u_3\omega^2 &= C_{55}U_3k_1^2 + (C_{55} + C_{13})U_1k_1k_3 + C_{33}U_3k_3^2\end{aligned} \tag{A.12}$$

U_1 and U_3 are eliminated in these two equations:

$$(C_{13}+C_{55})^2 k_1^2 k_3^2 = (\rho\omega^2 - C_{55}k_1^2 - C_{33}k_3^2)(\rho\omega^2 - C_{11}k_1^2 - C_{55}k_3^2) \qquad \text{(A.13)}$$

Equation A.13 is a quadratic equation in k_3^2 whose solutions are:

$$k_{3\pm}^2 = k_1^2 \frac{[-\overline{B} \pm \sqrt{\overline{B}^2 - \overline{A}\overline{C}}]}{2\overline{A}} \qquad \text{(A.14)}$$

With
$$\begin{aligned} \overline{A} &= C_{33}C_{55} \\ \overline{B} &= (C_{11}-\rho c^2)C_{33} + (C_{55}-\rho c^2)C_{55} - (C_{13}+C_{55})^2 \\ \overline{C} &= (C_{11}-\rho c^2)(C_{55}-\rho c^2) \end{aligned} \qquad \text{(A.15)}$$

c is the phase velocity of the waves in the direction X_1 and is related to the frequency by the relation:

$$c = \frac{\omega}{k} \qquad \text{(A.16)}$$

By using previous equations, the ratio U_3/U_1 is given by the relation:

$$\frac{U_3}{U_{1\pm}} = \frac{(\rho\omega^2 - C_{11}k_1^2 - C_{55}k_{3\pm}^2)}{(C_{55}+C_{13})k_1 k_{3\pm}} \qquad \text{(A.17)}$$

Now that k_3 and U_3/U_1 are determined, it is possible to construct the displacements u1 and u3 describing the propagation of Lamb waves. Given that the equation A.13 has 4 solutions for k_3, the displacements have the following form:

$$u_1 = e^{i(k_1 x_1 - \omega t)}\left[A e^{ik_{3+}x_3} + B e^{-ik_{3+}x_3} + D e^{ik_{3-}x_3} + E e^{-ik_{3-}x_3}\right] \tag{A.18}$$

$$u_3 = e^{i(k_1 x_1 - \omega t)}\left[\frac{U_3}{U_{1+}}\left[A e^{ik_{3+}x_3} - B e^{-ik_{3+}x_3}\right] + \frac{U_3}{U_{1-}}\left[D e^{ik_{3-}x_3} - E e^{-ik_{3-}x_3}\right]\right]$$

A, B, C and D are constants. The top and bottom surfaces of the plate are assumed to be stress free, which means that the displacements u_1 and u_3 must meet the following boundary conditions at $x_3 = \pm h$:

$$\begin{aligned} \tau_{33} &= C_{33}u_{3,3} + C_{13}u_{1,1} = 0 \\ \tau_{31} &= C_{55}u_{1,3} + C_{55}u_{3,1} = 0 \end{aligned} \tag{A.19}$$

Equations A.18 and A.19 can be written as:

$$\begin{bmatrix} F_+ e^{ik_{3+}h} & F_+ e^{-ik_{3+}h} & F_- e^{ik_{3-}h} & F_- e^{-ik_{3-}h} \\ F_+ e^{-ik_{3+}h} & F_+ e^{ik_{3+}h} & F_- e^{-ik_{3-}h} & F_- e^{ik_{3-}h} \\ G_+ e^{ik_{3+}h} & -G_+ e^{-ik_{3+}h} & G_- e^{ik_{3-}h} & -G_- e^{-ik_{3-}h} \\ G_+ e^{-ik_{3+}h} & -G_+ e^{ik_{3+}h} & G_- e^{-ik_{3-}h} & -G_- e^{ik_{3-}h} \end{bmatrix} \begin{bmatrix} A \\ B \\ C \\ D \end{bmatrix} = 0 \tag{A.20}$$

where

$$\begin{aligned} F_\pm &= C_{33}k_{3\pm}\frac{U_3}{U_{1\pm}} + C_{13}k_1 \\ G_\pm &= k_1\frac{U_3}{U_{1\pm}} + k_{3\pm} \end{aligned} \tag{A.21}$$

The matrix relation (A.20) has non trivial solution only if the determinant of the matrix 4×4 equals zero. It can be shown that this occurs when:

$$\frac{\tan(k_{3+}h)}{\tan(k_{3-}h)} = \left[\frac{F_+ G_-}{F_- G_+}\right]^{\pm 1} \tag{A.22}$$

Equation (A.22) is a relation between the phase velocity c and the frequency ω. This is the orthotropic Lamb wave dispersion equation. It must be satisfied for the propagation of Lamb waves. The exponent of the right term in equation (A.22) determines the mode of propagation of the wave. If it equals 1, the mode of propagation is symmetric. Then, in the expressions of u_1 and u_3, there are the following equalities: A=B and D=E. On the other hand, if the determinant is -1, the mode of propagation is antisymmetric. The equalities are A=-B and D=-E. Figure A.2 illustrates the lowest symmetric (S_0) and antisymmetric (A_0) modes of propagation.

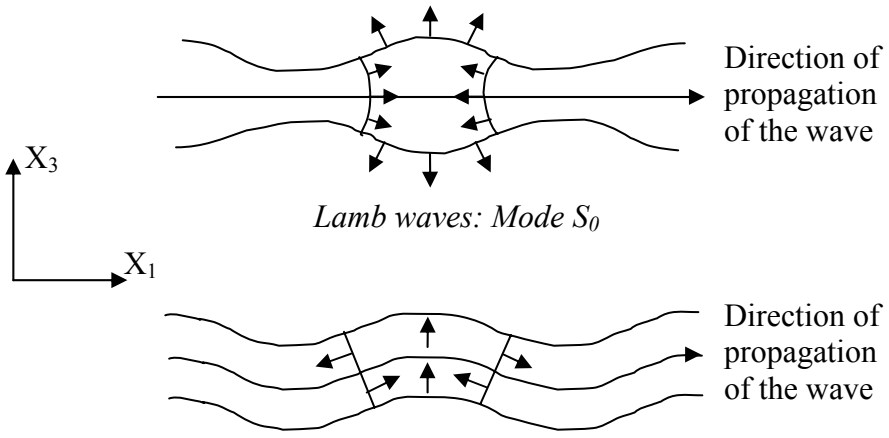

Figure A.2. The first two modes of propagation for Lamb wave in a plate

Because equation (A.22) is poorly conditioned, its solutions are difficult to compute. To avoid this drawback, it is convenient to use Schenck's method, which consists of the evaluation of the expression $\log(1+|\det(M)|)$ for a given frequency and a given phase velocity, where M is the matrix given by:

$$M = \begin{bmatrix} F_+ e^{ik3+h} & F_+ e^{-ik3+h} & F_- e^{ik3-h} & F_- e^{-ik3-h} \\ F_+ e^{-ik3+h} & F_+ e^{ik3+h} & F_- e^{-ik3-h} & F_- e^{ik3-h} \\ G_+ e^{ik3+h} & -G_+ e^{-ik3+h} & G_- e^{ik3-h} & -G_- e^{-ik3-h} \\ G_+ e^{-ik3+h} & -G_+ e^{ik3+h} & G_- e^{-ik3-h} & -G_- e^{ik3-h} \end{bmatrix}$$

The roots of the dispersion curves correspond to low values of this equation. In fact, there is a root when the determinant of the matrix M is zero, which means that the value $\log(1+|\det(M)|)$ should be zero.

A MATLAB numerical program has been written to plot the dispersion curves of orthotropic plate. More details can be found in the Projet de Fin d'Etude (PFE report), ENSAM-Metz, 2003, by Gex and Chen. The following figures show the sensitivity of dispersion curves to variation of 20% of specific elastic constants. For these curves, the thickness of the plate is 90 μm and the values of elastic constants are

C11 = 10.29 GPa	C13 = 0.15 GPa	C55 = 0.30 GPa
C22 = 5.34 GPa	C23 = 0.15 GPa	C33 = 0.15 GPa
C44 = 0.20 GPa		

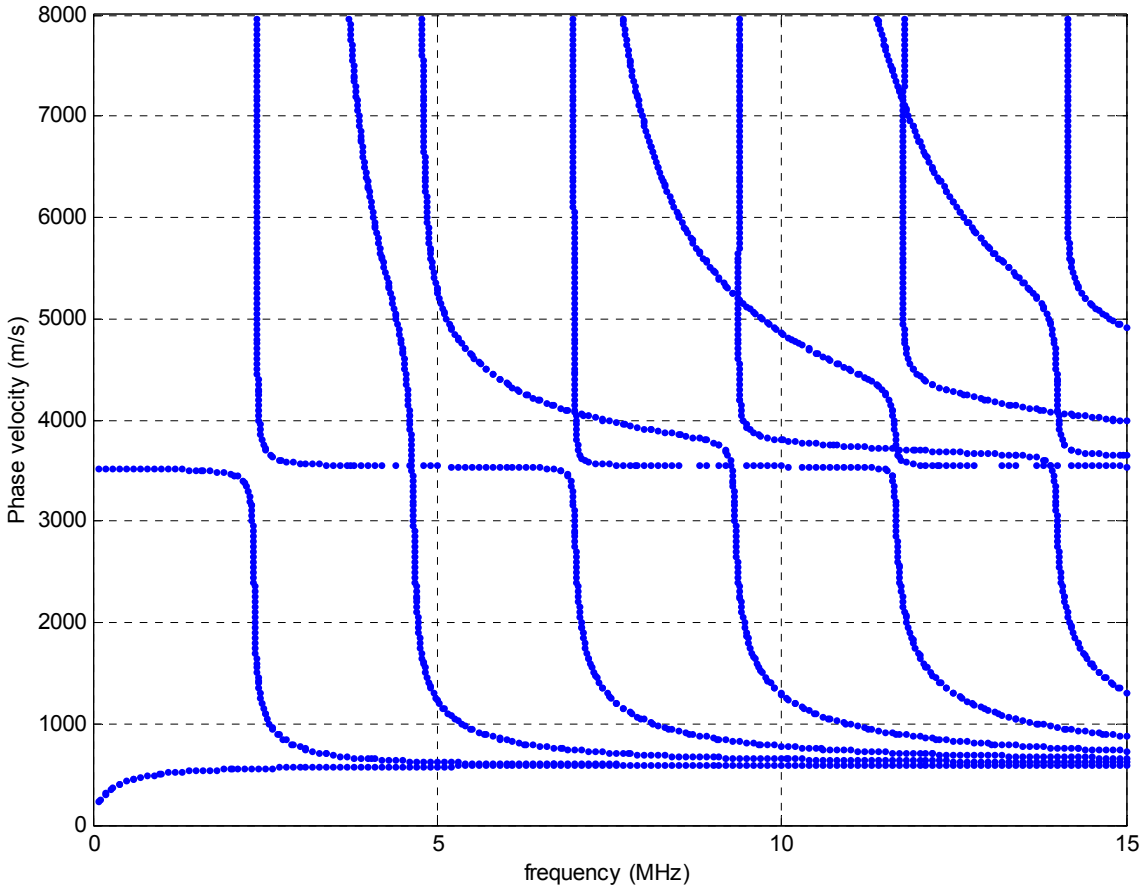

Figure A.3. Dispersion curves in an orthotropic plate

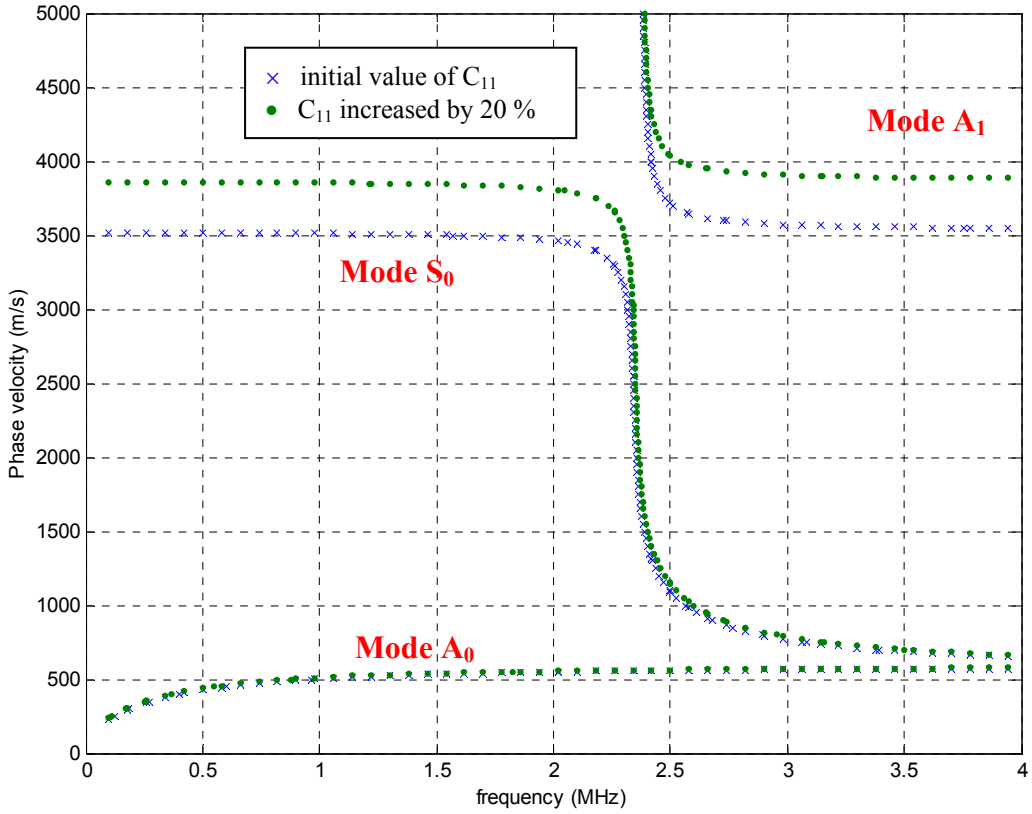

Figure A.4. Effect of the variation of C_{11} on the dispersion curves

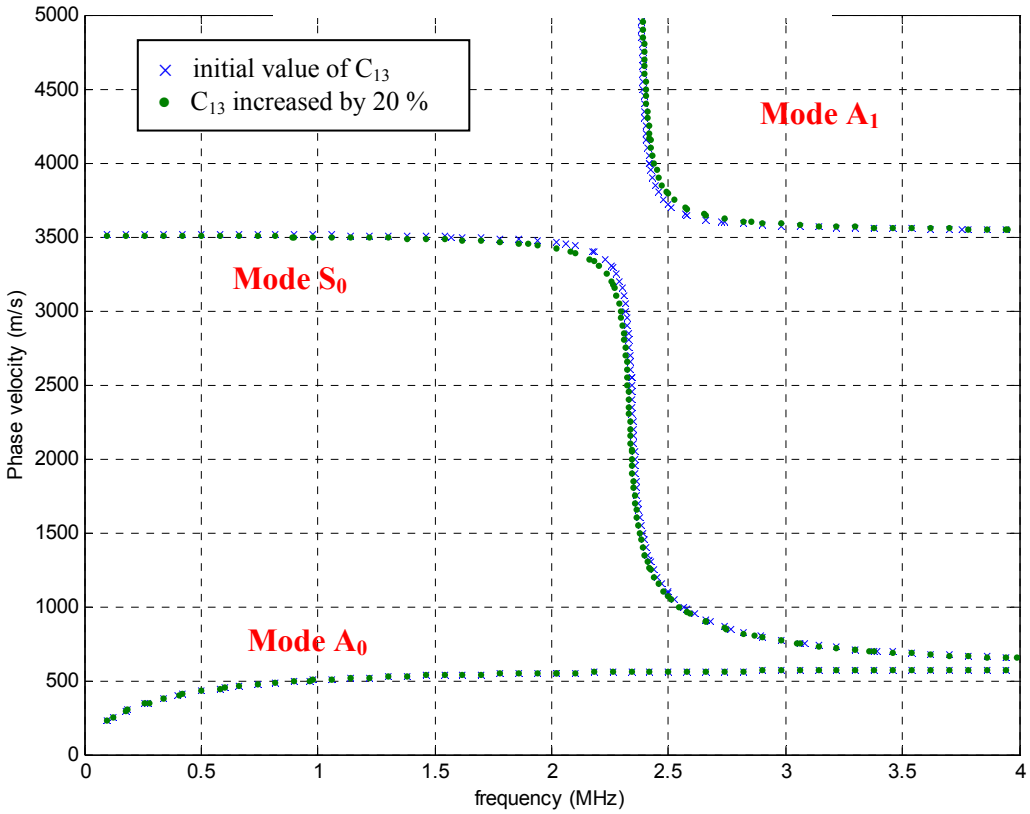

Figure A.5. Effect of the variation of C_{13} on the dispersion curves

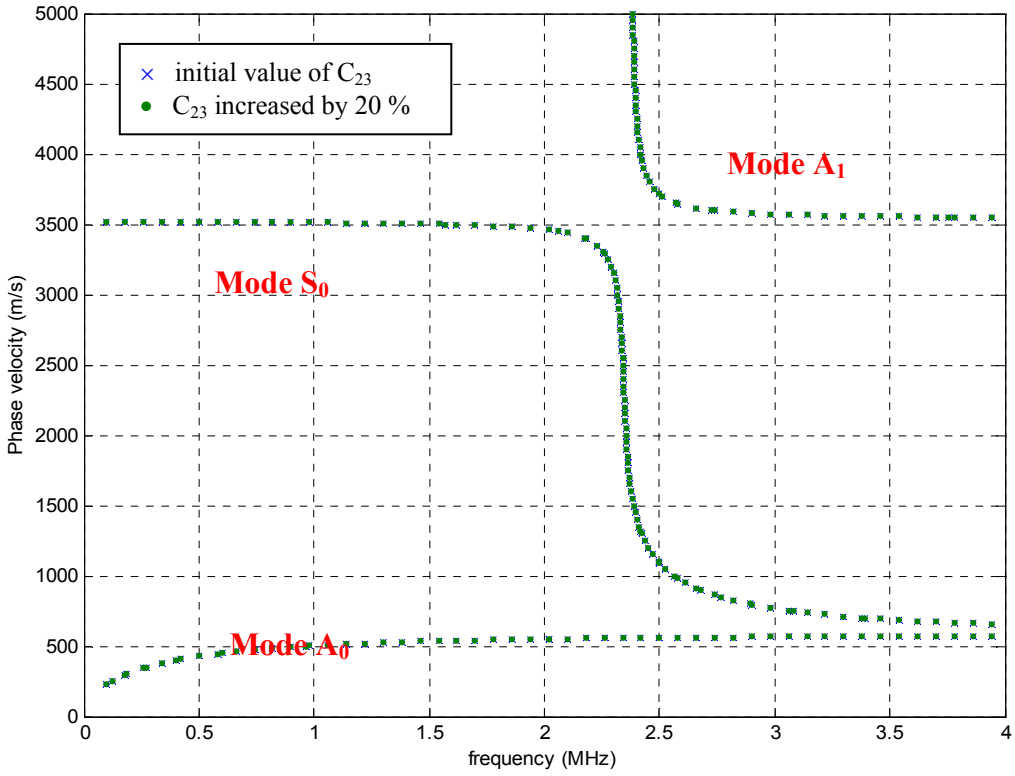

Figure A.6. Effect of the variation of C_{23} on the dispersion curves

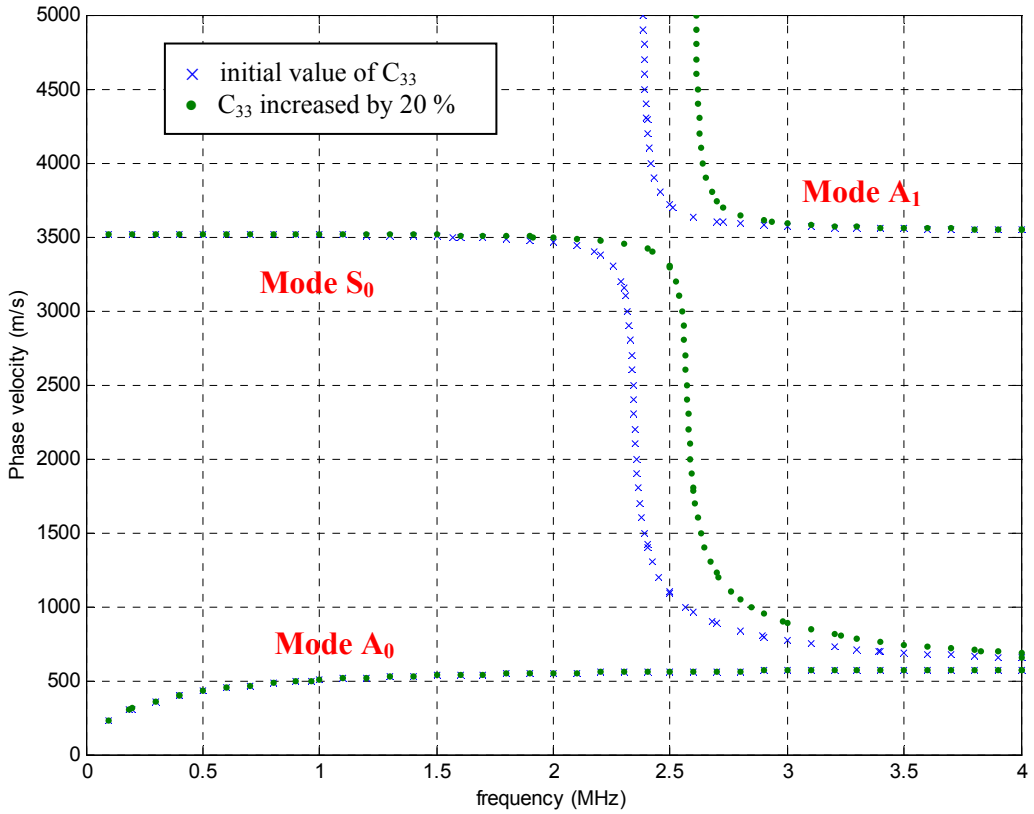

Figure A.7. Effect of the variation of C_{33} on the dispersion curves

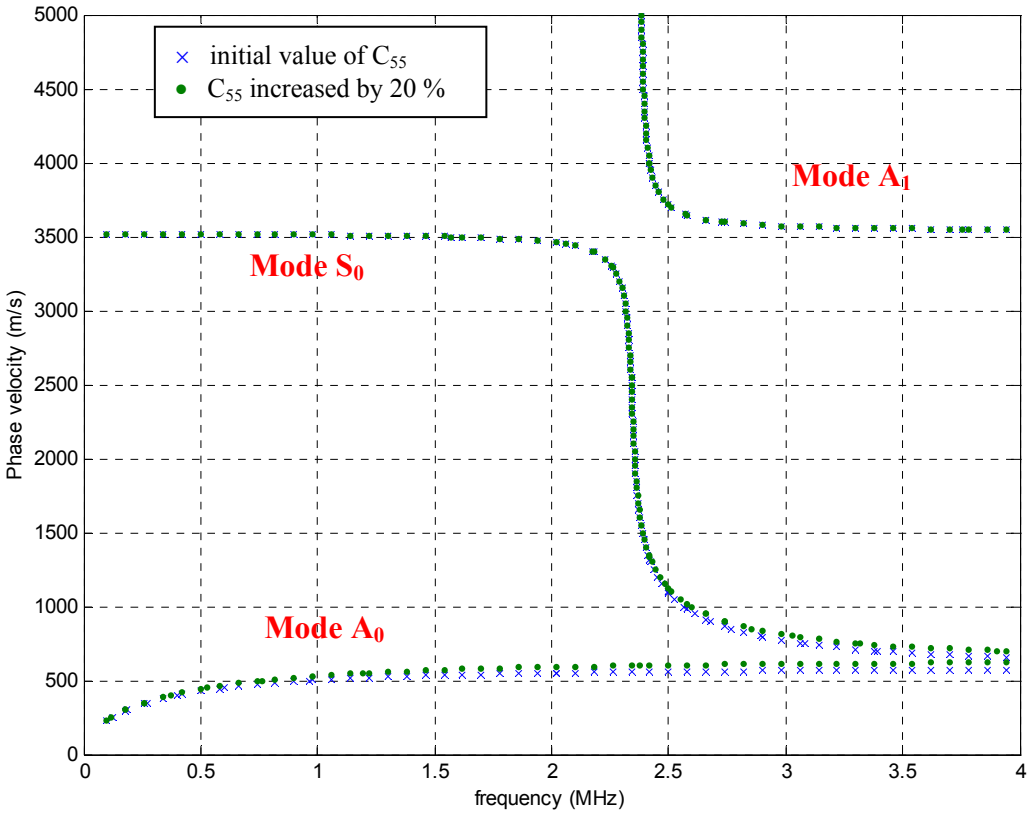

Figure A.8. Effect of the variation of C_{55} on the dispersion curves

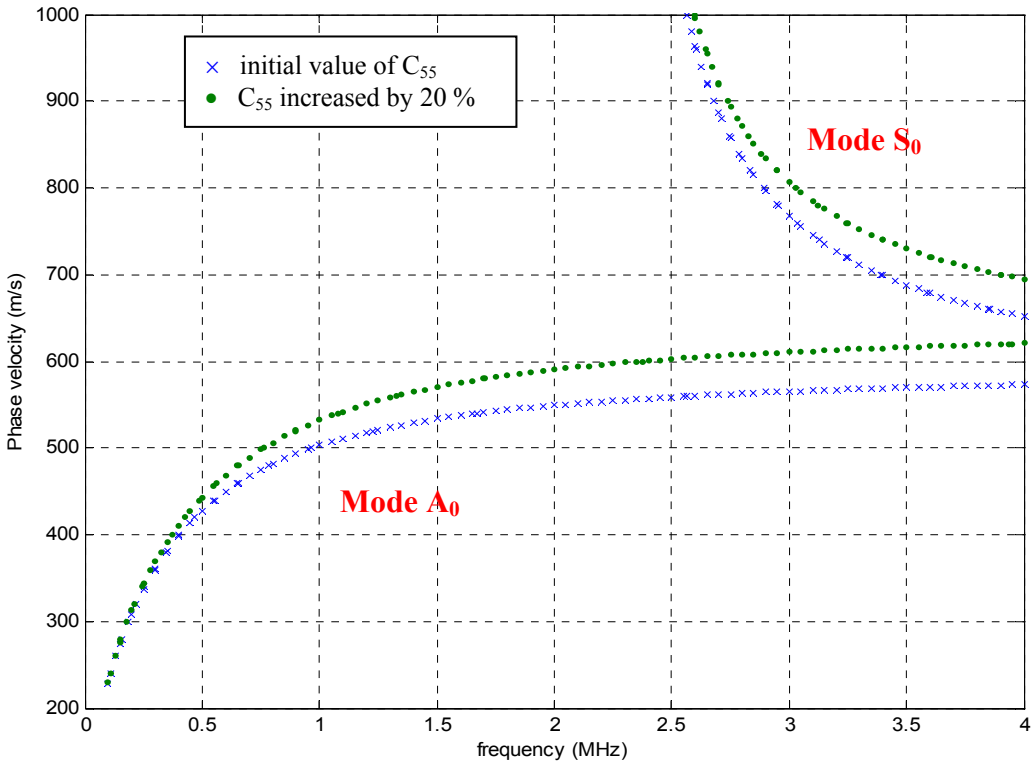

Figure A.9. Zoom on the effect of the variation of C_{55} on the dispersion curves

Finally, one can derive dispersion curve for the case chaere the boundary conditions at the bottom and top ($X_3 = \pm h$) are not stress free, but instead zero displacement. In this case equation A.19 is replaced by $u_1 = u_3 = 0$ at $X_3 = \pm h$. The resulting dispersion curve is shown in figure A.9.

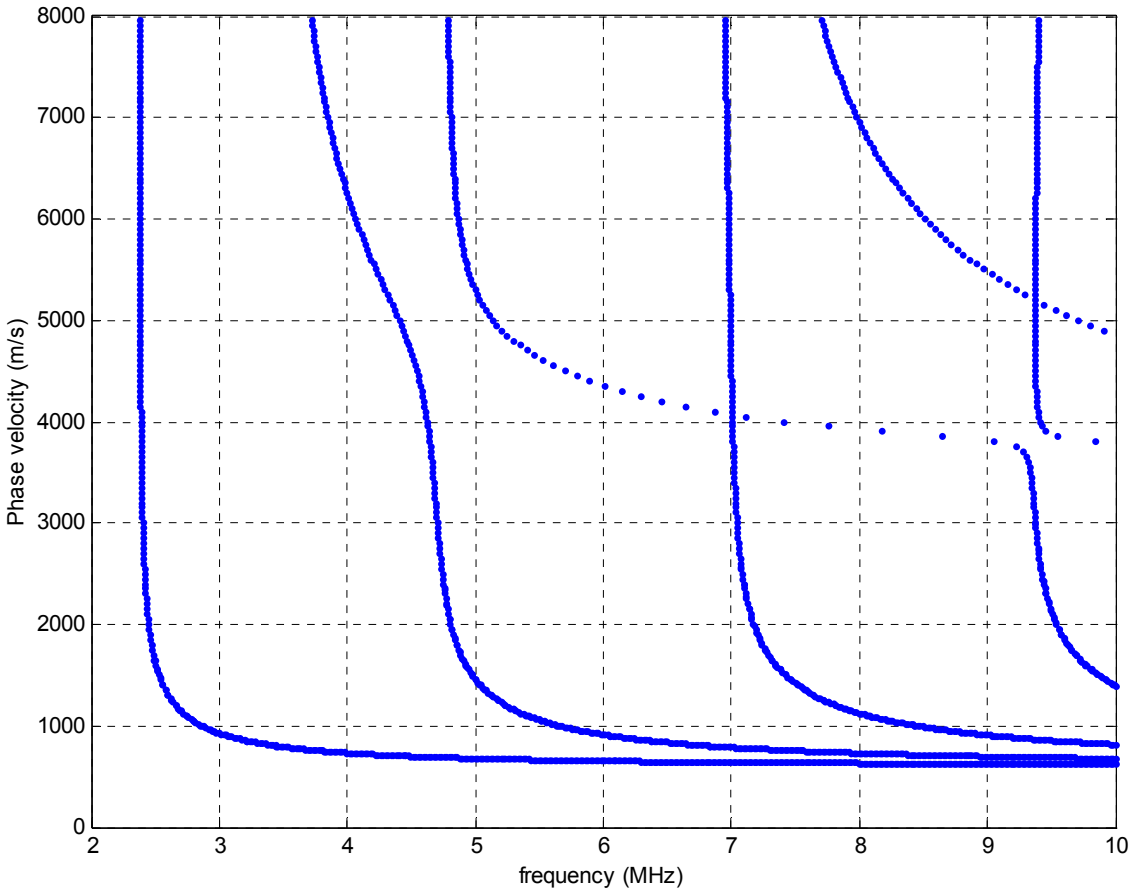

Figure A.10. Dispersion curves for an orthotropic plate with U_1=0 and U_3=0

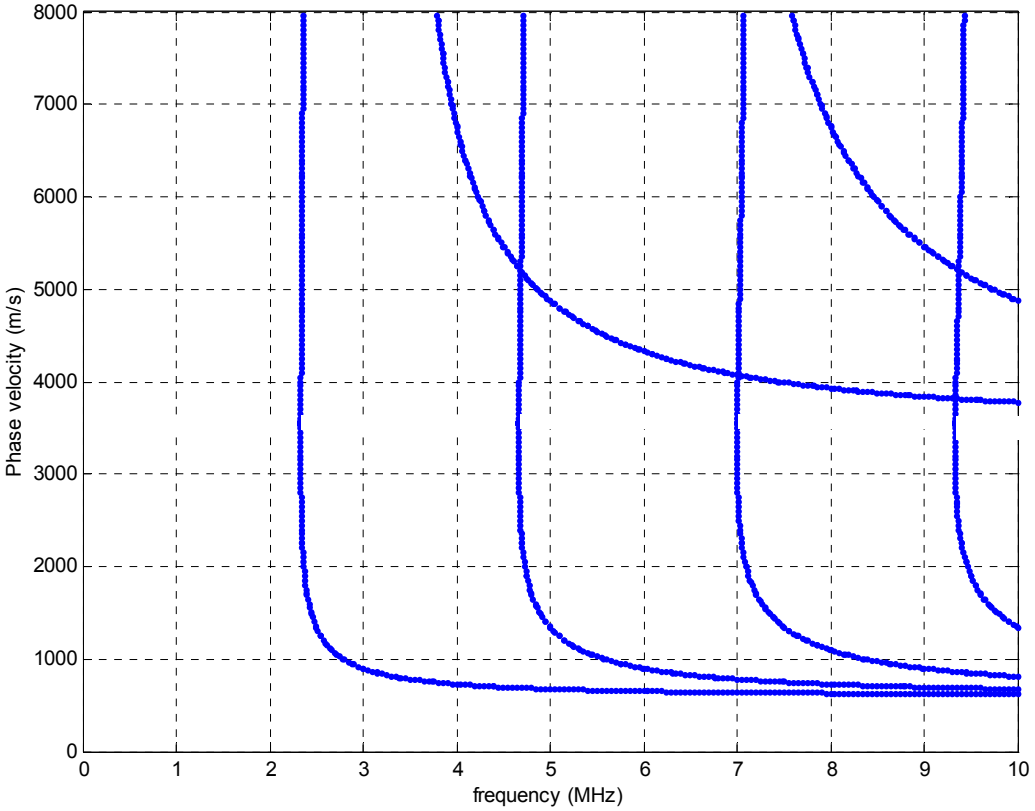

Figure A.11. Dispersion curves for an orthotropic plate with $U_1=0$ and $\tau_{33}=0$

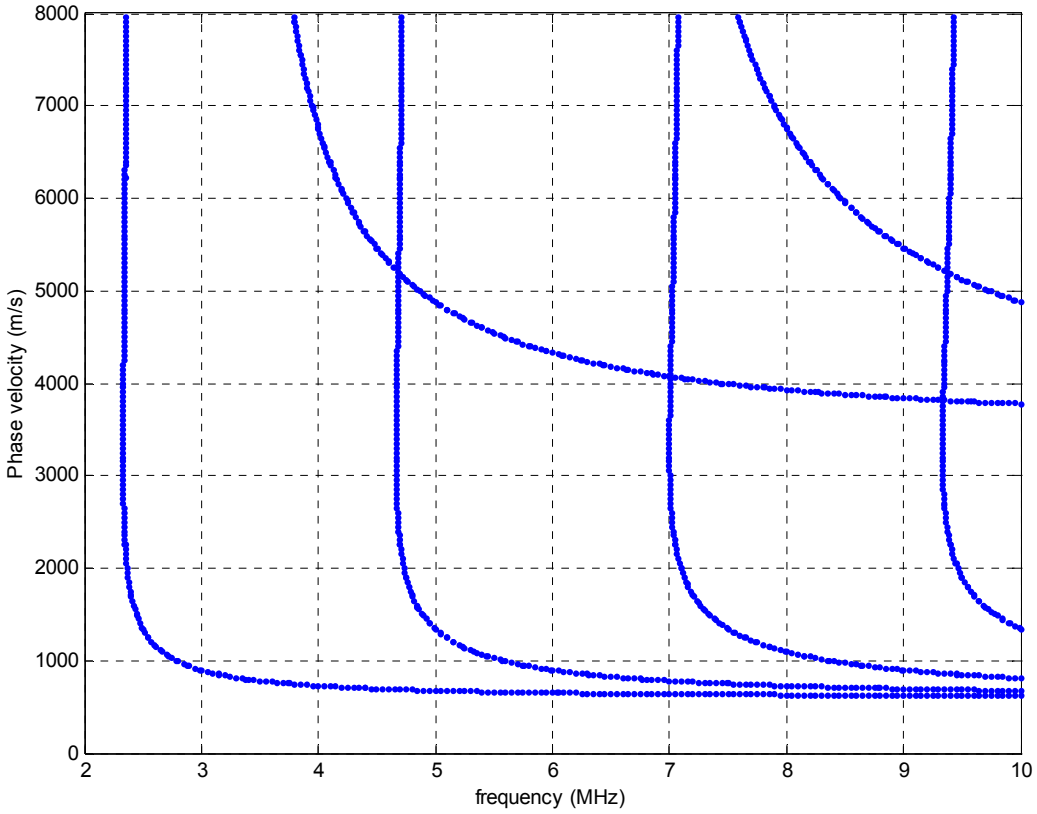

Figure A.12. Dispersion curves for an orthotropic plate with $U_3=0$ and $\tau_{31}=0$

APPENDIX B – DOME DISPLACEMENT

This appendix complements section 5.1.2 by showing dome height displacements at N = 200,000 cycles, N = 400,000 cycles, and N = 850,000 cycles, as well as hysteresis between dome-height displacement and applied voltage during the low frequency cycle (10 Hz).

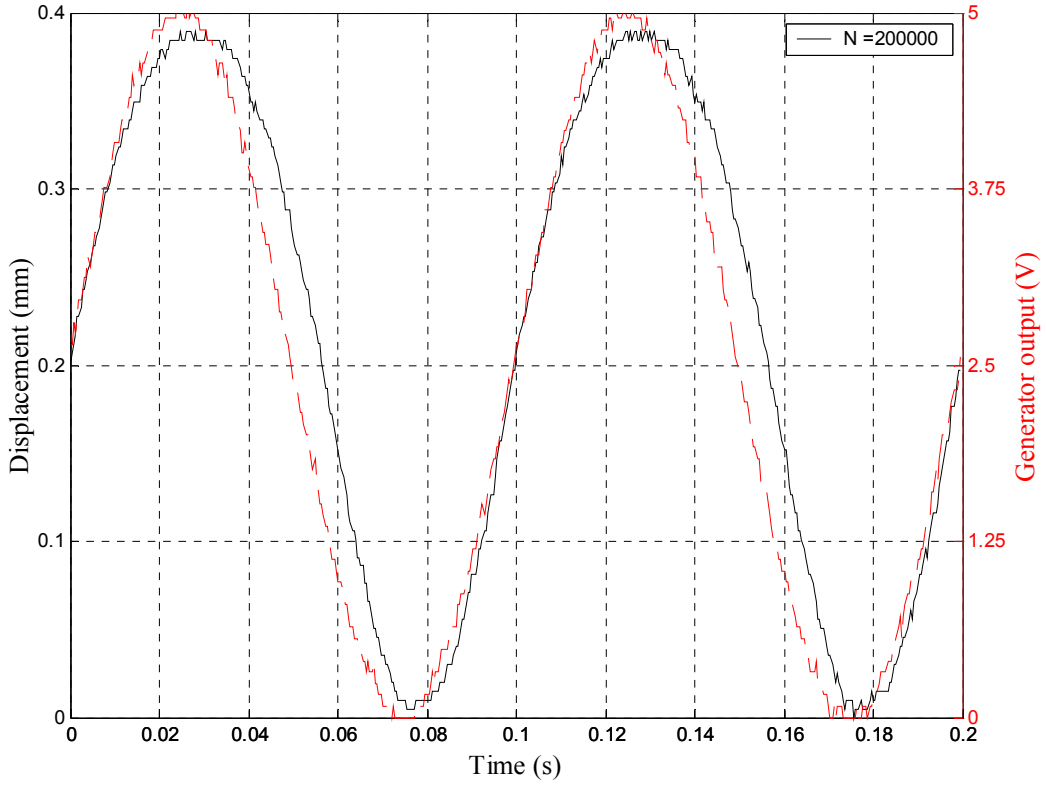

Figure B.1. Dome height displacement and generator output for N = 200,000 cycles

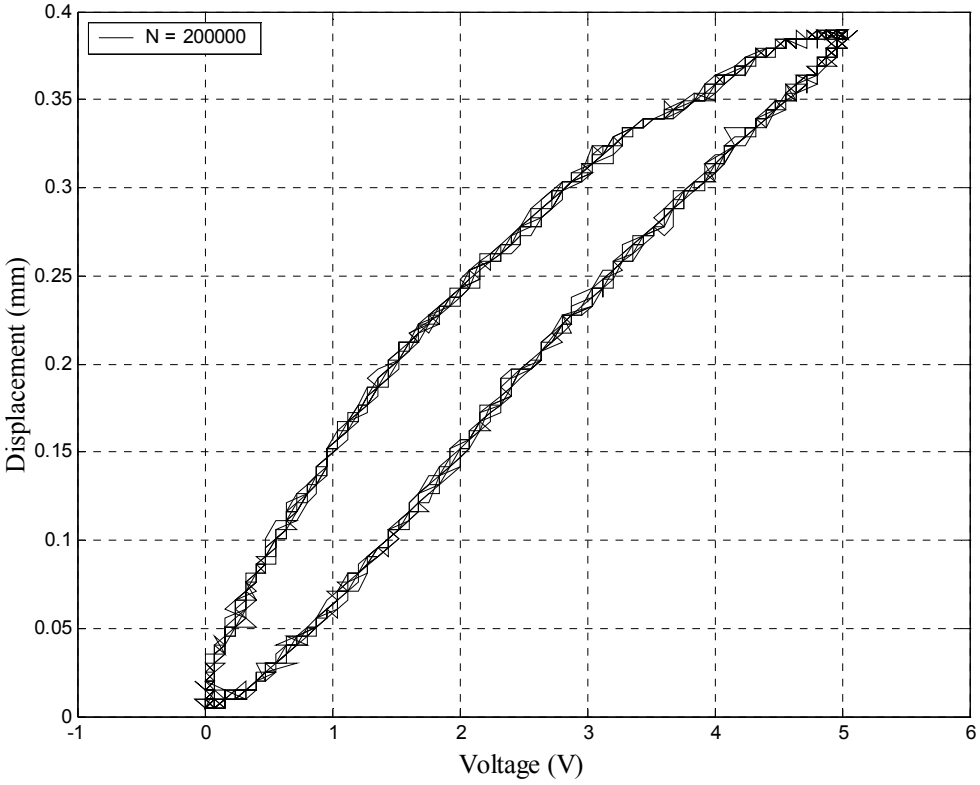

figure B.2 Hysteresis cycle of displacement vs voltage for N = 200,000 cycles

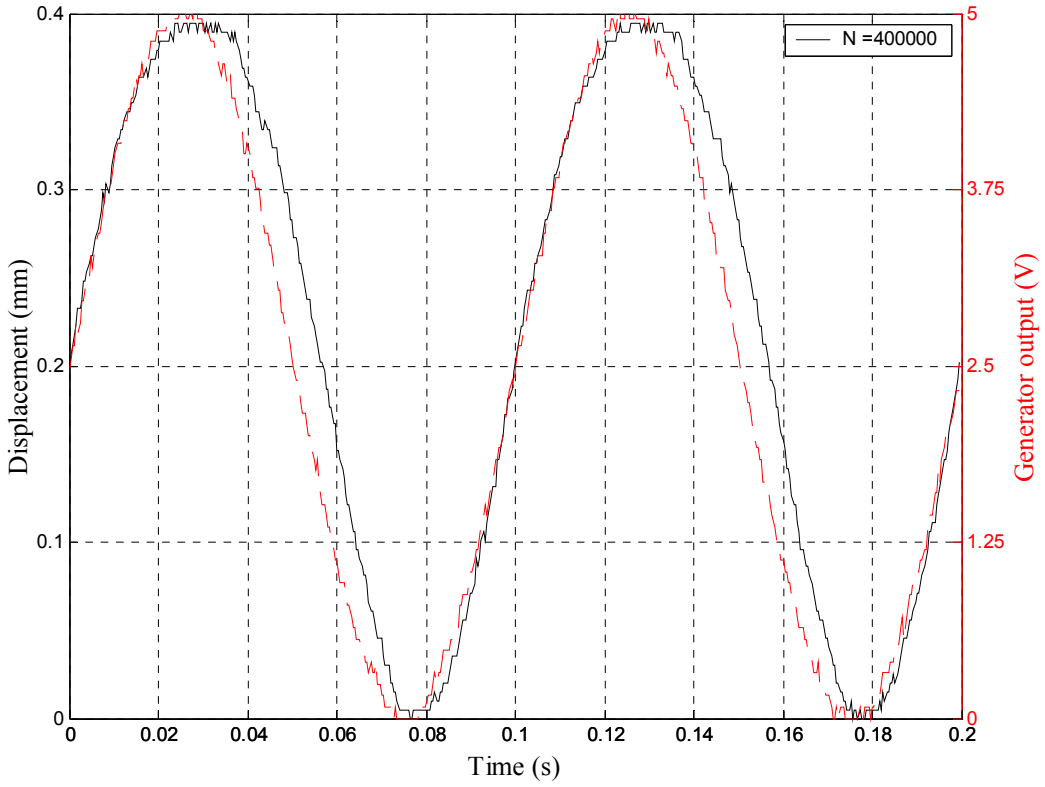

Figure B.3 Dome height displacement and generator output for N = 400,000 cycles

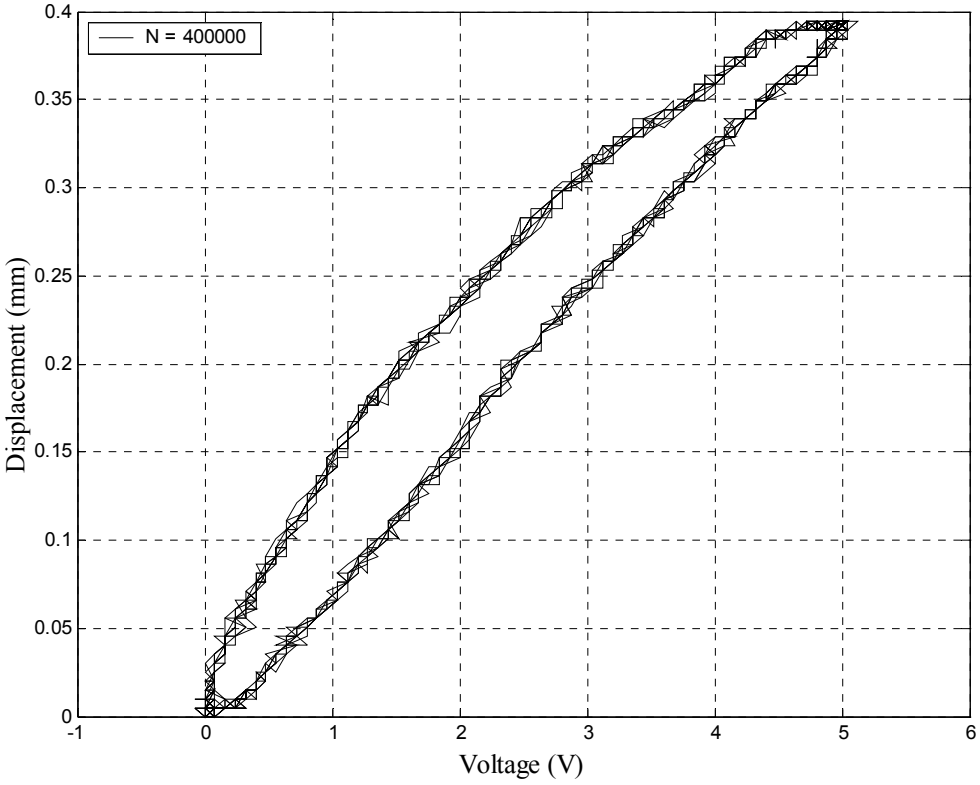

figure B.4 Hysteresis cycle of displacement vs voltage for N = 400,000 cycles

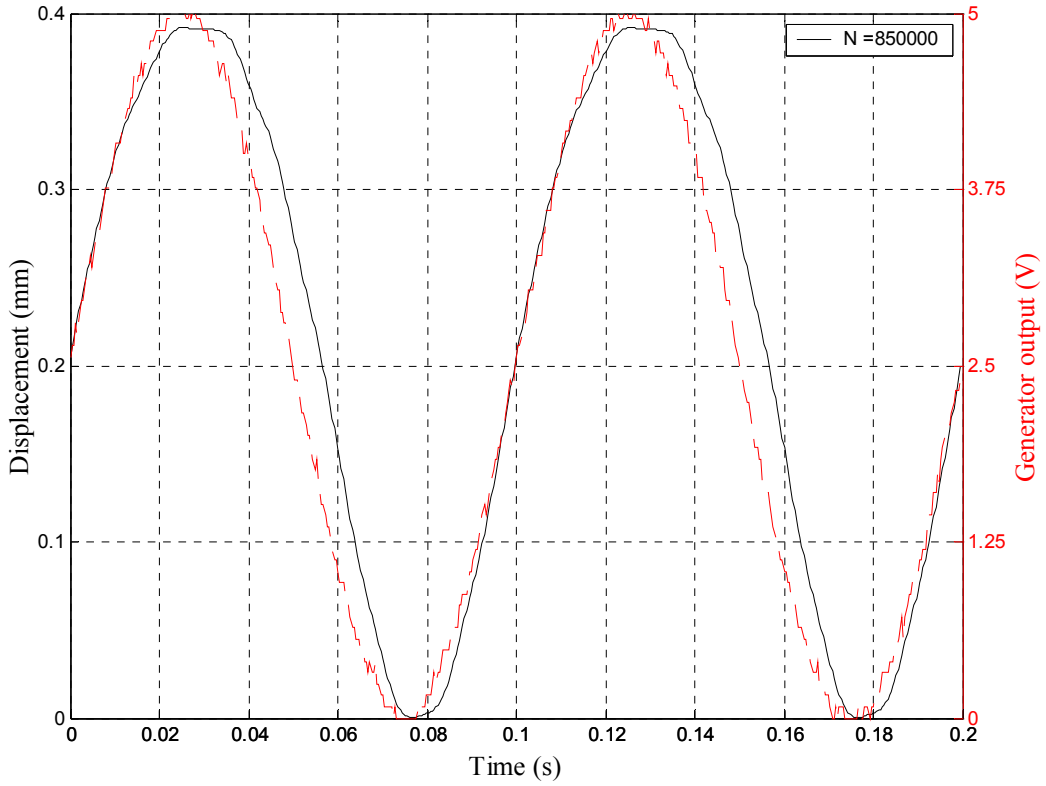

Figure B.5 Dome heigh displacement and generator output for N = 850,000 cycles

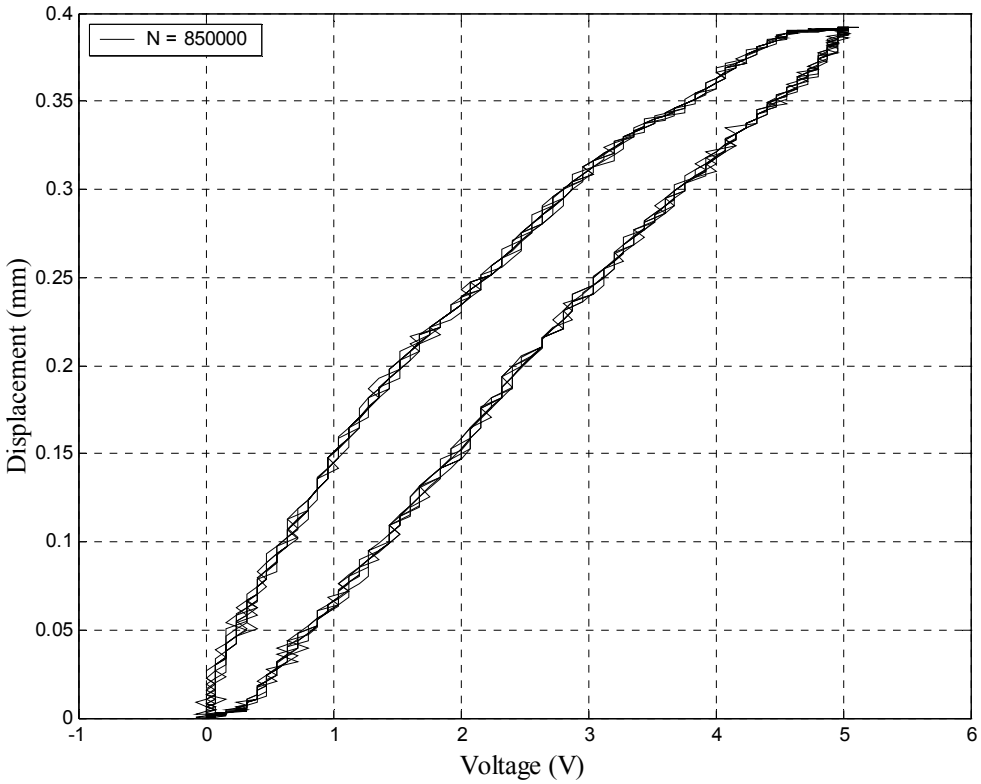

figure B.6 Hysteresis cycle of displacement vs voltage for N = 850,000 cycles

REFERENCES

Auld, B. A. 1990. Acoustic Fields and Acoustic Waves in Solids, Second Edition, Krieger, Malabar.

Bechet, A., Berthelot Y., and Lynch C. 2003. "A stress gradient enhanced piezoelectric actuator composite (GEPAC) with integrated ultrasonic NDE capability for continuous health monitoring,", submitted to J. Intel. Mat. Systems and Structures.

Bechet, A. 2003. "Ultrasonic detection of debonding within a gradient enhanced piezoelectric actuator (GEPAC),", MS Thesis, Gerogia Institute of Technology, Georgia, Atlanta .

Berthelot, Y., Bechet A., and Lynch C. 2003. "Development of a stress gradient enhanced piezoelectric actuator with integrated ultrasonic monitoring capability,", J. Acoust. Soc. Am. 114, No 4, Pt 2, 21671 (2001). Presented at the 146th meeting of the Acoustical Society of America, Austin, TX.

Blackstock, D. T. 2000. Fundamental of physical acoustics, A Whiley-interscience publication, Austin, Texas.

Channel Industries. Website: http://www.channelindustries.com

Chimenti, D. E. 1997. "Guided waves in plates and their use in materials characterization", Appl. Mech. Rev. Vol. 50, No 5, 247-284.

Francois, D., A. Pineau, and A. Zaoui. 1991. Comportement mécanique des matériaux, Hermes, Paris.

Goo, N. S., C. Kim, H. C. Park, and K. J. Yoon. 2001. "Performance evaluation of lightweight piezocomposite curved actuators", J. Intel. Mater. Syst. And Structures, Vol. 12, (9): 639-646.

Haertling, G.H. (1994). "Rainbow Ceramic: A New Type of Ultra High Displacement Actuator." American Ceramic Society Bulletin, Vol. 73, pp. 93-96.

Hellbaum, R.F., R.G. Bryant, and R.L. Fox (1997). Thin Layer Composite Unimorph Ferroelectric Driver and Sensor. United States Patent No. 5,632,841.

Hopkinson, D. 2003. "Development of stress gradient enhanced piezolelectric unimorph actuator composites", MS. Thesis, Georgia Institute of Technology, Georgia, Atlanta .

Jaffe, B., W.R. Cook, and H. Jaffe (1971). Piezoelectric Ceramics, Second Edition. Marietta, OH, Academic Press Limited, Reprinted by CBLS.

Lynch, C., Bethelot Y., Hopkinson D., Keller C., and Bechet A. 2003. "Development of Stress Gradient Enhanced Piezoelectric Actuator Composites with integrated ultrasonic NDE capability", IMECE. ASME International Mechanical Engineering Congress and Exposition, Washington DC.

Mallick, P.K. 1993. Fiber-Reinforced Composites: Materials, Manufacturing, and Design, Second Edition. New York, NY, Marcel Dekker.

Mossi, K.M. and Bishop, R.P. 1999. "Characterization of different types of high performance Thunder actuators", Proc of SPIE Conference, Vol. 3675: 43-52

Nayfeh, A. H. 1995. Wave Propagation in Layered Anisotropic Media, North-Holland,Elsevier Science, Amsterdam.

Smits, J.G., S.I. Dalke, and T.H. Cooney. 1990. "The Constituent Equations of Piezoelectric Bimorphs." *Sensors and Actuators A: Physical*, Vol. 28, pp. 41-61.

TRS Ceramics, Inc. 2003. 2820 East College Avenue, Suite J, State College, PA 16801, USA. Website: http://www.trsceramics.com

Yoon, K.J., J.H. Chung, N.S. Goo, and H.C. Park (2001). "Thermal Deformation and Residual Stress Analysis of Lightweight Piezo-Composite Curved Actuator Device." *Proceedings of SPIE*, Vol. 4333, pp. 418-425.

Yoon, K.J., K.H. Park, Y.B. Kim, Y.S. Kim, and H.C. Park (2002). "Experimental Performance Evaluation of Lightweight Piezo-Composite Curved Actuators." *Proceedings of SPIE*, Vol. 4699, pp. 315-322.

Yoon, K.J., K.H. Park, H.C. Park, and D. Perreux (2003). "Thermal Deformation Analysis of Curved Actuator LIPCA with a Piezoelectric Ceramic Layer and Fiber Composite Layers." *Composites Science and Technology*, Vol. 63, pp. 501-506.